

5-5-2017

Neuronal Tissue Deposition of Gadolinium following Single in Vivo Intravenous Exposure of Low Doses Of Gadodiamide In the Brains of Healthy Dogs and Comparison of Single- And Multi-Voxel Spectroscopy in the Normal Canine Brain at 3 Tesla

Alison Margret Lee

Follow this and additional works at: <https://scholarsjunction.msstate.edu/td>

Recommended Citation

Lee, Alison Margret, "Neuronal Tissue Deposition of Gadolinium following Single in Vivo Intravenous Exposure of Low Doses Of Gadodiamide In the Brains of Healthy Dogs and Comparison of Single- And Multi-Voxel Spectroscopy in the Normal Canine Brain at 3 Tesla" (2017). *Theses and Dissertations*. 3281. <https://scholarsjunction.msstate.edu/td/3281>

This Graduate Thesis - Open Access is brought to you for free and open access by the Theses and Dissertations at Scholars Junction. It has been accepted for inclusion in Theses and Dissertations by an authorized administrator of Scholars Junction. For more information, please contact scholcomm@msstate.libanswers.com.

Neuronal tissue deposition of gadolinium following single in vivo intravenous exposure
of low doses of gadodiamide in the brains of healthy dogs and comparison of
single- and multi-voxel spectroscopy in the
normal canine brain at 3 Tesla

By

Alison Margret Lee

A Thesis
Submitted to the Faculty of
Mississippi State University
in Partial Fulfillment of the Requirements
for the Degree of Master of Science
in Veterinary Medical Research
in the College of Veterinary Medicine

Mississippi State, Mississippi

May 2017

Copyright by
Alison Margret Lee
2017

Neuronal tissue deposition of gadolinium following single in vivo intravenous exposure
of low doses of gadodiamide in the brains of healthy dogs and comparison of
single- and multi-voxel spectroscopy in the
normal canine brain at 3 Tesla

By

Alison Margret Lee

Approved:

Jennifer M. Gambino
(Major Professor)

Erin Brinkman
(Committee Member)

Michaela Beasley
(Committee Member)

Jason Syrcle
(Committee Member)

Andrew J. Mackin
(Graduate Coordinator)

Kent H. Hoblet
Dean
College of Veterinary Medicine

Name: Alison Margret Lee

Date of Degree: May 5, 2017

Institution: Mississippi State University

Major Field: Veterinary Medical Research

Major Professor: Jennifer Gambino

Title of Study: Neuronal tissue deposition of gadolinium following single in vivo intravenous exposure of low doses of gadodiamide in the brains of healthy dogs and comparison of single- and multi-voxel spectroscopy in the normal canine brain at 3 Tesla

Pages in Study 169

Candidate for Degree of Master of Science

Proton MR spectroscopy is a tool that provides quantified brain bioprofiles. Two methods exist: single- and multi-voxel spectroscopy. No studies compare their clinical validity *in vivo*. Gadolinium based MR contrast agents are used to improve lesional conspicuity. Adverse events are reported. Brain deposition occurs following administration in people and murine models. In dogs, doses are anecdotal and deposition is not described. Eight normal dogs underwent MRI at 3 Tesla with two methods of spectroscopy and were administered varying doses of gadodiamide. No differences were seen between single- and multi-voxel spectroscopy when interrogating identical regions of interest. Brains were harvested and evaluated for gadolinium depots using inductively coupled plasma mass spectrometry. Gadolinium was found in the brains of all dogs with dose dependency. Further, adequate normal brain conspicuity was seen at a dose of 0.5 mmol/kg. Thus, clinical trials of gadolinium chelated contrast agents at this dose are recommended.

DEDICATION

Firstly, this work is dedicated to my parents Tom and Sabine, without whose eternal support, encouragement, and affirmation my journey to becoming a veterinarian and a radiologist would not have been possible.

Secondly, this work is dedicated to all my veterinary classmates, professors, clinicians, house officers, and colleagues, who taught me and inspired me in my journey.

Finally, and most importantly, this work is dedicated to my husband Kyle, a rock throughout my residency, who did so much for me during this process when I could do so little for him. I love you forever Kyle; thank you for everything you do.

ACKNOWLEDGEMENTS

This work would not be possible without the tireless support, assistance, and encouragement of my mentor and major professor Dr. Jennifer Gambino as well as my co-collaborators Dr. Michaela Beasley, Dr. Jason Syrcle, and my residency mentor Dr. Erin Brinkman. Thank you all. To all those who made this research possible, including Dr. Judy R. James, Dr. Robert Wills, Dr. Kristen Fizzano, Dr. Bridget Willeford, Jamie Walker, Gary Sorrels, Molly Nicholson, Dr. Jim Cooley, Dr. John Buchweitz, Amber Osborne, and especially DVM candidate Emerald Barrett, thank you. To those whom I work with day in and day out and contributed whatever was needed to finish this process, notably Dr. Brandy Pearson, Dr. Sasha Naugler, and Dr. Wade Won, thank you.

Ever grateful, AML

TABLE OF CONTENTS

DEDICATION	ii
ACKNOWLEDGEMENTS	iii
LIST OF TABLES	viii
LIST OF FIGURES	x
CHAPTER	
I. INTRODUCTION TO MAGNETIC RESONANCE IMAGING AND SPECTROSCOPY	1
Magnetic resonance imaging (MRI).....	1
Historical background	2
Basic principles of nuclear magnetic resonance.....	5
Classical and quantum MRI physics	5
Basic spin theory and net magnetization	8
The Larmor equation	10
Excitation and magnetization vectors.....	12
Free induction decay.....	13
Signal localization and magnetic field gradients.....	14
Fourier transformation and image generation	14
Tissue contrast	15
Proton magnetic resonance spectroscopy	17
Metabolites of interest	18
Acquisition of MRS.....	23
Types of MRS.....	25
Single-voxel spectroscopy (SVS).....	25
Multi-voxel spectroscopy (MVS).....	25
Comparison of MVS and SVS	26
Clinical use of MRS in people.....	26
Veterinary use of MRS	30
II. COMPARISON OF SINGLE- AND MULTI-VOXEL SPECTROSCOPY IN THE NORMAL CANINE BRAIN AT 3 TESLA	34
Study purpose	34

Hypothesis	35
Methods and materials.....	35
Study population.....	35
Technical information: conventional MRI imaging.....	36
MR spectroscopy	38
Cerebrospinal fluid analysis	43
Histopathology	44
Data analysis and post-processing.....	44
Statistics.....	45
Results	45
Metabolite concentrations	47
Comparison of SVS and MVS	50
Discussion.....	51
Differences between SVS and MVS	52
Comparison to prior studies.....	55
Additional experimental considerations	56
Limitations.....	58
Conclusion.....	58
III. INTRODUCTION TO MAGNETIC RESONANCE CONTRAST AGENTS.....	60
Contrast-enhanced MRI.....	60
Gadolinium	60
History	60
Physical properties.....	60
Environmental contamination	61
Toxicity.....	61
Chelation.....	63
Gadolinium-based chelated agents (GBCAs).....	65
Pathophysiology	65
History of GBCA use	66
Types of GBCAs	67
Open-chain versus macrocyclic.....	68
Ionic versus non-ionic	68
Extracellular vs organ-specific	70
Stability of GBCAs.....	71
Dosing	75
Veterinary use of GBCAs.....	75
Adverse reactions to GBCAs.....	76
Nephrogenic systemic fibrosis (NSF)	77
Adverse reactions in veterinary medicine	78
Survey of the American College of Veterinary Radiology	78
T1 hyperintensity following GBCA administration	79
Gadolinium tissue deposition	80
Warnings and current recommendations for use and surveillance	81

Conclusion.....	82
IV. CONSPICUITY OF VARIOUS LOW DOSES OF GADOLINIUM IN THE NORMAL CANINE BRAIN AT 3 TESLA	83
Study purpose	83
Hypothesis	84
Methods and materials.....	84
Study population.....	84
MRI imaging	85
Technical information: conventional magnetic resonance imaging	85
Contrast administration	86
Histopathology	88
Data analysis.....	88
Statistical analysis	91
Gadolinium based contrast use by the American College of Veterinary Radiology: a survey.....	91
Results	92
Agreement	92
Survey results	97
Discussion.....	97
Adverse effects	97
Conspicuity.....	97
Study limitations.....	99
Conclusions	102
V. INVESTIGATION OF NEURONAL DEPOSITION OF GADOLINIUM IN NORMAL DOGS FOLLOWING A SINGLE INTRAVENOUS EXPOSURE TO VARIOUS DOSES OF GADODIAMIDE.....	103
Study purpose	103
Hypothesis	103
Methods and materials.....	104
Study design and animal subject population	104
MRI imaging and GBCA administration	106
Tissue processing and histopathology	109
Inductively-coupled plasma mass spectrometry gadolinium analysis.....	110
Scanning and transmission electron microscopy with electron probe microanalysis	111
Statistical analysis	112
Results	113
Subject population	113
Effect of gadolinium exposure on tissue deposition.....	120
Statistical model with group 1 and group 2 dogs	124
Model with group 1 dogs.....	125

Model with group 2 dogs.....	127
Model with group 2 dogs comparing tissue type.....	128
Localization of gadolinium within neuronal tissue and assessment of histologic change	131
Discussion.....	131
Gadolinium deposition	132
Dose dependency	134
Prior studies	135
Physiology	136
Study limitations.....	139
Conclusion.....	141
REFERENCES	143
APPENDIX	
A. LIST OF ABBREVIATIONS.....	160
B. MR SPECTROSCOPIC METABOLITES OF INTEREST	163
C. BRAIN MRI PROTOCOLS	166
Typical MRI acquisition protocols.....	167
Typical MR sequences	169

LIST OF TABLES

1.1	Magnetic moments of medically useful nuclei	11
1.2	Gyromagnetic ratios for medically useful elements in MR	12
1.3	MR signal intensity characteristics of various tissues	16
1.4	Common metabolite changes in non-neoplastic disease states in people	20
1.5	Common metabolite changes in neoplastic disease states in people	21
1.6	Common metabolite changes in non-neoplastic disease states in animals	22
1.7	Common metabolite changes in neoplastic disease states in dogs	22
1.8	Mean metabolite ratios in normal dogs <i>in vivo</i> at 3 Tesla using single-voxel spectroscopy.....	31
2.1	MR spectroscopy acquisition parameters for single-voxel and multi-voxel studies.....	43
2.2	Hepatobiliary and renal serum biochemistry values for all dogs.....	47
2.3	Mean brain metabolite concentrations, given in machine (MACH) units, acquired using single-voxel spectroscopy in the thalamus, parietal lobe, and piriform lobe of six dogs.....	48
2.4	Mean brain metabolite concentrations, given in absolute ppm units, acquired using multi-voxel spectroscopy in the thalamus, parietal lobe, and piriform lobe of six dogs.	49
2.5	Metabolite ratios given for both single-voxel and multi-voxel spectroscopy performed in the thalamic, parietal, and piriform lobes of the brains of six dogs.....	50
3.2	FDA approved gadolinium based contrast agents	69
3.3	Chemical stability and excretion of the nine FDA approved gadolinium based contrast agents	73

4.1	Intravenous dosing scheme of gadodiamide (Omniscan) administered to the study population consisting of eight purpose-bred hound dogs	87
5.1	Hepatobiliary and renal serum biochemistry values for all dogs of groups 1, 2, and 3.....	115
5.2	Doses of gadodiamide as administered to dogs with information regarding tissue state, timing of sample collection and total time between tissue collection (and necropsy) and gadodiamide administration for all dogs.	118
5.3	Gadolinium deposition by lobe for all dogs of each group.....	121
B.1	MRS metabolites of interest, spins, and clinical importance.....	164
C.2	Typical minimum MR sequences and acquisition parameters acquired for all dogs in Chapters II and IV, and group 1 of Chapter V	169

LIST OF FIGURES

1.1	3T magnetic resonance images of a “ <i>brainy</i> ” orange.....	4
1.2	Quantum mechanics model.....	7
1.3	Proliferation of the number of publications regarding MR spectroscopy.....	27
2.1	MR Spectroscopy calibration obtained via a Probe-P phantom	38
2.2	Single-voxel and multi-voxel magnetic resonance spectral examples	39
2.3	Single-voxel and multi-voxel spectroscopic region of interest (voxel localization).....	41
2.4	Post-processed multi-voxel regions of interest	42
3.1	Open-chain vs macrocyclic GBCA structure.....	68
3.2	The 9 FDA approved gadolinium-based chelated agents, grouped by their class and charge.	70
4.1	Tagged image file format (TIFF) images of T1-weighted transverse images following various doses of gadodiamide in four normal dogs.....	90
4.2	Image score by dose (in mmol/kg) and by reviewer.....	94
4.3	Number of images given each score by reviewer	95
4.4	Images scored by dose by three reviewers.....	96
4.5	T1 shortening times of various GBCAs, as a function of their gadolinium concentration.....	101
5.1	Regression lines of gadolinium concentrations (ng/g) by dose (mmol/kg) for group 1 and group 2 dogs.....	125
5.2	Regression lines of gadolinium concentrations (ng/g) by dose (mmol/kg) for each brain lobe of group 1 dogs.	126

5.3	Regression line of gadolinium concentrations (ng/g) by dose (mmol/kg) for group 2 dogs.....	128
5.4	Regression line of gadolinium concentrations (ng/g) by dose (mmol/kg) for group 2 dogs.....	130
C.1	MRI acquisition parameters for the eight dogs described in Chapters II, IV, and group 1 of IV	168

CHAPTER I

INTRODUCTION TO MAGNETIC RESONANCE IMAGING AND SPECTROSCOPY

Magnetic resonance imaging (MRI)

The use of magnetic resonance (MR) imaging (MRI) in humans has grown exponentially over the past few decades, in part due to the excellent anatomical and pathological detail provided by this modality.^{1,2} The use of contrast enhanced MRI in veterinary medicine is no exception, and a growing number of veterinary patients have benefited and continue to benefit from the clinical use of this imaging modality. This growth is in part due to a growing understanding of the capabilities of the imaging modality as fostered by the American College of Veterinary Radiology (ACVR), its growing number of diagnostic imaging specialists, and a client base of pet owners willing and financially able to pursue this advanced technology through tertiary care referral centers and academic institutions.

With regard to brain imaging in particular, important and generally accepted advantages of conventional MRI over the use of computed tomography (CT) include the ability to directly acquire images with different sequences that exploit specific tissue contrasts, the ability to avoid beam hardening artifacts in regions of high bone density (such as the petrous temporal bone for evaluation of the pons, cerebellum and structures within the caudal fossa), and the ability to obtain detailed differentiation of gray-white matter tissue and ventricular structures. In addition to routine conventional MR sequence

protocols, there are more advanced applications, such as MR spectroscopy, vascular angiography (time of flight imaging or MR angiography), volumetric imaging, blood oxygen level dependent imaging and diffusion/perfusion weighted imaging, which can be performed to gain additional biomolecular and functional information beyond that of simple brain morphology and pathology.

Historical background

A complete overview of the history of nuclear magnetic resonance (NMR) imaging (NMRI) is beyond the scope of this thesis, and compiled histories can be found in numerous publications.³⁻⁷ The following is an abridged account of the historically significant milestones that contributed to the great success of MRI as one of the most valuable clinical imaging modalities of our era.

Isidor Rabi of Columbia University first described nuclear magnetic moment “beams” in 1938 and was awarded the Nobel Prize for his discovery.^{4,5} In the late 1940s, nuclear magnetic resonance became the focus of experimental exploration of physicists and chemists of that period. From 1946–1952 teams at Cambridge, Stamford and Massachusetts Institute of Technology (MIT) worked simultaneously, yet independently, toward the discovery of nuclear magnetic resonance imaging.³ Block (of Stamford) and Purcell (of MIT) won the Nobel Prize for physics in 1952 for their achievements and now famous prior publications.^{3,8,9} Around the same time (1950), Proctor, Yu and Dickinson were the first to discover that nuclei within the same atom absorbed energy at different resonance frequencies, while Shaw and Elksin were investigating the water content of vegetables.^{3,4,10-12} For 20 years, physicists, chemists and biologists explored molecular compounds and chemical structure (both *in* and *ex vivo*) using the basic magnetic

resonance principles proposed earlier. By the late 1950s, approximately 400 papers on the topic had been published, and the first established text about NMR made reference to all of them.^{3,13}

In 1955, Odeblad and colleagues pioneered investigations on animal and human tissues and fluids, which lead to numerous biologic investigations on the molecular characteristics of vitreal and lenticular fluids, blood cells, spinal fluid, saliva and muscle tissues.¹⁴ By 1966, Ernst and Anderson introduced pulsed MR and Fourier transformation.¹⁵ Investigations on whole organisms (ranging from bacteria to rodents), and later human subjects, naturally followed; however, it was not until the early 1970s that Raymond Damadian first proposed the medical use of NMR and hypothesized that NMR could be used to differentiate between abnormal or cancerous tissues and normal tissues.^{4,16} He patented his concept and later created the first whole body NMRI machine. Early in the same decade (1973), in Stony Brook, New York, Lauterbur, Mansfield and Grannell used magnetic gradients to produce the first images of live animals, demonstrating the NMR properties of tissue for which Lauterbur and Mansfield later shared the Nobel Prize in medicine (2003).^{4,6} Lauterbur called this technique *zeumatography*, which in Greek means “that which joins together.”⁶ In the late 1970s, publications applying methods of spatial localization began to surface using sequential point, line scanning, projection-reconstruction and two- and three-dimensional Fourier transformation began to surface.⁶ These techniques were, and still are, used to display slice images and achieve second and third planar imaging. Although essential to image production, a full discussion these techniques is beyond the scope of this work.

Detailed internal images of biological structures of fruits, vegetables, members of the animal kingdom (such as clams, mice, and rabbits) and eventually the first human MRI of a finger were published.¹⁶⁻¹⁸

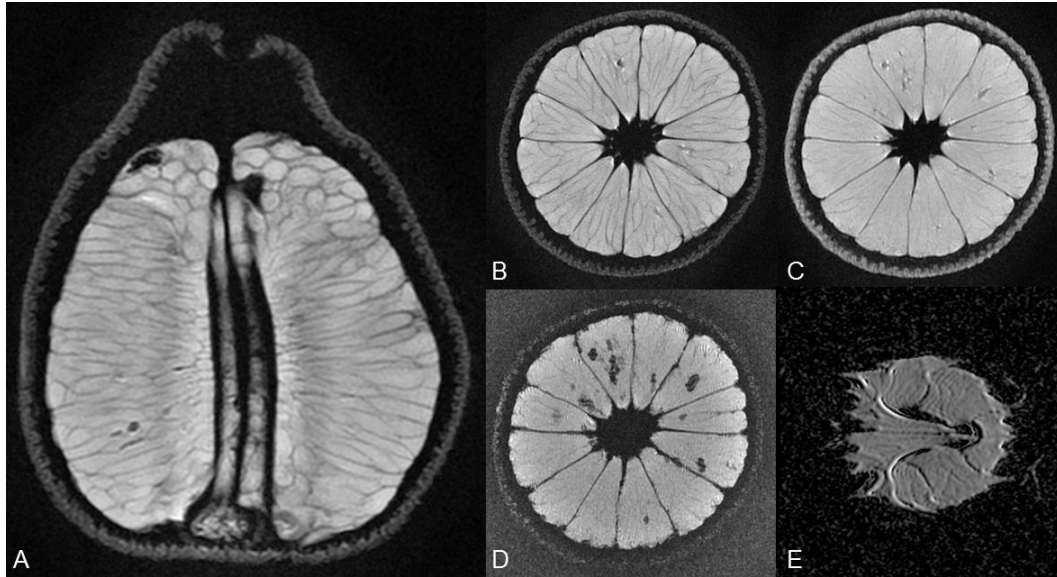


Figure 1.1 3T magnetic resonance images of a “brainy” orange

A and B– “Dorsal” and “transverse” planar images T2-weighted images. C– “Transverse” planar proton density image. D– “Transverse” planar gradient echo image. Notice the susceptibility artifact (black within the image) within the orange due to trapped gas. E– Diffusion tensor image, a measure of Brownian water molecular motion demonstrating free water movement along the “pathways” of least resistance of (hyperintense regions) and restricted regions, or membrane boundaries. *Courtesy J. Gambino and G. Sorrells – we scan our lunch.*

The low field images (on the order of 0.15T) showed different contrasts of different tissues, which arose from inherent properties of the object’s construction like tissue density, mobility and relaxation.¹⁶ The first images of the human thorax, head and abdomen of healthy volunteers preceded early images of the first descriptions of pathology in 1980s.¹⁹⁻²¹ Early diagnostic capabilities included the recognition of

hydrocephalus, a variety of intracranial tumors, aneurysms, arteriovenous fistulas and chronic sinusitis.⁶

The first high field, superconducting, MRI machine was installed by Oxford Instruments in London, at Hammersmith Hospital in 1981, with commercial magnets coming into use at clinical facilities shortly thereafter.⁷ MRI has become a staple of clinical human and veterinary radiology with incredible advances occurring between its advent in the early clinical use in the 1980s to today. The rapidly progressive interest of *in vivo* applications of this technology, in areas such as microimaging, spectroscopy, functional brain imaging and interventional imaging, have brought MRI to the forefront of medical imaging.

Basic principles of nuclear magnetic resonance

In order to discuss the clinical applications of MRI, contrast-enhanced imaging, and magnetic resonance spectroscopy (MRS), a basic understanding of MRI physics is essential.

Classical and quantum MRI physics

Two methods of physics are used to describe the NMR phenomena. In the classical description, molecular momentum is described in the reference frame of classical Newtonian derivatives. Vectors of magnitude, direction and frequency are used to explain the relationships between angular momentum, magnetic moment and the inherent spin of the nuclear components of elements. The motion of an object's molecular construct (in the case of MRI, nuclear particles, for example ^1H), is linear or rotational and its corresponding momentum is linear or rotational.⁴ The particle's motion can be

thought of as its tendency to remain in motion. In accordance with Newton's second law of motion, only a force can disrupt this tendency. Molecules may also have momentum at an angle, which can only be affected by the force of torque (or rotational force). At the same time it must be considered that such rotating objects have a charge, such that when in motion, according to Faraday's law of induction, an electrical current loop is created inducing a magnetic field.⁷ This magnetic field is characterized by a fundamental magnetic quantity associated with current, called a magnetic dipole moment. With regard to any periodic orbital motion, there is a fundamental relationship between magnetic moment and angular momentum where the magnetic dipole moment is the object's inherent classical gyromagnetic ratio.⁷ Thus, any time there is magnetism, charge and momentum, any two will induce the third.

Quantum mechanical theory and classical arguments arrive at the same relationship, where the magnetic dipole moment is inversely proportional to the gyromagnetic constant (characteristic to the nucleus under investigation) multiplied by the angular momentum of the spinning particle.⁷

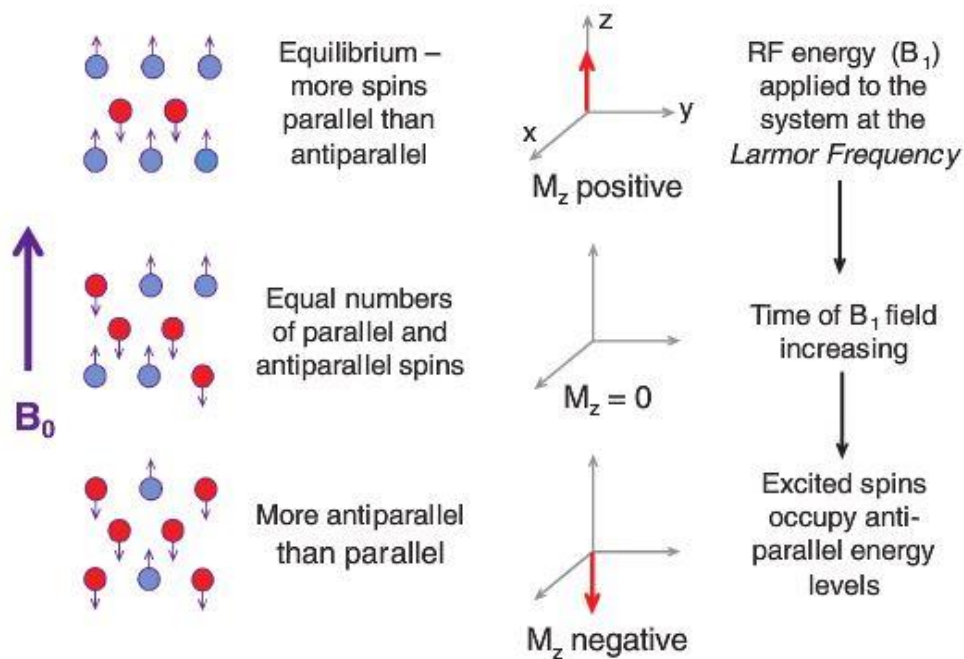


Figure 1.2 Quantum mechanics model

Diagram depicting the quantum mechanics model. Discrete energy absorption is shown over time, as the energy differences between the spin-up (blue) and spin-down (red) conditions. Discrete absorption of quanta of energy cause the protons to excite from alignment with the main magnetic field (spin-up or B_0) to the spin-down condition. This phenomenon is the origin of the signal that contributes to image creation. *Adapted from Bushberg, The essential physics of medical imaging,*⁷

In the author's opinion, a classical explanation falls short especially with regard to MR spectroscopy because it does not fully explain the intimate relationship between magnetic energy associated with magnetic moment and the general resonance condition.⁴ A quantum mechanical discussion is the only theory that can completely describe NMR phenomenon because it takes into consideration the amplitude of the spin of an elementary particle which is finite and limited, as well as its directions, which are discrete and specific.⁷ Furthermore, it takes into account changes in energy that the particles undergo and discusses the changes in terms of electromagnetic waves and nuclear spins.

Basic spin theory and net magnetization

In quantum mechanics, protons, neutrons and electrons have a spin quantum number that can be calculated using atomic mass and charge number under the following few summarized rules.⁷ For nuclei with odd atomic mass, spin quantum number is a half-integral.^{4,7} Examples include ^1H and ^{13}C for which spin quantum numbers are $\frac{1}{2}$ and $\frac{3}{2}$ respectively.⁷ For nuclei with even atomic mass and even charge, spin quantum number is zero with examples including ^{12}C and ^{16}O .⁷ For nuclei with even atomic mass and odd charge, spin quantum number is an integral number.⁷ For example, the spin quantum number for ^2H and ^{14}N are 1 and 2, respectively.⁷

For the hydrogen proton (^1H), 2 energy states exist: quantum spin $+\frac{1}{2}$ and quantum spin $-\frac{1}{2}$.^{4,7,22} The quantum theory describes these as spin up positions (or the low energy alpha spin state) and spin down position (or the high energy beta spin state). In a high field magnet, the lower energy (or spin up) state predominates with magnetic moments parallel to the main magnetic field, whereas the beta spin state has an antiparallel angular momentum.^{4,7} Between the two states exists an energy difference with the energy being greater in the spin down position.^{4,7} With regard to clinical MRI and image acquisition, a radiofrequency (RF) pulse is applied to manipulate the particles that are aligned in a main magnetic field of the magnet in order to generate the NMR phenomenon of precession. The energy of the applied oscillating magnetic field (or electromagnetic wave or RF), is equal to that of the energy difference between the spin up and spin down states.^{4,7}

In living systems in which we investigate ^1H , the low energy state predominates in that a greater population of protons is in the spin up state aligned with the main

magnetic field (B_0). For a macroscopic sample of living tissue containing one million nuclear spins at 3T, corresponding with the velocity of spin of 400 Mhz, the population difference between the two states is small, only 37–67 spins or 0.006%. The final signal received is proportional to this population difference and is the signal that contributes to final image construction and the perception of different tissue contrasts. MRI and MRS are far less sensitive when compared to other forms of spectroscopy (like mass spectroscopy) where the energy differences are much larger.⁴ Total signal is dependent however, on many factors (some predictable and some not) including sample volume, gyromagnetic ratio, temperature, natural abundance of the nucleus studied, (sample) noise, relaxation parameters and inherent tissue characteristics, the presence of artifact inducing conditions, the presence of relaxation enhancing contrast agents and magnetic field strength⁴.

MRI images are made based on the electromagnetic activity of ^1H within the body. Human bodies, and those of the mammalian species are predominantly composed of water. ^1H is very abundant in tissues. Protons and neutrons within atomic nuclei both have linear and rotational (spin) motion and momentum (or electromagnetic moment). The spins of the nuclear particles each have an individual axis and generate small internal magnetic fields with unchanging or constant linear momentum and speed.⁷ Momentum changes (acceleration and deceleration) result only when an external force is applied as per basic Newtonian principals. MR imaging is based on the concept of this nuclear spin being influenced by externally applied magnetic fields and radiofrequencies. When under the influence of a strong magnetic field and exposed to such radiofrequencies, these nuclei absorb and emit energy and undergo changes in angular (or directional)

momentum. Fluctuations in angular momentum from radiofrequency manipulations result in the superior soft tissue contrast resolution of the images.

The Larmor equation

Under normal circumstances, the spinning of the protons and neutrons in our bodies is a random event. Although we are “magnetized,” the magnetism of the Earth’s magnetic field (on the order of 50 μ T) is too small to have much of an effect. The high-field magnet at the author’s institution is a 3T magnet (on the order of 60,000 times the Earth’s gravitational force).⁷

The abundance of water in the human body makes the ^1H isotope almost 100% ubiquitous. ^1H also has the highest magnetic moment among stable nuclei.^{7,13} Oxygen is the next most abundant element, but it is not one to investigate given its lack of a suitable isotope and the artifacts it imparts on images.³ Phosphorus (^{31}P) is also 100% abundant with high magnetic moment. However, its concentration in living organisms is low. The abundance of carbon is less (approximately 1%) and its magnetic moment is very low making it unfavorable and difficult to exploit.⁴ Nitrogen isotopes are also unsuitable, having either low abundance or magnetic moment.³ Other compounds are used in research applications, but have a lower NMR sensitivity than ^1H . For example, ^{19}F is abundant, but has 83% of the MR sensitivity of ^1H .²³

Table 1.1 Magnetic moments of medically useful nuclei

Nucleus	Magnetic Moment
^1H	2.79
^3He	-2.13
^{13}C	0.70
^{17}O	-1.89
^{19}F	2.63
^{23}Na	2.22
^{31}P	1.13

Magnetic moment given in units= $5.05 \times 10^{-27} \text{ J T}^{-1}$

When living systems are placed in a clinical MR unit, it is ^1H that is exploited given its abundance, concentration and angular momentum. When the protons are exposed to a large magnetic field, the two magnetic fields, those of the externally applied B_0 , and those of the nuclei, interact. When they interact, the protons become still momentarily and shortly thereafter begin to regain movement or precess. This precession occurs at a frequency (ω_0), which is dependent on the strength of the external magnetic field. The Larmor equation

$$\omega_0 = B_0 * \gamma \quad (2.1)$$

defines the frequency at which precession occurs. The magnitude of B_0 is expressed in the unit Tesla. Gamma (γ) is the gyromagnetic ratio measured in MHz per Tesla, which is a constant for every atom at a given magnetic field strength (as given in Table 1.2).²⁴

Table 1.2 Gyromagnetic ratios for medically useful elements in MR

Nucleus	Gyromagnetic Ratio (MHz/T)
^1H	42.58
^{13}C	10.7
^{17}O	5.8
^{19}F	40.0
^{23}Na	11.3
^{31}P	17.2

Excitation and magnetization vectors

Because of the abundance of ^1H protons in the body, when placed under the influence of B_0 , the majority of the protons align with that main externally applied field and become a separate magnetic or static net magnetization vector. A second externally applied force, B_1 (or RF pulse) is then applied. This RF pulse, induces a flip or inversion of the net magnetic vector away from the main magnetic field (B_0 , or in the classical description, the M_z vector) and into the longitudinal and transverse planes (the M_x and M_y fields, respectively).⁷ As the transverse vector precesses around the receiver coil, it induces a current, as described in the previous section, and in accordance to Faraday's law of induction.²⁰

Nuclear magnetization can only be observed by rotating the net magnetization onto the transverse plane and inducing precessions about the B_0 and B_1 axes.⁴ Both magnetic fields act simultaneously at the Larmor frequency and induce an electromotive

force in the receiver coil surrounding the sample.⁴ A 90° pulse is applied, which moves the protons into the transverse vector resulting in a maximum M_{xy} . These protons are said to be in phase coherence. Intrinsic inhomogeneity in the tissues causes a loss of M_{xy} . This is called the free induction decay (FID). We described earlier that the subsequent current that the magnetization induces becomes the MR signal.²¹

Free induction decay

As described, externally applied RF pulses force the protons out of thermal equilibrium (which occurs in the direction of M_z / B_0 and is the natural state of the protons when tissues are placed in a strong magnetic field). The RF is then turned off, and the protons are again free to precess to their original states (and realign with B_0). This process is called free induction decay (FID) and it occurs in both the transverse and longitudinal planes (M_x, M_y).¹⁹ The term decay refers to a relaxation of the protons from the excitable state due to the RF pulse and a subsequent decrease in signal intensity. Decay in the longitudinal plane is referred to as T1 (spin-lattice) relaxation, whereas decay in the transverse plane is referred to as T2* and T2 (spin-spin) relaxation.⁷ Transverse and longitudinal decay occur simultaneously. Different tissues within the body and in the brain have different T1, T2* and T2 relaxations.

Free induction decay (FID) is an important component to the creation of MR spectral (or Lorentzian absorption and dispersion) line shapes. Following excitation, transverse magnetization occurs at ω_0 and decays with a characteristic time constant or T2* as time progresses. Complex three-dimensional FID can be described by two projections of the motion, the $M_x t$ (a real component) and $iM_y t$ (an imaginary component), where t is the characteristic time constant for the loss of phase coherence

amongst the spins.⁴ Although this FID is often presented as a single-exponential decay, local magnetic field inhomogeneities cause small variations in individual spin decays, which results in a multi-exponential decay pattern.

Signal localization and magnetic field gradients

Acquisition of MR images and signal detection by the MRI machine, inherent computer components and software are complicated processes. Detection of signal location is by way of a complicated extrapolation from gradients along the x, y and z axes and a mathematical process called Fourier Transformation, which translates the data obtained into a visible image in a domain called k-space.²² The acquisition gradients are termed slice selection (SSG), phase encoding (PE) and frequency encoding (FE) gradients.²² The slice selection gradient selects the target region of the RF pulse, and the steeper the gradient, the thinner the slice. Phase encoding occurs along the y-axis or longitudinal gradient. Frequency encoding (also called the read out gradient because it usually occurs when the echo is read out), occurs along the transverse or x-axis.²²

Fourier transformation and image generation

Once the MRI computer processor has all the information about the proton spins occurring in each of these planes, it can then compute the exact location and amplitude of the signal. This information is then stored in k-space, which is a matrix of voxels within which the raw imaging data resides.⁷ The center of k-space usually stores information regarding the gross morphology and tissue contrast, whereas the periphery of k-space stores information about the details of fine structures (or spatial resolution).¹⁷ The raw

data must then be Fourier transformed in order to display the typical MRI image seen on a computer monitor used for diagnostic evaluation.¹⁷

Tissue contrast

Two parameters in particular contribute to differences in contrast seen between the tissues on MRI images. These are time to echo (TE) and time to relaxation (TR). TR is the time in milliseconds between the application of the RF pulse and the start of the next RF pulse.¹⁹ TE is the time in milliseconds between the start of the RF pulse and the peak of the echo detected.¹⁹ Most pathologies have high signal intensity due to the density of their proton content and hence have high signal intensity on T2.

Table 1.3 MR signal intensity characteristics of various tissues

Signal Intensities	T1	T2	Signal Intensities
<u>Hypointense</u> (dark, black, or signal void)	Air Bone Calcifications/stones Fast flowing blood		<u>Hypointense</u> (dark, black, or signal void)
<u>Isointense</u> (medium grey)	Ligaments, tendons, scars <u>High bound water tissues</u> Liver, pancreas, adrenal glands, hyaline cartilage, muscle		<u>Isointense</u> (medium grey)
	<u>Edema/fluids</u> Urine, bile, cystic fluid, cerebrospinal fluid <u>High free water</u> <u>tissues</u> Kidneys, spleen	Bone islands	

Table 1.3 (Continued)

<u>Hyperintense</u> (light grey to white)	<u>Proteinaceous fluid</u> Abscess, complex cyst, synovial fluid		<u>Hyperintense</u> (light grey to white)
	Fat Bone marrow Methemoglobin Slow flowing blood Paramagnetic contrast	<u>Edema/fluids</u> Urine, bile, cystic fluid, cerebrospinal fluid <u>High free water</u> <u>tissues</u> Kidneys, spleen <u>Blood products</u> Oxyhemoglobin Extracellular methemoglobin	

T1-weighted and T2-weighted signal characteristics of various tissues. The shared T1 and T2 characteristics are placed in the centered cell, while different characteristics between T1 and T2 are placed in the divided cells. *Table Adapted from Bitar et. al.*²⁴

Proton magnetic resonance spectroscopy

Although the MR appearance of multiple disease processes of the brain, including neoplastic, infectious, and immune-mediated disorders, have been well described in both human and veterinary literature, the specificity of MRI for definitive diagnoses remains limited.²⁵⁻²⁸ In people, the sensitivity of MR for brain tumor diagnosis is reportedly 95%–99%, whereas the specificity is 70%–76%.^{25,29} This relatively low specificity is due to signal overlap in MR imaging characteristics and lesion morphology between various

disease etiologies (and is seen in both people and dogs).^{26,29} When spectroscopy is added to conventional MR imaging interpretation, the sensitivity for disease detection is reportedly 80%–100% and the specificity increases to 78%–100%.^{30,31}

Metabolites of interest

Magnetic resonance spectroscopy (MRS) is a non-invasive, U.S. Food and Drug Administration (FDA)-approved, complementary MR imaging technique which allows for the interrogation of numerous inherent tissue biological markers.³² With regard to the brain, biomarkers of interest typically include N-acetyl aspartate (NAA), creatine (Cr), choline, (Cho), myo-inositol (mI), lactate (Lac), lipids, glutamine-glutamate complex (Glx), and taurine (Tau).^{32,33} MRS allows for the *in vivo* quantization of these markers, thus providing qualitative and quantitative data regarding the metabolic and functional status of the imaged tissue; which conventional MR acquisition pulse sequences do not provide.^{32,34} Spectroscopic data can be particularly useful in acting as a complement to conventional MR images in improving interpretation accuracy in the brain.³⁴⁻³⁶ As stated above, the addition of spectroscopy can increase the sensitivity of the scan to 80%–100% and the specificity of the scan to 78%–100%.^{30,31}

Briefly, lipids (which resonate at a ppm of 0.9–1.4) are products of brain destruction.³¹ Lactate, which resonates at 1.3 ppm, is a product of anaerobic glycolysis, and is increased in cases of meningoencephalitis.³¹ N-acetyl aspartate (NAA), which resonates at a ppm of 2.0, is a neuronal marker present in neurons, axons, and dendrites, representing axonal number and dendritic and axonal density. The NAA fraction is decreased in tumors, including gliomas and meningiomas, as well as hepatic encephalopathy.^{31,37,38} The glutamine-glutamate complex (Glx complex), which resonates

at 2.2–2.4 ppm, is composed of two neurotransmitters.³¹ Glutamine is involved in detoxification and regulates neurotransmitter activity. Glutamate is excitatory and is involved in mitochondrial metabolism.³¹ Increases in fractions of the Glx complex can be seen with traumatic brain injury, oligodendroglioma, and epilepsy.^{39,40} Creatine (Cr, which resonates at 3.0 ppm) is involved in energy metabolism and is increased in hepatic encephalopathy.^{31,38} Choline (Cho), which resonates at 3.2 ppm, is a cell membrane marker and is involved in cellular synthesis and degradation. It is elevated in gliomas and meningioma but is decreased in hepatic encephalopathy and can also be elevated in certain inflammatory conditions.^{31,37,38} Resonating at 3.5 ppm, myo-inositol (mI) is a pentose sugar and is a glial cell marker involved in the triphosphate intracellular second messenger system.³¹ This metabolite may be elevated in extra-axial choroid plexus tumors, in gliosis, in Alzheimer's disease in people, or following the administration of mannitol.^{31,34} Alanine, an amino acid, (resonating at 1.48 ppm) is present and typically seen in meningiomas.³¹ Taurine (3.4 ppm) is an osmoregulator and a moderator of neurotransmitter action and can be elevated in high grade malignancies.³¹ Please refer to Appendix B for more information regarding these metabolites. Tables of common elevations in disease states in people and animals are given below.

Table 1.4 Common metabolite changes in non-neoplastic disease states in people

Disease	mI	Cho	Lac	Lip	Succinate
Subacute infarct			+		
Focal cortical dysplasia			++		
Pyogenic abscess	+		ND	+	+
Delayed radiation necrosis			ND	+	
Peritumoral edema			+	ND	
Herpes encephalitis		+	++		
Arachnoid cyst			++		
Epidermoid cyst			++		
Hydatid cyst			++		
Toxoplasmosis			+		

ND=none detected. *Adapted from Kingsley et al.*⁴¹

Table 1.5 Common metabolite changes in neoplastic disease states in people

Disease	mI	Cho	Lac	Lip
Pilocytic Astrocytoma		+	ND	ND
Diffuse Astrocytoma		+	ND	ND
Oligodendroglioma		+++	ND	ND
Anaplastic Astrocytoma		+++	+	ND
GBM		+++	+	+
Ependymoma		+++	ND	ND
Medulloblastoma		+++	ND	ND
Meningioma		+++	ND	ND
Metastasis		++	ND	++
Lymphoma	++	+++	++	++

ND=none detected. Adapted from Kingsley et al.⁴¹

Table 1.6 Common metabolite changes in non-neoplastic disease states in animals

Disease	mI	Cho	Cr	Glx	NAA	Lac	Lip	Succ	Tau
Feline immunodeficiency virus			-	+	-				
Canine hepatic encephalopathy	-	-	ND	+	-				
Abscess (caprine)		-	-		-	+	+	+	
Canine noninfectious meningoencephalitis						+			+

Succ=succinate. ND=none detected. Adapted from Carrera et al 2014,³⁸ Carrera et al 2016,⁴² Power et al,⁴³ and Dennler et al.⁴⁴

Table 1.7 Common metabolite changes in neoplastic disease states in dogs

Disease	mI	Cho	Cr	NAA	Lac	Lip
Glioma		+++		-	+	+
Meningioma		+++		-	+	+

Adapted from Stadler et al.³⁷

Metabolites may be present in increased or decreased concentrations, or may be absent all together in varying pathologic conditions.³³ Many of these conditions can have overlapping biomarker signal intensities and similarities in their respective brain bioprofiles, such that accurate interpretation only comes from evaluation of the clinical

presentation, the conventional MR images, and functional MR imaging, if performed (Jennifer Gambino, personal communication, January 17, 2017). With regard to human brain tumors, it is common to see elevations in Cho, lactate, and lipids, while there is usually a decrease in NAA and Cr.³¹ A metabolite not normally present in brain tissue is lactate, and lactate may be seen in increased concentrations in varying pathologic conditions such as neoplasia, ischemia and coagulative necrosis.³³ In the author's experience, in the dog, mild to moderate Lac/Lip fraction elevations seen in conjunction with mild Cho and Cr depression and lack of moderate NAA depression, can make infarction distinguishable from intra-axial tumors (specifically of glial cell origin) in which Cho and NAA depression trends are noted. (Gambino unpublished data).

Acquisition of MRS

MRS is typically performed following the acquisition of a complete study of conventional morphologic brain MR images. Magnet shimming, to correct for magnetic field inhomogeneities is essential in spectroscopic acquisitions. Additionally, water suppression must be performed, because the concentration of water in biological samples is much higher than the metabolites in question. If water suppression is not performed, the water peak would be much larger (up to 100,000 times that of water) than the metabolites, and the necessary scaling would make the metabolite peaks impossible to see.⁴ Water suppression is accomplished by either a chemical shift selective (CHESS) or inversion recovery (IR) technique, coupled with a stimulated echo acquisition mode (STEAM) or point resolved spectroscopy (PRESS) acquisition.^{4,22} An MRS pulse sequence is applied, and the resultant data is displayed as a set of signal peaks derived from the inherent quantum spin of the metabolites of interest.⁴⁵ This data is what forms

the spectrum. The spectral data is presented in graphical format with two axes. The vertical y-axis corresponds to signal intensity, which is given in arbitrary units (machine or MACH units for single-voxel acquisitions and relative or absolute machine units for multi-voxel acquisitions). These units correspond closely to the number of millimoles (mmols) of atoms (versus the molar concentration of water). The concentration of these atoms can then be presented as either a general proprietary MACH unit, an absolute value, or as a value relative to the concentration of water in the imaged tissue depending on the MRS probe acquisition applied. With regard to the bioprofile, the horizontal x-axis corresponds to frequency, given in either absolute (Hertz, Hz) or relative (parts per million, ppm) measure.³² Generally, Hz units are converted to ppm because of differences in the Hz values for metabolites between magnets of different field strength.^{46,47} The ppm for metabolites remains constant for molecules, because the separation in Hz is proportional to field strength.^{46,47} The equation for the conversion of Hz to ppm is given by:

$$df = \frac{f \times ppm}{10^6} \quad (2.2)$$

where df is the peak frequency in Hz, ppm is the peak variation, and f is the center frequency of the metabolite in Hz.

As described above, specific metabolites have inherent (fingerprint) quantum spins, which correspond to frequency shifts relative to a frequency standard, given in ppm, on the horizontal axis. The frequencies for these metabolites of interest are well described in the literature and allow for identification of these metabolites on the x-axis of the spectrum.^{31,32} The signal measured from the imaged tissue depends on a variety of factors, including magnet strength, voxel size, pulse sequence, echo times, number of

signal averages, and T1 and T2 relaxation times.³³ Due to these confounding factors, metabolite signal amplitude are normally calibrated against a reference signal of known metabolite concentration, generally via use of a phantom.^{33,48}

Types of MRS

Two distinct methodologies of performing spectroscopic examination exist: single-voxel and multi-voxel spectroscopy.^{22,33}

Single-voxel spectroscopy (SVS)

With single-voxel spectroscopy (SVS), a single sample obtained from a one-dimensional volume, with a typical measurement of approximately $\geq 1 \text{ cm}^3$, is placed over a region of interest (ROI). The spectral data are then obtained from that single-voxel using point resolved spectroscopy (PRESS) or stimulated echo acquisition mode (STEAM) acquisition modes.^{33,45} Single-voxel spectroscopy can generally be performed with faster scan times as compared to multi-voxel spectroscopy.⁴⁵ Additional advantages of SVS include minimal lipid contamination, improved magnetic field homogeneity, and improved water suppression.^{45,49} Placement of the voxel in single-voxel spectroscopy is crucial, as slight errors in voxel placement can lead to errors in interpretation of the spectral data, due to the inclusion of unintentional and undesirable regions of the brain, bone, gas filled sinuses or adipose tissue.⁴⁵ Of the two methodologies, SVS results in a spectrum with a lower signal-to-noise (SNR) ratio.²²

Multi-voxel spectroscopy (MVS)

In contrast, multi-voxel spectroscopy (MVS) uses chemical shift imaging (CSI) acquisition to acquire multi-dimensional spectra from multiple smaller voxels within the

same volume of tissue, which can be presented as individual spectra.^{33,45} Multi-voxel spectroscopy allows for the placement of smaller voxels within the tissue and can be used to acquire spectra from multiple locations.⁴⁹ Multi-voxel spectroscopy, however, typically requires longer acquisition time to perform when compared to single-voxel spectroscopy and, due to its use of CSI, is more susceptible to contamination from adjacent voxels, notably air, bone, and adipose tissue. The SNR, however, is generally higher for MVS.⁴⁵

Comparison of MVS and SVS

Despite the variation of the two methods, few studies exist comparing results garnered.^{22,50} No studies exist in the medical or veterinary fields that statistically compare the metabolite concentrations and or ratios generated from these two methodologies *in vivo* in the clinical setting.

Clinical use of MRS in people

Clinical and research applications of MR spectroscopy are well described in the medical literature. A large body of literature exists regarding specific metabolites and their concentrations with regard to the human brain and numerous disease processes afflicting central neuronal tissue.^{30,31,34,45,51-53} Clinical applications have been described for multiple other tissues such as the prostate and breast.^{30,45} In people, MRS has been shown to be clinically valuable in the characterization of various brain lesions, including neoplastic, infectious, inflammatory lesions, as well as traumatic brain injury.^{30,31,36,54-60} In contrast, the veterinary literature is limited to short descriptive pilot studies and limited clinical applications of MRS.^{37,38,49,50,61}

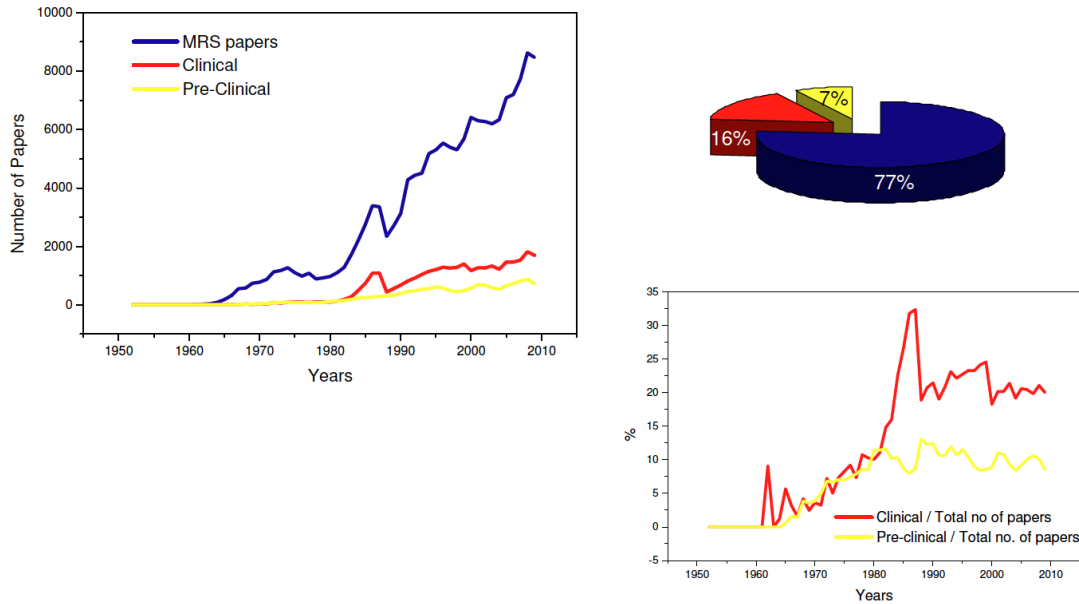


Figure 1.3 Proliferation of the number of publications regarding MR spectroscopy

Publications regarding MR spectroscopy (blue), and its clinical (red) applications and pre-clinical (yellow) applications. Notice the increase in total papers until the 1990s, and the relative plateau from 1990–2010. *Adapted from Rosario Lopez, University of Glasgow, The future of MRS, 2010.*

Over the past 3 decades, the popularity of spectroscopy increased and then plateaued. Limited reviews and the multiple factors that contributed to the rise and decline of the clinical utility of MRS's frequent uses are discussed below. Meta-analyses of MRS techniques and applicability, especially when combined with conventional MR imaging, have clinical value in aiding physicians in the task of differentiating various disease states in people. When using MRS for the diagnosis of prostatic cancer, in one meta-analysis of 31 reports, dating from 1998 to 2008, the sensitivity and specificity (when combined with conventional MR images) were high (on the order of 75–95%) and reported to be as high as 100% in some studies.⁶² A separate meta-analysis, which included 19 studies ranging from 1998 to January 2012, showed similar results when

using spectroscopy for distinguishing benign versus malignant breast nodules. When combined with MRI, the pooled sensitivity in this analysis was 73%, whereas the pooled specificity was 88%.⁶³ A meta-analysis of hepatic changes in people, which included 46 articles ranging from 1983 to 2009, found a sensitivity of 72.7%–88.5% when using MRS alone, which was similar to both ultrasound and CT and less than that of MRI alone. However, the specificity of MRS was 92.0%–95.7%, which was higher than that for ultrasound, CT, or MRI (for which the sensitivity was 82% and specificity was 89.9%).⁶⁴ A meta-analysis of brain disease, including 24 studies ranging from 1995–2013, found that MRS has a sensitivity of 80.05% and a specificity of 78.46% when imaging brain tumors in people.⁶⁵ It was also concluded that in general over the studies in the analysis, MRS performed better, with higher sensitivity and specificity, than conventional MRI for diagnosing brain tumors.⁶⁵ Finally, MRS has clinical value even in brain states which lack morphologic lesions on conventional MR imaging or macroscopic evidence of disease such as epilepsy and schizophrenia.⁶⁶ When looking at changes associated with schizophrenia in people, an analysis of 64 papers found that there was a perceptible decrease in NAA in various tissues in the brains of affected patients.⁶⁶ However, these same meta-analyses also found numerous discrepancies between reports. For instance, when imaging patients with prostate cancer, specificity was reported to be as low as 33%, while the sensitivity was reported to be as low as 14%.⁶² These conflicting reports are only a part of the reason why MRS is not currently widely used clinically.

The units in which MRS data are reported are arbitrary and proprietary based on the software used for acquisition.⁴ In principle, all spectra obtained by MRS can be used to derive absolute concentrations via the following equation:

$$[M] = [R] \frac{S_M}{S_R} C_{MR} \quad (2.3)$$

where $[M]$ is the metabolite concentration, $[R]$ is a calibration reference of known concentration, S_M is the detected signal from the metabolite, S_R is the detected signal from the known reference, and C_{MR} is a correction factor which accounts for differences in relaxation times for T1 and T2, diffusion, the gyromagnetic ratio, magnetic susceptibility, and generally any other differences between the reference compound and the metabolite.⁴ These factors can be different with different proprietary software packages. Understandably, the calculation of a reliable correction factor (C_{MR}) is challenging and can be time consuming.⁴ Instead, ratios of metabolites (for instance, NAA/Cr) are used when making comparisons across different systems.⁴ However, care must be taken when interpreting ratios, as changes in ratios may be due to one of many different factors.⁴ For instance, if Cho/Cr increases, it may be due to 1) an increase in the Cho concentration, 2) a decrease in the Cr concentration, 3) a change in both Cho and Cr, or 4) a change in relaxation parameters for either or both metabolites.⁴ Thus, patterns of recognition should be interpreted with conventional images, post gadolinium-based chelated agents (GBCA) enhancement patterns and the clinical presenting picture. Further, ratio changes do not indicate the degree of change in either metabolite if both metabolites are abnormal.

MRS is not currently widely clinically available. There are numerous reasons for this lack of availability. The aforementioned discrepancies between historical studies of MRS have called into question its value as a clinical tool, and the proprietary nature of the units makes it difficult to draw meaningful conclusions between systems.

Additionally, there are no accepted, standardized clinical techniques for performing MRS. For example, tumor evaluation comparing the periphery or center of the tumor can yield varying profiles such that even comparisons across the same tumor type may vary significantly, lending further credence to the notion that patients are best served by interpreting MRS in concert with the total clinical picture (Jennifer Gambino, personal communication, March 2, 2015). Partly as a result of these multiple factors, insurance companies do not cover spectroscopy as a clinical test. Partially as a result of this, there is reluctance to accept its clinical and the test is not generally available (Michael Garwood via Jennifer Gambino, personal communication, March 1, 2012). As a result of this unavailability, the majority of the data available concerning MRS is from clinical studies and research.⁴

Veterinary use of MRS

The available veterinary literature supports the feasibility of MRS as an imaging technique for the canine brain.^{37,38,49,50,61} Previous veterinary studies have reported metabolite concentrations in the brains of both healthy and diseased tissues in dogs using both SVS and MVS.^{37,49} Normal concentrations of N-acetyl aspartate, choline, creatine, myo-inositol, glutamine-glutamate complex, and glutathione in the basal ganglia, thalamus, parietal lobe, occipital lobe, and cerebellum in healthy dogs at 3T are described using SVS.⁴⁹ However, few studies exist reporting metabolite concentrations obtained via MVS in the normal canine brain.⁴⁹ Additionally, no data exists regarding MVS concentrations in the parietal lobe of the normal canine brain. MRS concentrations in additional tissues, including the prostate and abdominal organs, are not described.

Table 1.8 Mean metabolite ratios in normal dogs *in vivo* at 3 Tesla using single-voxel spectroscopy

Lobe of brain	NAA/Cr	Cho/Cr	Glx/Cr	mI/Cr	Glutathione/Cr
Basal ganglia	1.01	0.31	1.875	1.035	0.265
Thalamus	1.235	0.36	1.80	1.17	0.305
Parietal lobe	1.275	0.315	2.01	1.295	0.30
Occipital lobe	1.04	0.27	1.78	1.26	0.31
Cerebellum	0.98	0.29	1.78	1.53	0.32

Data from Carrera et al⁴⁹

In clinical veterinary use, at 3 Tesla, multi-voxel MR spectroscopy has the ability to distinguish between neoplastic and inflammatory processes in the canine brain.^{37,67} In a clinical, prospective population of 33 dogs with intracranial disease, MRS (specifically a the N-acetyl aspartate to choline ratio) was 82.7% accurate at differentiating neoplastic and inflammatory (meningoencephalitis of unknown etiology) intracranial disease processes.³⁷ In addition, MRS has the ability to distinguish normal dogs from those with spontaneous hepatic encephalopathy due to portosystemic shunting.³⁸ Relevant spectral changes in dogs with hepatic encephalopathy included diminished concentrations of glutamine and glutamate, myo-inositol, choline, and N-acetyl aspartate. Additionally, single-voxel MRS can distinguish between dogs with tick-borne encephalitis and normal

dogs.⁶⁷ Relevant changes in the affected dogs included mild decreases in NAA and Cr, and a mild increase Glx.⁶⁷ MR spectroscopy has also been performed in a Toggenburger goat with a cerebral abscess.⁴⁴ The spectral changes included increases in succinate, acetate, lipids, and amino acids, as well as a mild increase in lactate. Both Cho and NAA were decreased.⁴⁴ Despite not having normal values for this species, clinicians were able to distinguish this as an abscess based on the characteristic increase in succinate, acetate, and amino acids.⁴⁴ Normal MRS concentrations have been reported in non-human primate species, but not in any additional animal populations.

Additional *ex vivo* studies in animals also exist. An *ex vivo* study using MRS investigating the spectroscopic differences between normal, reactive, and metastatic lymph nodes found that the Cho SNR was significantly higher for metastatic lymph nodes compared to both reactive and normal nodes.⁶⁸ However, no differences were seen in the Cho SNR between reactive and normal lymph nodes.⁶⁸ Unfortunately, the veterinary radiology department at that institution no longer exists. This is a feature not unique to veterinary institutions across North America, given the unilateral migration of veterinary radiologists to the private sector. Although there is a growing body of literature describing metabolite concentrations and ratios in the normal dog (especially with multi-voxel spectroscopy), gaps in the veterinary literature remain and are subject to such dilemmas. Further, no studies in the literature exist comparing the clinical utility of SVS and MVS *in vivo* in companion animals. The paucity of literature becomes especially important in situations where time is of the essence (as all animal clinical patients are under general anesthesia when undergoing MRI) and, in some cases where magnet throughput for human patients takes precedence over that of companion animals.

The dog is a historically viable translational model for brain physiology and disease states. Concerning the research topics discussed herein, improvements in the body of knowledge of advanced MRI techniques (or ancillary techniques exclusive of conventional MR imaging) such as MRS; and evaluating GBCA use, administration and tissue deposition in the brains of healthy dogs, not only advances knowledge for the veterinary clinician, but provides a translational platform for expanding knowledge for medical practitioners.^{69,70}

CHAPTER II
COMPARISON OF SINGLE- AND MULTI-VOXEL SPECTROSCOPY IN THE
NORMAL CANINE BRAIN AT 3 TESLA

Study purpose

The purpose of this portion of the study is to prospectively evaluate the validity of raw data single-voxel MRS compared to post-processed multi-voxel MRS in the normal canine brain at 3 Tesla in the parietal lobe, thalamus, and piriform lobe, to determine if metabolite concentrations and ratios obtained by these two methodologies are statistically different, and to describe for the first time the normal multi-voxel metabolite concentrations and compare the ratios and quality of data obtained by both techniques for each of the described brain lobes.

An additional purpose of this study was to add to the available veterinary literature regarding metabolite concentrations in the brains of normal dogs using both SVS and MVS. Specifically, MVS metabolite concentrations have not previously been reported in the piriform lobe in dogs. Additionally, no studies exist comparing *in vivo* SVS and MVS results in the veterinary population. One aim of this study was to provide this comparison. SVS is easier, and in most cases faster, to perform when compared to MVS. At some institutions, as is the case at the author's institution, limited time for use of the magnet may influence the ability to perform MVS. In addition, post-processing

software availability, upgrade costs, and the complexity of use even of freeware, may also limit the clinical utility of MRS at some institutions.

Hypothesis

The author and cohorts hypothesized that although performed using different acquisition techniques, single- and multi-voxel spectroscopy would yield comparable spectra and metabolite ratios, with a lack of a statistically significant difference between the two methodologies.

Methods and materials

Design and execution of *in vivo* portions of this study and subsequent surgical laboratories, were subject to institutional review board oversight (Institutional Animal Care Use Committee protocol numbers 15012, 12065, and 15075). Financial support was provided by Dr. Gambino through the Department of Clinical Sciences and by the American College of Veterinary Radiology. In addition, Dr. Gambino provided direction and had oversight over all aspects of the current study concept, design, drafting, revision, final approval and had full control of the acquisition, analysis, and interpretation of all data.

Study population

This prospective, pilot, study population consisted of 8 healthy juvenile purpose-bred hound dogs. Ages ranged from 5 to 13 months (mean=8.6 months, IQR=5 months). Two dogs were intact males, five were intact females, and one was a spayed female. Weights ranged from 17.3–24.8kg (mean=23.76 kg, IQR=8.65). Dogs were deemed normal based on physical and neurophysical examination performed by a first year

radiology resident, laboratory animal veterinarian, and a board-certified neurologist. Complete blood count, serum biochemistry, serum occult heartworm, and serum titers for *Ehrlichia canis*, *Rickettsia rickettsii*, *Borellia burgdorferi*, and *Babesia canis* (ProtaTek Reference Laboratory, Mesa AZ) were performed. All study subjects underwent CT scout scanning with a 64 detector helical CT (Lightspeed VCT 64-slice, GE Healthcare, Milwaukee, WI) scanner as a whole body metal (implanted or ingested) screening prior to MRI of the brain. Following MRI examination in all dogs, all subjects underwent cerebrospinal fluid aspiration and analysis for cytology and West Nile virus titer testing (Diagnostic Center for Population and Animal Health, Lansing MI). Further exclusion criteria for subject selection were not applied.

Technical information: conventional MRI imaging

A daily quality assurance for functional magnetic resonance imaging (fMRI) was performed the morning prior to all MRI and MRS scanning, consisting of a base echo planar imaging (EPI) sequence on a phantom. In addition, a week or less prior to all scans, an American College of Radiology (ACR) phantom scan was performed, the results from which are evaluated yearly by a licensed medical physicist. Additionally, a week prior to all MRS scans, calibration was performed for the spectroscopy using a probe-P phantom (MI385AM, IC6 Medical Advances).

All dogs were sedated with acepromazine (0.01 mg/kg, PromAce, Fort Dodge Animal Health, Overland Park, KS) and hydromorphone (0.1 mg/kg, Dilaudid, West-Ward, Eatontown, NJ) intramuscularly. Animals were induced with propofol (2.3 mg/kg, PropoFlo, Abbot Animal Health, Abbott Park, IL) and were maintained on an admixture of isoflurane (Attane, Piramal Healthcare, Bethlehem, PA) inhalant anesthesia and

oxygen according to a standard clinical protocol and under supervision of the institutional anesthesia service. Conventional morphologic MR was performed with a 3T magnet (Signa 3T Excite, General Electric Healthcare, Milwaukee, WI). All animals were scanned in sternal recumbency with a quadrature knee coil (M1385AM, IGC [Intermagnetics General Corporation], Latham, NY). A typical clinical conventional MR imaging protocol was performed in multiple image planes to include: sagittal T1-weighted (T1-W) fluid-attenuating inversion recovery (FLAIR); dorsal T2-weighted (T2-W); sagittal and transverse T1-W fast spoiled gradient echo (FSPGR); transverse T2-W FLAIR, T2* fast gradient echo (FGRE), transverse diffusion tensor (DTI); transverse diffusion weighted imaging with apparent diffusion coefficient mapping (DWI, ADC); transverse time of flight (TOF) imaging; and a 3-D reconstructable, transverse T1-W FSPGR series following the intravenous administration of a gadolinium chelated contrast agent, gadodiamide (Omniscan, 0.5 mmol/mL, General Electric Healthcare, Milwaukee, WI). As part of a separate study, dogs were administered variable, fractional doses of the contrast agent as follows: 0.1 mmol/kg (n=2), 0.05 mmol/kg (n=2), 0.025 mmol/kg (n=1), 0.0125 mmol/kg (n=1), and 0.006 mmol/kg (n=1), via the right cephalic vein. Following intravenous contrast administration, intravenous fluids (0.9% sodium chloride, Baxter Healthcare, Deerfield IL), at a standard anesthetic flow rate dose of 5 mL/kg/hr, were administered. Morphologic images were reviewed by a board-certified radiologist and a second year imaging resident. Animals were included only if morphologic MR brain images were normal.

MR spectroscopy

Calibration for the single-voxel spectroscopy was performed using a Probe-P phantom with known concentrations of metabolites to ensure accuracy of the spectra.

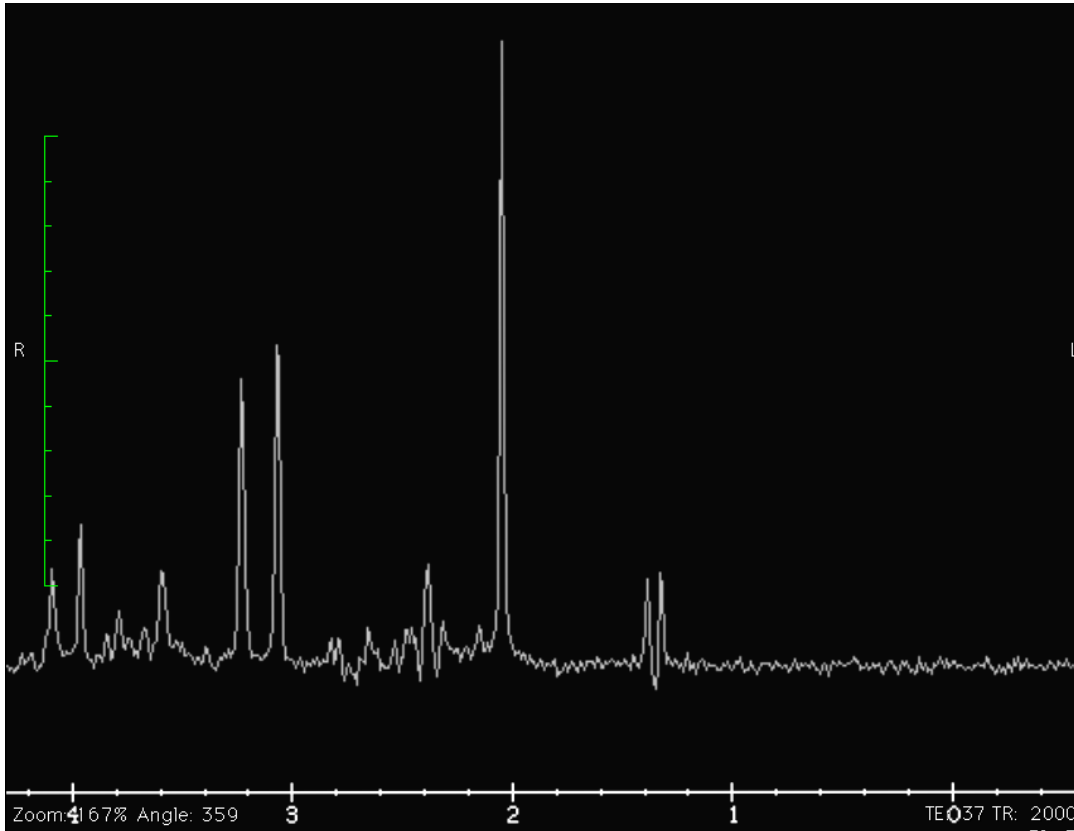


Figure 2.1 MR Spectroscopy calibration obtained via a Probe-P phantom

Spectrum obtained from a Probe-P phantom demonstrating proper calibration for 3T MRI prior to spectroscopic imaging. This calibration was performed weekly prior to all spectroscopic imaging in the study.

Following the acquisition of conventional morphologic brain MR images, single- and multi-voxel spectroscopy was performed on all dogs in one of each of the following brain regions: parietal lobe (n=3), thalamus (n=2), and piriform lobe (n=3).

Prior to spectroscopic imaging, third order shimming was performed to correct for any inhomogeneity in the magnetic field. Water suppression was additionally performed in order to acquire spectra for the required metabolites. Full width at half maximum (FWHM) smoothing was performed as a measurement of the width of the signal and to improve magnet homogeneity and optimize the signal-to-noise (SNR) ratio for the spectra. Maximum FWHM value for the spectroscopic study was 8 Hz. Animals were included only if the FWHM value was less than 12 MHz.

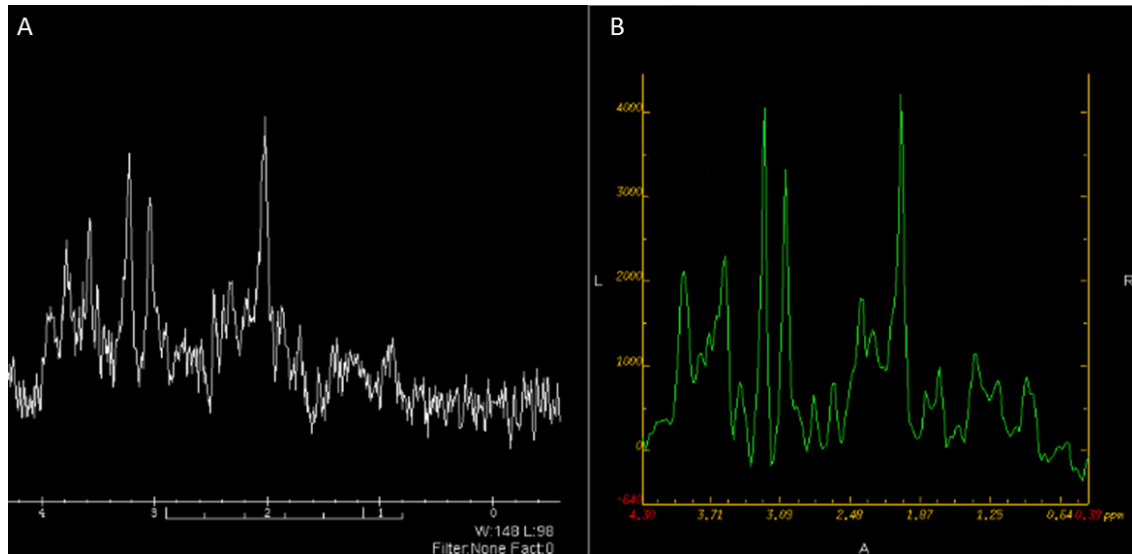


Figure 2.2 Single-voxel and multi-voxel magnetic resonance spectral examples

Spectra from the thalamus of a neurologically normal dog with normal brain morphology. Spectrum from each of the two described. A– Resultant single-voxel acquisition from the right hemisphere and B– Resultant multi-voxel acquisition.

For consistency for single-voxel acquisition, a single rectangular ROI was placed in the left hemisphere at the following locations: parietal lobe (3 dogs), thalamus (2 dogs), and piriform lobe (2 dogs), using the transverse T2-W images for localization. The dimensions of this voxel were recorded and an identical voxel was created and used for

the multi-voxel spectroscopy on the same lobe in the contralateral (right) hemisphere (Figure 2.3). All voxels were placed by a licensed MRI technologist under the supervision of a board-certified radiologist, board-certified neurologist, and/or second year radiology resident once protocol was established.

For multi-voxel acquisition, the transverse T2-W images were again used for localization purposes. A voxel ROI with identical dimensions to the ROI used for single-voxel acquisition was placed in the right hemisphere in the same region of the brain as the SVS acquisitions: parietal lobe (3 dogs), thalamus (2 dogs), and piriform lobe (3 dogs). Following removal of the animal from the magnet, post-processing of two smaller ROIs from the larger, rectangular MVS acquisition were performed. Briefly, a smaller, 5 mm square voxel ROI and a 5 mm diameter circular ROI within this original larger MVS ROI were interrogated (Figure 2.3).

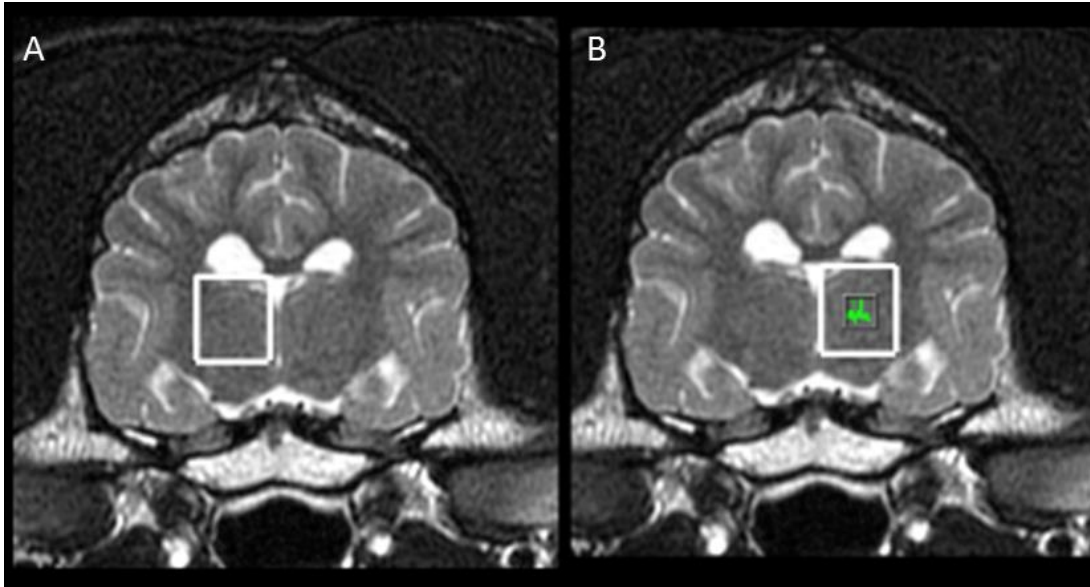


Figure 2.3 Single-voxel and multi-voxel spectroscopic region of interest (voxel localization)

A– Single-voxel and B– multi-voxel spectroscopic voxel placements within the thalamus of a morphologically normal canine brain. In B, notice the smaller green spectrum within the larger localization, giving a read out for that specific localization such that multiple regions within a given interrogation can be evaluated.

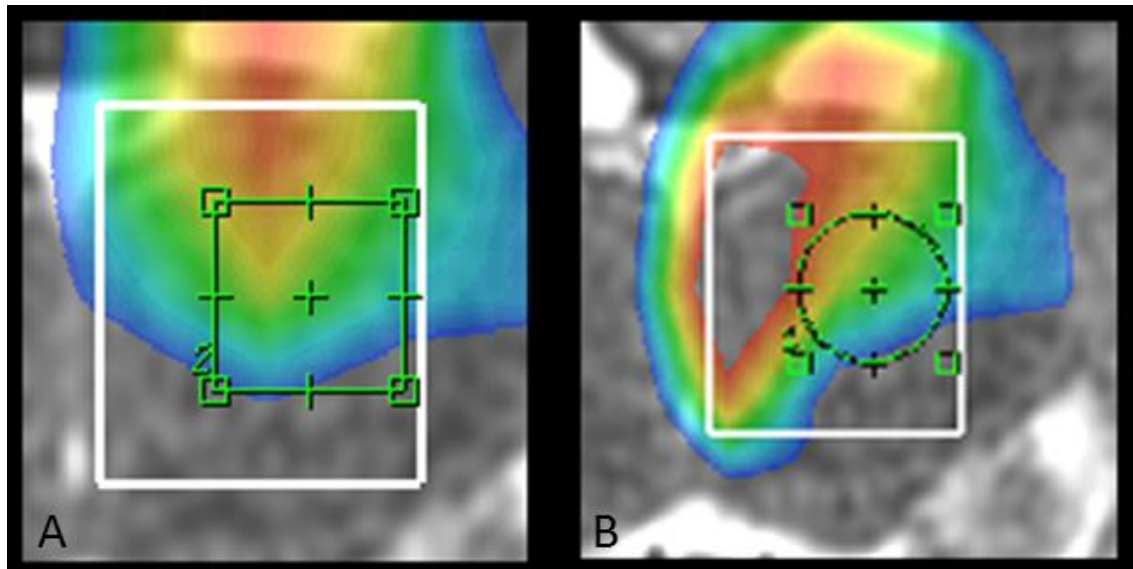


Figure 2.4 Post-processed multi-voxel regions of interest

Post-processed multi-voxel regions of interest created from the same multi-voxel spectroscopic voxel in Figure 2.3. A– Small square, and B– small circular region of interest. Each has a width (or with a diameter) of 5 mm respectively. These smaller regions were created following removal of the subject from the magnet bore at the console for comparison to the two original larger voxels and the single-voxel spectral acquisition from a region of interest placed in the same region within the contralateral hemisphere.

Details of post-contrast single- and multi-voxel acquisition parameters are given below in Table 2.1.

Table 2.1 MR spectroscopy acquisition parameters for single-voxel and multi-voxel studies

Parameter	Single-voxel	Multi-voxel
TR (ms)	1500	1500
TE (ms)	30	30
NEX	16	4
Flip angle	90°	90°
Echo train	1	1
Echo number	1	1
Spectroscopic matrix	1x1	18x18

Cerebrospinal fluid analysis

Following conventional morphologic and spectroscopic imaging, all dogs underwent cisternal cerebrospinal fluid centesis by a board-certified veterinary neurologist (MB) during the immediate imaging recovery phase. All dogs then received subcutaneous carprofen (4 mg/kg, Rimadyl, Zoetis, Florham Park, NJ) and were recovered from anesthesia uneventfully. Only dogs meeting the criteria of cerebrospinal fluid (CSF) analysis results within normal reference ranges, with no evidence of xanthochromia, infectious organisms or abnormal cellular concentrations, and negative CSF titers for West Nile Virus were included.

Histopathology

Following imaging and recovery, all dogs were surrendered to an unrelated non-imaging terminal surgical laboratory. Upon completion of that study, animals were euthanized. The brains of each of the subjects were harvested no more than four hours following euthanasia. Brains were stored in formalin and fixed neurologic tissue from each of the evaluated lobes was submitted for histopathologic evaluation to confirm the normal status of the tissue. All dogs met the inclusion criteria of having normal gross and histopathologic brain evaluation by a board-certified pathologist in the frontal, parietal, and piriform lobes, thalamus, cerebellum, brainstem, motor cortex, and hippocampus.

Data analysis and post-processing

SVS spectra resulted in data processed in MACH values (arbitrary machine units) according to the inherent post-processing algorithm for NAA, Cho, Cr, MI, and H₂O. Additionally, MACH values for each individual ppm along the horizontal axis of the spectra were obtained. MVS spectra were evaluated in both relative (to water) and absolute concentrations according to the inherent post-processing algorithm (Func Tool, FuncTool Performance, General Electric Healthcare, Milwaukee, WI) for NAA, Cho, Cr, mI, Lip, Lac, Ala, and Tau. Concentrations were evaluated for all methods of MVS acquisition (large SVS-like rectangular ROI, smaller square within lobe of interest and circular ROI).

Prior to metabolite evaluation, baseline water and lipid correction post-processing were applied to the MVS data sets. Metabolite peaks for NAA, Cr, Cho, and mI were obtained from via automated processing with FuncTool. NAA, Cr, Cho, mI, Lac, Lip, and Tau peaks were obtained for all three regions of interest utilized during multi-voxel

spectroscopy. Absolute values, as well as relative values, for these peaks were archived for the multi-voxel spectroscopy technique.

Statistics

All statistical analyses were performed by an epidemiologist/statistician. A mixed model analysis was conducted using PROC MIXED in SAS for Windows v9.4 (SAS Institutes Inc., Cary, NC). For each metabolite measured, a model was fit with fixed effects of lobe imaged and technique used (SVS vs MVS). Dog identity was included as a random effect with a compound symmetry covariance structure. Differences in least squares means (lsmeans) with Tukey-Kramer adjustment for multiple comparisons were determined for outcomes with a significance fixed effect. An alpha level of 0.05 was used to determine statistical significance for all methods. All data were normally distributed.

Mean metabolite values were obtained for both single-voxel and post-processed multi-voxel techniques in all three imaged regions of the brain (Tables 2.4 and 2.5). Ratios for each of the methodologies (single- and multi-voxel) were compared (Table 2.6). The following ratios were compared: Cho/Cr, Cho/NAA, NAA/Cho, NAA/Cr, Cr/Cho, and mI/Cr. Calculation of ratios was performed to compare the peaks of the spectra from both single- and multi-voxel techniques without needing to convert the MACH numbers of the single-voxel spectroscopy to the relative or absolute part per million results of the multi-voxel spectroscopy.

Results

Conventional and advanced MRI examinations were successfully performed in all dogs and deemed normal by a board-certified veterinary radiologist, 2nd year imaging

resident and board-certified veterinary neurologist. Advanced protocols demonstrated normal brain diffusion and perfusion. A total of 6/8 dogs had successful spectroscopy performed bihemispherically and these spectra were deemed normal based on historically available comparisons in the available canine literature.^{49,50} All images were of excellent diagnostic quality and none were excluded from the image scoring. No complications were observed in any dog secondary to the phlebotomy, gadolinium chelated contrast administration, MRI examinations or cisternal cerebrospinal fluid centesis. All hepatorenal values were normal in all dogs, as given in Table 2.3. Infectious disease titers for *Ehrlichia canis*, *Rickettsia rickettsii*, *Borellia burgdorferi*, and *Babesia canis* were negative, all dogs tested heartworm negative, and CSF analyses and cytology results were unremarkable (protein quantification <30 mg/dL with nucleated < 5 cells/uL) in all animals. All animals recovered uneventfully from anesthesia.

Table 2.2 Hepatobiliary and renal serum biochemistry values for all dogs.

Subject number	Alk Phos U/L (reference range 11–140 U/L)	ALT U/L (reference range 10–90 U/L)	T Bili mg/dl (reference range 0.2–0.6 mg/dL)	BUN mg/dl (reference range 8–24 mg/dL)	Creat mg/dl (reference range 0.5–1.4 mg/dL)
1	120	12	0.6	9	0.6
2	130	10	0.3	8	0.8
3	138	13	0.2	8	0.6
6	135	16	0.3	12	0.81
4	86	28	0.4	9	0.87
7	73	36	0.3	10	0.78
5	92	27	0.3	10	0.14
8	90	34	0.2	8	0.76

All dogs had normal hepatobiliary and renal values.

Metabolite concentrations

Two spectra were excluded from the study. The parietal voxel in dog 1 was excluded due to suboptimal voxel ROI placement. The piriform voxel ROI placement in dog 6 was also excluded, as the voxel was too small, and the resultant spectral data were non-diagnostic due to a high signal-to-noise ratio. In the remaining 6 dogs, diagnostic, quality spectra were obtained in the thalamus (n=2), parietal lobe (n=2), and piriform lobe (n=2).

Table 2.3 Mean brain metabolite concentrations, given in machine (MACH) units, acquired using single-voxel spectroscopy in the thalamus, parietal lobe, and piriform lobe of six dogs

Metabolite	Thalamus (n=2)	Parietal lobe (n=2)	Piriform lobe (n=2)
NAA	21	25.5	20
Cr	14.5	17.5	14
Cho	18.5	18	16.5
mI	11	13	13
H ₂ O	22383.5	27353	21890

Table 2.4 Mean brain metabolite concentrations, given in absolute ppm units, acquired using multi-voxel spectroscopy in the thalamus, parietal lobe, and piriform lobe of six dogs.

Metabolite	Thalamus (n=2)	Parietal lobe (n=2)	Piriform lobe (n=2)
NAA	2175	2227.167	1780
Cr	1404	1396.5	918.167
Cho	1624	1440	1499.167
mI	1091	1389.833	1465.333
Ala	8.3	96.4	43.133
Lac	459	340.667	506.222
Lip	508	345	575.167
Glx	1014.9	1264.34	813.306
Tau	458.147	517.235	186.709

Single-voxel spectroscopy was compared for the three sampled lobes of the brain for the following metabolites: NAA, Cho, Cr, and mI. Water was also included in this analysis. The large, SVS-like rectangle, small square, and small circle post-processed MVS voxels were compared for the following metabolites: NAA, Cho, Cr, mI, Lac, Lip, Glx, Ala, and Tau. Metabolite ratios were compared for SVS and the three post-processed MVS voxels. The specific ratios compared were: Cho/Cr, Cho/NAA, NAA/Cho, NAA/Cr, Cr/Cho, and mI/Cr.

Table 2.5 Metabolite ratios given for both single-voxel and multi-voxel spectroscopy performed in the thalamic, parietal, and piriform lobes of the brains of six dogs.

Ratio	Thalamus (n=2)		Parietal lobe (n=2)		Piriform lobe (n=2)	
	SVS	MVS	SVS	MVS	SVS	MVS
Cho/Cr	1.27	1.16	1.03	1.01	1.21	1.62
Cho/NAA	0.88	0.75	0.71	0.63	0.83	0.85
NAA/Cho	1.14	1.34	1.41	1.63	1.22	1.19
NAA/Cr	1.45	1.55	1.46	1.62	1.45	1.92
Cr/NAA	0.69	0.65	0.69	0.62	0.70	0.53
mI/Cr	0.75	0.76	0.74	0.98	0.95	1.58

Comparison of SVS and MVS

In line with the proposed hypothesis, statistically significant differences were not seen between SVS and the identically sized (large rectangular) MVS acquisitions for any given lobe. In addition, when comparing the MVS acquisitions, no statistically significant differences were found between the larger rectangular MVS acquisitions and either the small circle or the small square MVS ROIs.

For Cr/NAA, statistically significant differences were seen between the (large) SVS ROI, and the smaller, post-processed MVS ROIs (the small square and SVS ($p=0.0442$); and the small MVS post-processed circle and SVS ($p=0.0223$). Finally, for NAA/Cr, a statistically significant difference was seen between the SVS and the smaller, post-processed MVS circle ($p=0.0456$).

Irrespective of technique, no significant differences in regional concentrations were seen between the thalamus and parietal lobe for any metabolite or ratio. Statistically significant differences were, however, seen for Cho/Cr between the piriform and the parietal lobes ($p=0.002$) and between the piriform lobe and the thalamus ($p=0.0067$). For mI/Cr, statistically significant difference was also seen between the piriform the parietal lobes ($p=0.0281$) and between the piriform lobe and the thalamus ($p=0.0047$).

Discussion

Both single- and multi-voxel spectroscopy were successfully performed in 6/8 dogs in this study, with no adverse effects from the spectroscopic procedures, contrast administration, or CSF centesis observed. In addition, metabolite concentrations were successfully obtained for both SVS (MACH units) and MVS (parts per million) in all three interrogated regions of the brain (Tables 2.4 and 2.5). There are a few reports that describe normal regional SVS and MVS concentrations in dogs; however, this study is the first to compare SVS and MVS ratios in a normal, juvenile dog population. Collectively, the results of the current study provide clinicians with the regional concentrations of metabolites for the sections investigated for which the previous literature is sparse or non-existent. An objective baseline quantification of the metabolite reference values in the normal juvenile canine brain (for the thalamus, parietal lobe, and piriform lobes), included herein provides veterinarians interpreting MR brain spectra a measurable parameter allowing for future comparison to various disease states.

Differences between SVS and MVS

No significant differences were detected between the bihemispheric metabolite ratios obtained by way of the two different spectroscopic methodologies (SVS versus MVS) when using identically sized and shaped, rectangular ROIs. In addition, no significant difference was seen between the smaller ROIs (both the rectangular and circular), and the large rectangular MVS ROI. However, differences were seen for some ratios obtained by way of SVS when compared to the smaller (rectangular and the circular) MVS ROIs. These differences were attributed to signal volume averaging across the entire SVS ROI, which can be dramatic in SVS acquisition data sets, versus more manipulable for a given MVS ROI. Signals furthest from the center of the given SVS ROI contribute to decreased SNR and a greater amount of signal degradation.³³ This finding is due to an averaging of the signal coming from the periphery of the ROI, where the signal to noise ratio is lower.³³ Thus, in general (for both techniques), the larger a given ROI, the greater the degree of contamination of the final, resultant spectrum by degraded signals coming from the periphery of the ROI. This peripheral signal degradation and sample averaging are the likely reasons that comparing the SVS acquisition to the smaller MVS acquisitions, which were obtained from a central region within the large (rectangular, SVS-like) MVS acquisition, resulted in significantly different values for a limited number of ratios and metabolites. The raw SVS data set was a large volume that included the peripheral signal degradation, whereas the smaller MVS acquisitions excluded the areas of poor signal and only included the strongest contributing signals in addition to eddy current and lipid and water baseline correction post-processing. In addition, smaller voxels are more easily placed in the tissue of

interest, minimizing contamination from other regions of the brain. This may prove to be especially important in clinical patients, where lesions may be smaller than the initial large volume, and only those voxels over the lesion would need to be selected for the post-processing. It is possible and likely that, had we post-processed our single-voxel data, and diminished the effect of the averaged peripheral signal, using MRS post-processing software (for example, LCModel^a), we likely would have not seen any significant difference between these ratios. However, we decided to compare raw-data SVS to post-processed MVS as this would mimic the clinical situation at our institution. Despite the availability of MRS freeware (such as Tarquin^b, SIVIC^c, and jMURI^d), the author decided to test the current limitations of the scanner that does not include the software package to allow for post-processing of the SVS data set. Regardless, results from the study indicate that, when the same volume of tissue interrogated (same in size and shape), from the same region of brain, there is no statistically significant difference between raw data SVS and post-processed MVS methodologies. Although the removal of eddy current and lipid contamination is desirable for obtaining a “perfect” spectra from an ROI, it may not offer a perceptible clinical difference, and it is this point that is contrary to previous literature that claims that SVS was not as clinically useful as MVS.⁵⁰ Although there is no argument that MVS is a more robust test, results of the current study support the use of raw data SVS and ratios as a clinically relevant test for institutions that have similar software limitations. When using the same volume ROI, the results between SVS and MVS are not statistically different. This point brings into question the risks and benefits of choosing SVS (a shorter, albeit less perfect) acquisition protocol over MVS in the clinical setting when time is of the essence (especially true in veterinary MR imaging,

given that patients are anesthetized for the duration of the scan). In addition, results from this study support the notion that data (specifically ratios) garnered from different institutions using different spectroscopic methodologies and proprietary software, can be compared and/or compiled for future work and disease metabolite profile banking, allowing for a greater number of spectroscopic collaborations given the need for larger cohort studies in clinical patients with brain disease states.

Concerning the regional concentrations and the difference noted, irrespective of technique, differences were detected between the piriform and parietal lobes and the piriform lobe and the thalamus for Cho/Cr. A statistically significant difference was also seen between the piriform and parietal lobes, and between the piriform lobe and the thalamus for mI/Cr. This difference between lobes is similar to prior studies for both humans and dogs, which reported differences in metabolite concentrations in various lobes of the brain.^{49,71} A previous canine study reported differences in NAA, Cho, Cr, and mI for the following regions: basal ganglia, thalamus, parietal lobe, occipital lobe, and cerebellum.⁴⁹ In addition, we did not find a difference between the parietal lobe and the thalamus, which is in contrast to a prior study in dogs.⁴⁹ There are several possible reasons for this discrepancy. The placement of our voxels in these regions may have been slightly different than previous reports due to a human estimating the relative ROI and due to differences in the exact size of the ROI placed upon these regions, which is a well described caveat to voxel placement for spectroscopic evaluation in that repeatability is often difficult with regard to precision. Furthermore, although unlikely, we cannot definitively rule out that none of the samples in our, or in previously reported studies were completely free of lipid contaminant. The difference may also be attributable to the

low numbers of dogs and comparative voxel placements for each of the regions interrogated in our study.

Comparison to prior studies

There is an abundance of research and clinical spectroscopic data in people that has, over the past three decades, enhanced the sensitivity and specificity of conventional brain imaging.²⁵⁻²⁸ As previously stated, MR sensitivity in the brain is reported at 95%–99%, while the specificity is reported to be 70%–76%.^{25,29,72} The lower specificity is due to signal overlap in MR imaging characteristics and lesion morphology between various disease etiologies in the canine brain.²⁶ When spectroscopy is added to conventional MR imaging, the sensitivity is reported to be 80%–100%, however, the specificity increases to 78%–100%.^{30,31} Better pattern recognition, due to a higher number of published cases, is postulated to be the reason for the increasing specificity in later studies.³⁰

Many of the studies described employ the use of an identical ROI within the presumed normal, contralateral, hemisphere for comparison.⁴⁹ Previous studies in both people and dogs demonstrated only few statistically significant differences between hemispheres for the same regions of the brain, including the basal ganglia, thalamus, parietal lobe, occipital lobe, and cerebellum.^{49,73-75} Specifically, in dogs, mI/Cr differed between hemispheres in the parietal lobe in dogs.⁴⁹ Additionally, a small but significant difference between the two hemispheres for the thalamus is described.^{49,76,77} By and large, there were no significant regional differences in this study, within the limited metabolic profile evaluation, with the only significant differences seen being the Cho/Cr between the piriform and the parietal lobes ($p=0.002$) and between the piriform lobe and

the thalamus ($p=0.0067$) and for mI/Cr between the piriform the parietal lobes ($p=0.0281$) and between the piriform lobe and the thalamus ($p=0.0047$).

At the author's institution, when pathologic brain changes are unique to one hemisphere, an ROI in the contralateral hemisphere at the same location is placed for internal comparison, allowing the patient to serve as its own control. This is an ideal practice, given variations of normal affected by age and brain region.^{35,51,78} The author chose to perform SVS on one hemisphere and MVS on the other hemisphere because it reflected what is routinely done in the clinical setting at the author's institution. Given the findings of this and previous studies, it is highly unlikely that there is any significant difference between the two hemispheres for any lobe.^{49,76,77} However, slight differences between the lobes may exist, which would confound comparison of spectral data obtained by way of different protocol methods (namely, SVS and MVS).

The dogs in this study were juvenile, with a mean age of 8.6 months. The results of this study are similar to results in human pediatric and juvenile patients, where pertinent findings include low/normal NAA (due to developing neurons and axons), low/normal Cr, which is believed to be due to glial changes, and relatively normal mI, Cho, and GLX concentrations, as compared to the adult values.³⁵

Additional experimental considerations

There were a few limitations to the current study. The animals used in this study were all juvenile, with a mean age of 8.6 months. The juvenile status of the study population may therefore not be the ideal dataset for which to compare datasets obtained from geriatric patients. Although the MR evaluation of the maturation of grey and white matter have been reported to reach adult appearance by 16 weeks of age in dogs,

spectroscopic differences are reported for metabolite concentrations and ratios throughout maturation in people; and when comparing between juvenile, adult, and geriatric patients (in people and dogs).^{76,77,79-81} In dogs, increases in Cho/Cr are noted in young dogs compared to adult and geriatric dogs, with the proposed mechanism being increased myelination in younger animals.⁸⁰ In addition, NAA to choline is reportedly significantly lower in young and geriatric dogs compared to adults.⁸⁰ All animals in our study were of a similar age. It is likely that the shift from the juvenile to adult spectroscopic concentrations and ratios occurs at varying ages in dogs and over a period of time, though likely not entirely analogous to people given the differences in life span. Due to the narrow age range of the canine subjects evaluated in the current study, it is unlikely that there would be large enough differences between the animals to significantly affect the metabolite concentrations and ratios. Furthermore, comparisons made between ROIs of the SVS and MVS acquisitions were performed in different hemispheres of the same animal. However, small differences could feasibly affect results. Finally, interspecies differences (given the wide variety of existing veterinary patient species) are likely to be encountered such that the dataset presented herein is not intended to be viable for comparison across species. Further investigation is needed to determine metabolite concentrations and ratios in a range of ages in dogs and cats.

Different doses of gadolinium contrast agent were administered to these dogs during the MRI examination as part of a separate study (refer to Chapter IV). The effect of gadolinium contrast agents and their effect on the resulting spectra have been investigated. No statistically noted differences for NAA/Cr, Cho/Cr, and NAA/Cho are noted in patients with intra-axial brain tumors before and after administration of a

gadolinium contrast agent.⁸² It is a generally well accepted principle that these agents do not affect the baseline concentrations of brain metabolite composition.^{82,83}

The current study population included both male and female dogs. Historically, gender has no significant effect on baseline brain metabolite concentrations.^{49,76,77,81} The authors consider the heterogeneous population adventitious and representative providing data for both sexes

Limitations

There are several limitations to the study. The most significant limitations are the low number of study subjects and limited age group evaluated. However, when compared to the limited available literature there was good correlation with metabolite ratios suggesting sound methodology. A larger cohort of dogs will be required to confirm these preliminary/pilot results. Although voxel size was maintained for each lobe of the brain, placement of the voxels was subject to both human error and slight variations in the anatomy of the dogs imaged. Additionally, this study used a specific age and breed of dog. A larger study, incorporating a larger variation in age, breed, and size of dog, may show differences that were not detected in the current study.

Conclusion

In conclusion, both SVS and MVS were successfully performed on this pilot study cohort of 6/8 dogs in the thalamus, the piriform lobe, and the parietal lobe. The two exclusions were due primarily to inconsistencies of exact voxel placement and human error, an issue not specifically unique to the authors of the current study. This issue has previously been discussed as a limitation when following brain lesions in the same

patient over time and is, to date, an unavoidable problem. One spectra was excluded due to poor placement of the voxel, and one spectra was excluded due to small voxel size, leading to a low signal-to-noise ratio. There was no statistically significant difference seen between SVS and large rectangular MVS, although for NAA/Cr and Cr/NAA, a difference was found between the SVS spectra and the smaller round and square ROI MVS, again likely due to a number of factors such as signal strength at the center of the MVS ROI being superior to that of the SVS ROI whose signal is contaminated by that of the periphery. Differences were seen between the piriform lobe and thalamus and piriform and parietal lobes for select metabolite ratios. Additional studies, with larger numbers of dogs, are needed for further exploration and comparison of metabolite ratios and concentrations in different ages groups of the dog and in other species, such as the cat, in which MR is routinely performed for clinical and research applications for which greater diagnostic and baseline MR specificity and sensitivity are warranted.

Footnotes:

a: LCModel, <http://s-provencher.com/lcmodel.shtml>

b: Tarquin v 4.3.10, <http://tarquin.sourceforge.net/>

c: SIVIC, <https://sourceforge.net/projects/sivic/>

d: jMURI, v 6.0, <http://www.jmrui.eu/>

CHAPTER III
INTRODUCTION TO MAGNETIC RESONANCE CONTRAST AGENTS

Contrast-enhanced MRI

Gadolinium

History

With respect to the use of MR contrast agents in MR imaging, chemists have focused their attention fairly uniformly on one element: gadolinium. Gadolinium was first discovered in 1880 by a Swiss chemist names Jean-Charles Galissard de Marginac via mass spectroscopy.⁸⁴ It was isolated in 1886 by the French chemist Paul-Emile Lecoq de Boisbaudran, who then named it after the Finnish chemist Johann Gadolin.⁸⁴

Physical properties

Gadolinium is a rare earth, lanthanide series element, with an atomic number (Z) of 64. It is present at 5 ppm (approximately 6.2 mg/kg), or 100 times the concentration of iodine, in the earth's crust.⁸⁴ It is malleable and forms close-packed crystals at room temperature.⁸⁵ At room temperature, gadolinium is paramagnetic but becomes more ferromagnetic than iron when cooled to temperatures lower than 25 °C.⁸⁴ The metal is too reactive to exist naturally, and it adopts the oxidation state +3. The most common halide encountered is gadolinium (III) chloride, and the oxides can be dissolved in acid to obtain the separate salts.⁸⁵ Gadolinium features seven unpaired electrons in its positively charged ionic form (Gd^{+3}), which is more than any other element.^{86,87} This molecular

conformation results in large paramagnetic susceptibility.^{86,88} Approximately 400 tons of pure gadolinium are produced each year, and mines exist in the United States, China, Brazil, Sri Lanka, India, and Australia, the majority being for medical use.⁸⁵

The gadolinium ion, which is a metallic salt, was favored as the active center for first generation commercial contrast complexes, given multiple favorable physiochemical properties. These properties include seven unpaired electrons (distributed isotropically in its 4f shell), which offer an electrically charged magnetic center that exhibits the strongest effect of all the known elements on T1 relaxation time, its long electronic relaxation time, and its nine coordination sites.^{86,87} Gadolinium results in the largest T1 relaxation time of any known element, making it ideal as an MR contrast agent.⁸⁶

Environmental contamination

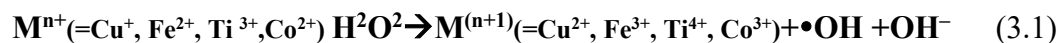
In 1996, the first report of gadolinium anomalies in surface waters was generated.^{89,90} High concentrations of gadolinium were eventually discovered in several rivers, lakes, and the North Sea.⁸⁹ Comparison of the concentration of gadolinium with other rare earth metals in these waterways showed that gadolinium was the only elevated rare earth metal. This finding confirmed that the increase in gadolinium was anthropogenic and due to increased use of gadolinium-based MR contrast agents.^{89,90}

Toxicity

All transition metals exhibit intolerable toxicity.³ Despite favorable properties and its efficiency as a paramagnetic substance, the Gd^{+3} aqueous ion is not unique and is highly toxic to the body.⁸⁷ It forms acid solutions in water and insoluble hydroxides or phosphates in solutions of neutral pH, which accumulate rapidly within the

reticuloendothelial system (RES) following intravenous (IV) administration via phagocytosis by the Kupffer cells in the liver.^{86,87} Gadolinium is not as toxic as other heavy metals like cadmium and lead.⁹¹ However, gadolinium has similar biologic and chemical characteristics (and thus toxicities) to other metals, including cerium, samarium, and europium.⁹² In rats and dogs, subchronic toxicity studies demonstrated that vacuolization of the proximal tubules (osmotic nephrosis) was the most obvious sign of toxicity in subjects administered up to 5 mmol/kg, daily for 4 weeks.³ Generally, the osmotic load produced by administration of typically used doses (such as 0.1 mmol/kg) is considered to be extremely low. Thus, this feature and consideration led to the synthesis of chelated gadolinium complex, which have reduced osmotic activity.³

In addition, the ionic radius of Gd^{3+} (107.8 pm) is similar in size to that of Ca^{2+} (114 pm), and has similar charge. Both of these factors contribute to the ability of the gadolinium ion to block many voltage gated calcium channels, even at very low (nanomolar to micromolar) concentrations.^{84,92} This channel blockage was first described in the rat atrium in 1994 via blockage of the stretch-activated natriuretic peptide secretion by gadolinium.⁹³ The free gadolinium ion is neurotoxic. It is known to inhibit mitochondrial function via nanotube-induced cellular necrosis and DNA damage, and has been shown to induce oxidative stress in cortical neurons in rats.^{54,94-98} Although theoretical for the free gadolinium ion according to some authors,⁹⁸ with regard to transition metals in general and oxidative stress, the majority of free radicals generated *in vivo* come from transmetallation and the metal catalyzed breakdown of hydrogen peroxide according to the Fenton reaction:



where M^{n+} is a transition metal ion.^{98,99} Factors affecting the release of the gadolinium ion are dependent on metals with high affinity for gadolinium binding ligands such as copper, zinc, and iron in addition to the presence of ligands that have high affinity for gadolinium such as phosphorus and carbonate.¹⁰⁰ Gadolinium release increases with decreasing pH. A proposed mechanism for this phenomenon is via uptake of the gadolinium (in unknown form) into a lysosome containing an inherently low pH such as occurs within the renal proximal tubules.¹⁰⁰

Further, the free gadolinium ion can inhibit muscle contraction, blood coagulation, nerve impulses, the activity of numerous calcium-dependent enzymes, including ATPase, kinases, dehydrogenases, and glutathione S-transferases due to its competition with the Ca^{2+} ion at various calcium-gated channels and calcium-dependent enzymes.^{84,92,94,95} The LD50 for gadolinium chloride ($GdCl_3$), when given to mice and rats intravenously, is 0.4 to 0.5 mmol/kg, respectively.^{84,100}

Chelation

Chelation complexes can increase safety by a margin of 20 such that toxic effects are demonstrated only at very high doses, making the LD50 in the range of 8–10 mmol/kg in rats, dogs, rabbits and mice.²⁷ Since tolerance of the gadolinium ion in laboratory animals was not sufficient to allow clinical studies, detoxification without altering its inherent paramagnetic properties was achieved by way of coordination chemistry to various suitable ligands rendering the paramagnetic magnetopharmaceutical less toxic than the free ion or free organic ligand.⁸⁷ The chelate, gadolinium

diethylenetriaminepentacetate (gd-DTPA), was first described in 1984, and successful clinical experiences in patients were reported later in that same year.^{101,102} Gd-DTPA, also known as Magnavist, was FDA approved for clinical use in 1988.¹⁰³ In order to mitigate toxicity, manufactured chelates are formed via a chelating process, in which an electronegative atom donates an electron to the positively charged ion.⁸⁷ Resultant large organic molecules form a more stable compound surrounding the gadolinium ion.^{88,104,105} When ion and ligand are bound together, neither can (in theory and historical belief) react *in vivo* to replace physiologic ions (such as calcium), nor can the supramolecular complex trap other ions (such as zinc).⁸⁷ Zinc is the second most abundant transition metal in the body (after iron), with the average human having about 2.3 grams of total zinc in the body. In theory, zinc is unable to replace gadolinium in the ligand (see equation 3.1).⁸⁷ Chelation results in a dramatic alteration of pharmacological and toxological properties.⁸⁷ These gadolinium-based chelated agents (GBCAs) are considered highly soluble in water at neutral pH, highly concentrated, and hydrophilic, rendering a stable aqueous solution; this is a general prerequisite for diagnostic agents administered intravenously in small volumes.⁸⁷

Beyond the scope of the current discussion, other, non-gadolinium based MR contrast agents can be used in MR imaging. Magnesium sulfate can be administered orally for use in MR imaging of the small intestine.¹⁰⁶ Calcium (II) and magnesium (III) ions are both currently being investigated as potential contrast agents.¹⁰⁷ Gadolinium-based chelated agents, however, remain the mainstay of contrast enhanced magnetic resonance imaging (CEMRI).

Gadolinium-based chelated agents (GBCAs)

Pathophysiology

The mechanism of action of chelated agents is complex.⁸⁴ Multiple physical factors including motion, temperature, viscosity, binding to biomolecules, and compartmentalization all influence the relaxation rates of bulk water and the relaxivity of paramagnetic materials.⁸⁷

When chelated gadolinium is administered intravenously, contrast enhancement results from the shortening of the T1 and T2 relaxation times of tissues, as the seven unpaired electrons of Gd^{+3} match the Larmor frequency, thus increasing the rate of transfer of energy and decreasing relaxation time.^{86,88} Unlike typical iodinated intravenous contrast agents, the contrast effect of GBCAs is indirect. The perceived hyperintensity on T1-weighted sequences is due to local micromagnetic fields which act to shorten the T1 relaxation times of the adjacent tissues. Therefore, rather than the brightness of the image occurring due to the quantity of contrast arriving within vessels at the tissue bed, as with iodinated or barium contrast agents, the brightness of MR contrast agent is due to the indirect effect of the agent on the surrounding tissues, not actually seeing the agent itself in the image.⁸⁷

The effectiveness of the contrast agent depends greatly on multiple variables. One of the greatest influencing variables is the applied MR sequence, with the best enhancement being generated with techniques having the shortest TR and TE such as T1-weighted spin echo (with a TR <600 milliseconds and short echo delay time TE less than 40 milliseconds) and gradient echo techniques, provided an adequate pulse angle is applied.^{87,88} Contrast enhancement is greater at higher field strengths due to longer

intrinsic relaxation times of the tissue protons.^{87,88} Multiple tissue properties/factors regulate the enhancement ability of a given tissue. Tissues with a large distribution volume of a paramagnetic contrast agent and long intrinsic relaxation time exhibit the most significant change in relaxation.⁸⁷ Therefore, marked enhancement is visible in lesions with increased extracellular space or areas of increased distribution volume, such as large accumulations of fluid like within the urinary bladder. Tissues with small distribution volumes and short intrinsic relaxation times, such as the normal brain, liver and muscle, do not exhibit a significant increase in signal intensity following the administration of contrast.⁸⁷ A third factor regulating the contrast-enhancing ability of the tissue is the concentration and relaxivity of the agent.⁸⁷ *In vivo*, low concentrations of paramagnetic species are needed to reduce T1 relaxation times, with concentrations as low as 0.012 mmol L⁻¹ being sufficient to elicit a strong effect on signal intensity.⁸⁷ In contrast, T2 relaxation (or susceptibility effect) dominates at very high concentrations (greater than 5 mmol L⁻¹).⁸⁷

Administered intravenously, GBCAs have an extracellular concentration analogous to iodinated radiographic agents with rapid, unchanged renal excretion by way of glomerular filtration with a half-life of 1–2 hours in people.⁸⁷ Greater than 90% of an administered dose can be recovered from the urine 3 hours following intravenous administration in people.⁸⁷ Elimination is similar in animals.^{88,104,108}

History of GBCA use

As discussed above, gadolinium-diethylenetriaminepentacetate (gd-DTPA; gadopentetate, Magnevist), developed in the early 1980s, was the first commercial MR contrast agent to be approved for clinical use in 1998.^{87,88} Clinical trials in the early

1980s demonstrated excellent patient tolerance of gd-DTPA, with adverse drug reactions being less common than with iodinated radiographic contrast agents. In addition, no hemodynamic alterations were noted in patients following intravenous administration of gadopentetate with doses up to 0.3mmol/kg in the first clinical reports.⁸⁷ Thus, despite of their lack of specificity, first generation compounds were considered to be safe.^{87,88} Conspicuity of abnormalities in tissues was determined to be adequate at 0.1–0.2 mmol/kg, and this dose was recommended in many early clinical reports.⁸⁷ This dose scheme has continued to current day recommendations.⁹² There are currently nine FDA-approved GBCAs available in the United States, as provided in Table 3.1. By 1993, over 7 million people had undergone GBCA enhanced MR studies and to date, over 200 million doses have been administered worldwide.^{87,109,110}

Few reports of overdoses of gadolinium exist. A case report from 2010 described an accidental overdose of 6 mL intrathecal gadopentetate dimeglumine which was mistaken for an iodine-containing contrast media.¹¹¹ Clinical signs associated with this overdose included global aphasia and vomiting; these signs progressed to stupor, rigidity, and intermittent seizures.¹¹¹

Types of GBCAs

Within the class of chelated agents, there are four subtypes into which these agents can be classified. These include the structure of the metalloligand (open-chain vs macrocyclic) and the charge of the ligand (ionic vs non-ionic). Additionally, GBCAs can be classified into extracellular or mixed extracellular/organ-specific (hepatocyte) agents.

stable.⁸⁷ A list of the FDA-approved GBCAs, as well as their structure and charge, is provided in Table 3.1 below, as well as in Figure 3.2.

Table 3.2 FDA approved gadolinium based contrast agents

Chemical Name	Trade Name	Manufacturer	Class	Charge
Gadodiamide	Omniscan	GE Healthcare	Linear	Non-ionic
Gadoversetamide	OptiMARK	Mallinckrodt Inc	Linear	Non-ionic
Gadopentetate dimeglumine	Magnevist	Bayer HealthCare	Linear	Ionic
Gadobenate dimeglumine	MultiHance	Bracco	Linear	Ionic
Gadoxetic acid disodium	Primovist/ Eovist	Bayer HealthCare	Linear	Ionic
Gadofosveset trisodium	Vasovist/ Ablavar	Lantheus Medical Imaging	Linear	Ionic
Gadoteridol	ProHance	Bracco	Macrocyclic	Non-ionic
Gadobutrol	Gadavist/ Gadovist	Bayer HealthCare	Macrocyclic	Non-ionic
Gadoterate meglumine	Dotarem	Guerbet	Macrocyclic	Ionic

The compounds in this table are listed in order of least (gadodiamide) to most (gadoterate meglumine) stable. *Adapted from Idee et al 2009.*⁸⁴

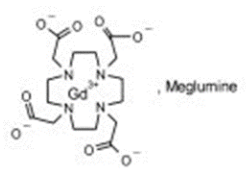
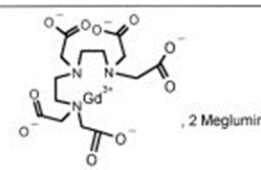
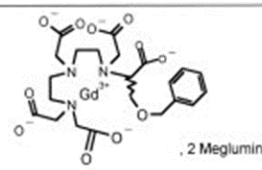
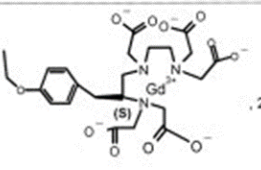
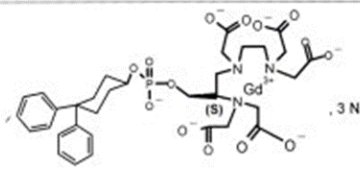
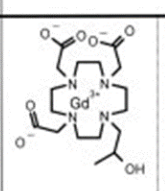
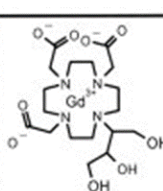
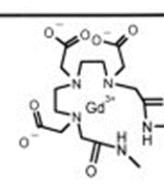
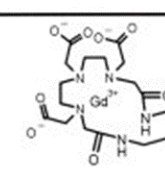
	Macrocyclic	Open-Chain		
Ionic	 Gd-DOTA, gadoterate meglumine, Dotarem®	 Gd-DTPA, gadopentetate dimeglumine, Magnevist®	 Gd-BOPTA, gadobenate dimeglumine, MultiHance®	
		 Gd-EOB-DTPA, gadoxetic acid disodium salt, Primovist®	 MS325, gadofosveset, Vasovist®	
Non-ionic	 Gd-HP-DO3A, gadoteridol, ProHance®	 Gd-BT-DO3A, gadobutrol, Gadovist®	 Gd-DTPA-BMA, gadodiamide, Omniscan®	 Gd-DTPA-BMEA, gadoversetamide, OptiMARK®

Figure 3.2 The 9 FDA approved gadolinium-based chelated agents, grouped by their class and charge.

Linear agents are listed on the right column and macrocyclic agents are listed on the left column. Ionic agents are listed on the top row, while the non-ionic agents are listed on the bottom row. *From Idee et al.*⁸⁴

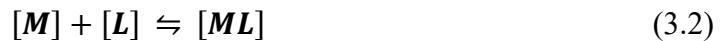
Extracellular vs organ-specific

Finally, GBCAs can be classified according to their biodistribution as either extracellular or mixed extracellular/organ-specific (hepatocyte). Extracellular agents generally do not show appreciable binding to proteins within the body, and are solely excreted by the kidneys (see Table 3.2).¹¹² Organ-specific agents, which do bind to

proteins within the body, are excreted in part by the biliary system, as well as the kidneys (see Table 3.2).¹¹² Although their immediate biodistribution following intravenous injection are similar to extracellular agents, organ-specific agents allow for a longer intravascular interval due to this protein binding and uptake by hepatocytes.¹¹² Additionally, organ-specific agents often have higher relaxivity and demonstrate greater (though clinically negligible) tissue brightening.¹¹² Gadoteric acid disodium (Eovist), gadofosveset trisodium (Vasovist), and gadobenate dimeglumine (Multihance) are organ-specific agents; the remainder are extracellular.^{112,113}

Stability of GBCAs

The stability of the gadolinium chelated compounds is generally discussed via two different, albeit similar concepts: thermodynamic stability and kinetic stability. All chelates are nine-coordinate complexes, which have 8 binding sites for the metal center (gadolinium ion) and a ninth site which is occupied by a water molecule.⁸⁸ The stability of the chelate is described by the equilibrium between the metal center (M), the ligand (L), and the chelate (ML) as follows:⁸⁸



The thermodynamic stability is defined by the energy required for the release of the gadolinium ion from the metalloligand.¹⁰⁹ If the thermodynamic stability is high, then less gadolinium ion is released from the chelate. If the thermodynamic stability is low, then more Gd³⁺ ion is released from the metalloligand.¹⁰⁹ It is generally described as the final equilibrium state of the gadolinium-ligand complex, or how much gadolinium will dissociate over time at a pH of 1.¹⁰⁹

Conditional stability, a constant, is described as the thermodynamic stability at a physiologic pH of 7.4, and it is a more representative descriptor than thermodynamic stability of the *in vivo* stability of these chelates in normal physiologic conditions within patients.⁸⁴

The kinetic stability of the chelate is characterized by its dissociation rate. It describes how fast a steady-state equilibrium is achieved, and thus how fast the Gd^{3+} ion is released from the chelated complex.¹⁰⁹ If the kinetic stability is low, the dissociation rate is high, and the gadolinium ion is released from the ligand quickly.⁸⁴ If the kinetic stability constant is low, then the dissociation rate is also low and the release of gadolinium is too slow to be physiologically important.¹⁰⁹ Kinetic stability is described as the speed at which the ligand and gadolinium dissociate. It is generally reported at a pH of 1, because if performed at physiologic pH of 7.4, some ligands would take months to years to reach equilibrium.

Kinetic and conditional stability constants are given in Table 3.2, with other safety and excretion considerations.

Table 3.3 Chemical stability and excretion of the nine FDA approved gadolinium based contrast agents

Trade Name	Thermodynamic stability	Conditional stability	Kinetic stability (pH 1)	Kinetic stability (pH 7.4)	Excretion	Kinetic stability
Omniscan	16.8	14.9	<5 s	5-7 days	Renal	Low
OptiMARK	16.6	15.0	N/A	N/A	Renal	Low
Magnevist	22.1	18.4	10 min	5-7 days	Renal	Low
MultiHance	22.6	18.4	N/A	N/A	95% renal 4-5% hepatobiliary	Medium
Primovist/ Eovist	23.5	18.7	N/A	N/A	50% renal 50% hepatobiliary	Medium
Vasovist/ Ablavar	22	18.9	N/A	N/A	95% renal 4-5% hepatobiliary	Medium
ProHance	22.8	17.2	2-3 hr	>1000 years	Renal	High
Gadavist/ Gadovist	21.8	15.5	7.9-24 hr	>1000 years	Renal	High

Table 3.3 (Continued)

Dotarem	25.4	19.3	9–60 hr	>1000 years	Renal	High
---------	------	------	---------	-------------	-------	------

a: Low: long-time index < 0.3; Medium: long-time index 0.3 to 0.95; High: long-time index > 0.95. Long-time index is equal to the ratio of the paramagnetic relaxation rates after 50 hours. N/A=not available. Adapted from Idee et al, Lohrke et al, and Ramalho et al.^{84,103,109}

Dosing

In people, enhancement of the MR signal occurs at a typically administered dose of 0.1–0.2 mmol/kg, for magnet strengths over 0.5 Tesla, with a median lethal dose (LD50) of approximately 10 mmol/kg, resulting in a safety factor of 50–100, superior to that of iodinated compounds. Animal experiments have demonstrated excellent cardiovascular tolerance, with toxic effects at high doses with the aforementioned LD50 in rats, mice, rabbits and dogs. Additionally, in rats and dogs administered doses up to 5 mmol/kg daily over a period of 4 weeks, subtoxic effects occurred resulting in vacuolization of the proximal tubules (osmotic nephrosis).⁸⁷ In veterinary patients, a similar dose range is described, yet to date, dosages have been extrapolated from the human literature or from clinical experience, and are largely unsubstantiated.¹¹⁴ An optimal dose for veterinary patients has not been thoroughly investigated.¹¹⁴

Veterinary use of GBCAs

The use of gadolinium chelated contrast agents is also currently prevalent in veterinary medicine. Early reports, beginning in the late 1980s, described the use of gadolinium chelated contrast agents to better evaluate tissues such as the kidney and brain, and also to better highlight such lesions as neoplasia (carcinoma) and hemorrhage in research animals such as rabbits and rats.¹¹⁵⁻¹¹⁹ Veterinary institutions began installing their own MR scanners in the 1990s, which were initially used to image the canine brain and head.¹¹⁹⁻¹²¹ The applications of MRI were soon extended to include many spinal and orthopedic conditions, and became available for the medical evaluation of many other companion animal species, from cats to horses.^{120,122} MRI and GBCAs are now readily clinically available for veterinary patients in both the academic and private sectors.¹²⁰

Adverse reactions to GBCAs

Although historically regarded as generally safe, with a low incidence of adverse reactions and a high safety index, numerous reports of adverse reactions to intravenous administration of GBCAs in both people and animals exist.^{86,123-130} In people, the incidence of adverse events associated with GBCAs administration at clinical doses (0.1–0.2 mmol/kg) is low and ranges from 0.07% to 2.4%.^{123,125,127,128,131-133} One institutional study reports an adverse reaction in 5.9 per 10,000 injections, with a severe reaction occurring every 1 in 40,000 injections.¹²⁸ Although uncommon, reactions to intravenous GBCA injection can be acute or delayed. Reactions occurring 30 minutes or more after the administration of the chelated agent are considered delayed.¹³⁴ Acute reactions are seen more commonly, with 70% of these reactions occurring within the first 5 minutes post-administration.^{134,135} Reactions can be further divided into mild, moderate, or severe.¹³² Mild reactions generally do not require intervention, whereas moderate or severe reactions require intervention in the form of antihistamines, bronchodilators, emergency drugs including epinephrine and atropine, and hemodynamic support.¹²⁹

Reported reactions include those that are mild and physiologic including injection site coldness, warmth, pain, nausea with or without vomiting, headache, paresthesia, and dizziness.¹³³ In addition, allergic-like reactions similar to those seen with the intravenous administration of iodinated contrast media, such as skin irritation, urticaria, facial edema, nasal congestion, and throat symptoms (itching or tightening, 0.004%–0.7%), as well as transient dyspnea (4%–14%) are documented.¹³³ Severe potentially fatal, life threatening reactions including respiratory and cardiovascular arrest are exceedingly rare (0.001%–0.01%), and there is an increased risk of adverse reaction in patients with underlying

asthma or chronic respiratory disease.^{123-125,127,128,136-139} In addition, some cardiodepressive and hypotensive effects are dose dependent in both people and rats.¹⁴⁰⁻¹⁴² The American College of Radiology (ACR) reports that additional risk factors for adverse reactions include a previous reaction to a GBCA, history of allergic-like reactions, and renal compromise.¹³⁹ The incidence of mild adverse reactions (including nausea and vomiting, cough, warmth, headache, dizziness, shaking, itching, and altered taste sensation) for the various types of GBCAs is 0.11%, whereas the incidence of severe reactions (including laryngeal edema, profound hypotension, and arrhythmias) is 0.02%.¹³³

Nephrogenic systemic fibrosis (NSF)

In patients with acute renal injury or chronic renal disease, nephrogenic systemic fibrosis (NSF), a systemic fibrotic disorder, has been strongly associated with the intravenous administration of gadolinium chelated contrast agents.¹⁴³⁻¹⁴⁵ First described in 2000, this rare disorder is characterized by scleroderma-like skin lesions and widespread extracutaneous fibrosis, notably muscle, with more than 500 cases being reported to the FDA since 2010.¹⁴⁶ Although the disease occurs almost universally in patients suffering from renal failure, there are reports of NSF-like lesions or gadolinium toxicity in patients with normal renal function.¹⁴⁷ The incidence of NSF has all but disappeared with more judicious screening tests prior to GBCA administration and careful selection of more stable agents in high-risk patients.¹³⁹

GBCAs accumulate in the skin and internal organs of people with NSF.^{105,148,149} The use of extremely high (off-label) doses of GBCAs has largely been abandoned, and off-label uses are uncommon within the latitude of reasonable, clinical, per case

justification.¹³⁹ Although not routinely performed in patients with hepatic or renal insufficiency, the medical community is now beginning to entertain the clinical use of fractional dosing (specifically 0.5 mmol/kg, with the most stable agents) in patients undergoing serial examinations and patients under 18 years of age.¹⁵⁰ Although rats given high doses of GBCAs develop changes in their skin similar to affected NSF patients, nephrogenic systemic fibrosis following intravenous gadolinium chelated contrast administration is not reported in animals.¹⁰⁴ Although the reason for this remains unknown, it is possible that the shorter lifespan of our companion animals precludes development of the disease. It is also possible that the disease does occur in companion animals and has not yet been recognized.

Adverse reactions in veterinary medicine

The body of veterinary literature describing reactions to intravenously administered GBCAs is limited, and thus the incidence of such reactions is currently unknown. However, multiple reactions are described and include facial swelling, hypotension, both bradycardia and tachycardia, and in one case cardiovascular collapse in dogs and bradycardia, tachycardia, hypotension, and hypertension in both dogs and cats.^{126,129,130,151,152}

Survey of the American College of Veterinary Radiology

Due to the sporadic nature of reports of GBCA related adverse events and concern amongst college members, the author designed a survey about the use of GBCAs in the veterinary radiology community. This survey was distributed to the American College of

Veterinary Radiology (ACVR) via an e-mail May 10, 2016. Results from this survey are discussed in Chapter IV.

T1 hyperintensity following GBCA administration

The first report of unenhanced T1 hyperintensity in the brain was made in patients with multiple sclerosis, with the report concluding that the hyperintensity was due to the disease.¹⁵³ In 2011, a report was made of regional T1 hyperintensity in unenhanced brain images in patients with normal renal function.¹⁵⁴ All of these patients had undergone radiation therapy, and thus it was originally thought that this hyperintensity was due to radiation. However, more reports of unenhanced T1 hyperintensity emerged in patients who had not undergone radiation therapy and did not suffer from multiple sclerosis.¹⁵⁵⁻¹⁵⁷ While this was first reported in adults with normal renal function, the hyperintensity has also been shown in rats and in pediatric patients.^{155,157} All of the patients in those reports had undergone multiple contrast-enhanced MRIs, and all had received linear agents.

The described hyperintensity is primarily seen in the dentate nucleus, pons, globus pallidus, and basal ganglia.^{109,156,158-163} This hyperintensity is progressive with increasing numbers (frequency) of dose administrations, and is independent of renal function in these patients, however, this hyperintensity has not been shown in patients administered macrocyclic GBCAs.^{153-157,160,162} In murine models, T1 signal hyperintensity of the deep cerebellar nucleus occurs after multiple high intravenous doses.^{109,155} This was not documented with similar doses of gadoterate meglumine, an ionic macrocyclic agent.¹⁵⁵

Gadolinium tissue deposition

Gadolinium tissue deposition was first seen in the bones of patients who had undergone femoral head and neck osteotomy following the intravenous injection of linear GBCAs.^{164,165} Gadolinium deposition was next found in the skin of patients who were suffering from NSF.^{148,149} Gadolinium deposition has more recently been discovered to deposit within the human brain. Evaluation of post mortem brain samples of 13 people with normal renal function undergoing multiple (at least 4) GBCA enhanced MRI studies with IV gadodiamide, a linear agent, demonstrated dose dependent deposition of gadolinium with transmission electron microscopy (TEM) and ICP-MS, independent of renal function.^{109,166} Gadolinium brain deposits following multiple exposures to the linear agents gadopentetate dimeglumine and gadoteridol in varying combinations have also been shown.^{109,166} Globus pallidus, dentate nucleus and bone gadolinium deposition of non-group 1 and macrocyclic agents is documented in 9 patients with systemic illness.¹¹³ Single or multiple administrations of both nonionic, macrocyclic agents (gadoteridol and gadobutrol) and non-group 1, protein binding linear agents (gadobenate and gadoxetate), result in brain deposition with an inability to pattern differentiate the levels of deposition.¹¹³ Additionally, bone deposition levels of gadolinium were found in one study to be a median 23 times greater than brain deposition.¹¹³ This finding raises a concern that bone deposition may serve as a reservoir for continued deposition of the toxic gadolinium into the blood or other organs. In people, a relationship between neural gadolinium deposition and increased clinical disability, lesion load, brain atrophy or brain irradiation may exist.^{109,153,154,166,167}

In murine models, cerebellar histologic gadolinium deposits are noted following multiple doses of a linear agent, gadodiamide. Cerebellar, cerebral, and subcortical brain gadolinium concentrations measured via inductively coupled plasma mass spectrometry (ICP-MS) were significantly higher in rats given gadodiamide compared to gadoterate meglumine.¹⁵⁵ Both agents produce focal and generalized myoclonus over several hours when injected into the lateral ventricle, with the cerebellar region having the greatest sensitivity to gadodiamide.⁹⁴ Significant increased seizure frequency is noted in 50% and 75% of dogs with osmotically induced disruption of the blood brain barrier (BBB) when given gadopentetate dimeglumine at doses of 0.1 mmol/kg, and 0.2 mmol/kg, respectively.¹⁶⁸

Warnings and current recommendations for use and surveillance

The perception that chelation practically eliminates gadolinium ion disassociation within the bloodstream and tissues is no longer a well-accepted theory and brain deposition is now a dilemma facing physicians who rely on contrast enhanced MRI (CEMRI) for increased specificity. In 2015, the FDA issued a GBCA safety announcement.^{86,105,169} Investigation and research to understand the mechanisms of gadolinium retention and risks posed with regard to neuronal brain deposition following multiple IV administrations in people are ongoing.^{166,170} The FDA and National Institutes of Health (NIH) advise limiting the use of GBCAs to necessary clinical circumstances, reassessing the need for repetitive use in MRI studies of well-established protocols until further evaluation of risks can be investigated and heeding NIH recommendations for clinical use.^{169,170} Combined, mounting accumulative evidence resulted in a safety warning announcement by the FDA, released on July 27, 2015.¹⁶⁹ In summary, the

statement announced safety concerns and a current ongoing FDA investigation through the continued research through its National Center for Toxicological Research to understand the mechanisms of gadolinium retention and to determine what risks, if any, are posed by the deposition of gadolinium in the brains of human patients, following the intravenous administration of multiple doses. The warning statement advises clinicians to limit the use of GBCAs to necessary clinical circumstances and to reassess the clinical necessity of repetitive use of GBCAs in MRI studies of established treatment protocols. The statement further promises investigation into the safety of GBCAs and description of the associated risks involved with their administration.¹⁶⁹

Conclusion

The dog is a historically viable translational model for brain physiology and disease states. Thus, improvements in our knowledge of advanced MRI techniques (or ancillary techniques exclusive of conventional imaging) such as MRS; and evaluating GBCA use, administration and tissue deposition in the brains of healthy dogs, not only advances knowledge for the veterinary clinician, but provides a translational platform for expanding knowledge for medical practitioners.^{69,70} Given the dose-dependent nature of both adverse reactions to GBCA administration and gadolinium tissue deposition, finding a lower clinical dose of GBCAs is an important problem to investigate. In addition, research into gadolinium tissue deposition is non-existent in the dog; thus there is a need to expand the literature on deposition in higher phylogenetic species than mice.

CHAPTER IV
CONSPICUITY OF VARIOUS LOW DOSES OF GADOLINIUM IN THE NORMAL
CANINE BRAIN AT 3 TESLA

Study purpose

The use and dosing of gadolinium-based chelated agents (GBCAs) in companion animals has been anecdotal and extrapolated from murine dose research and dosing in people. Several factors provided an impetus for investigating an ideal and minimum dose needed to achieve adequate conspicuity of normal brain and other tissue lesions. First, reports of reactions to contrast injection in companion animals are only sporadic in the scientific literature. Second, a discussion at the Annual Scientific Meeting of the American College of Veterinary Radiology in 2014 in St Louis, Missouri focused on mounting concerns of unreported, but experienced adverse events ranging from urticaria to death (Jennifer Gambino, personal communication, October 28, 2014). Finally, there is recent concern in the medical field of gadolinium deposition in human tissues (skin, bone and brain). The purpose of this portion of the study was to determine if lower-than accepted clinical doses of gadodiamide could be given in healthy dogs with adequate conspicuity of normally enhancing structures

Hypothesis

The author and cohorts hypothesized that normal patterns of enhancement would be seen at fractional doses of gadolinium chelated contrast agents with adequate conspicuity, in search for a viable lower dose for clinical use.

Methods and materials

Design and execution of *in vivo* portions of this study and subsequent surgical laboratories were subject to institutional review board oversight, (Institutional Animal Care Use Committee protocol numbers 15012, 12065, and 15075). Financial support was provided by Dr. Gambino through the Department of Clinical Sciences, and the American College of Veterinary Radiology. In addition, Dr. Gambino provided direction and had oversight of all aspects of the current study concept, design, drafting, revision, and final approval and had full control of the acquisition, analysis, and interpretation of all data.

Study population

This prospective, pilot study population consisted of 8 healthy juvenile purpose-bred hound dogs. Ages ranged from 5 to 13 months (mean=8.6 months, IQR=5 months). Two dogs were intact males, five were intact females, and one was a spayed female. Weights ranged from 17.3–24.8 kg (mean=23.76 kg, IQR=8.65). Dogs were deemed normal based on physical and neurophysical examination performed by a first-year radiology resident, laboratory animal veterinarian, and a board-certified neurologist. Complete blood count, serum biochemistry, serum occult heartworm, and serum titers for *Ehrlichia canis*, *Rickettsia rickettsii*, *Borellia burgdorferi*, and *Babesia canis* (ProtaTek Reference Laboratory, Mesa AZ) were performed. All study subjects underwent CT scout

scanning with a 64 detector helical CT (Lightspeed VCT 64–slice, GE Healthcare, Milwaukee, WI) scanner for pre-MRI whole body metal (implanted or ingested) screening prior to MRI of the brain. Following MRI examination all subjects underwent cerebrospinal fluid centesis and analysis for cytology and West Nile virus titer testing (Diagnostic Center for Population and Animal Health, Lansing MI). Further exclusion criteria for subject selection was not applied.

MRI imaging

Technical information: conventional magnetic resonance imaging

A daily quality assurance for functional magnetic resonance imaging (fMRI) was performed the morning prior to all MRI scanning, consisting of a base EPI sequence on a phantom. In addition, a week or less prior to all scans, an American College of Radiology (ACR) phantom scan was performed, the results of which are evaluated yearly by a licensed medical physicist.

All dogs were sedated with acepromazine (0.01 mg/kg, PromAce, Fort Dodge Animal Health, Overland Park, KS) and hydromorphone (0.1 mg/kg, Dilaudid, West-Ward, Eatontown, NJ) intramuscularly. Animals were induced with propofol (2.3 mg/kg, PropoFlo, Abbot Animal Health, Abbott Park, IL) and were maintained on an admixture of isoflurane (Attane, Piramal Healthcare, Bethlehem, PA) inhalant anesthesia and oxygen according to a standard clinical protocol and under supervision of our institutional anesthesia service. Conventional morphologic MR was performed with a 3T magnet (Signa 3T Excite, General Electric Healthcare, Milwaukee, WI). All animals were scanned in sternal recumbency with a quadrature knee coil (M1385AM, IGC [Intermagnetics General Corporation], Latham, NY). A typical clinical conventional MR

imaging protocol was performed in multiple image planes to include the following: sagittal T1-weighted (T1-W) Fluid Inversion Recovery (FLAIR); dorsal T2-weighted (T2-W); sagittal and transverse T1-W fast spoiled gradient echo (FSPGR); transverse T2-W FLAIR, T2* fast gradient echo (FGRE), transverse diffusion tensor (DTI); transverse diffusion weighted imaging with apparent diffusion coefficient mapping (DWI, ADC); and transverse time-of-flight (TOF) imaging; and a 3-D reconstructable, transverse T1-W FSPGR series following the intravenous administration of a gadolinium chelated contrast agent, gadodiamide (Omniscan, 0.5 mmol/mL, General Electric Healthcare, Milwaukee, WI). Dogs were administered variable, fractional doses of the contrast agent as follows: 0.1 mmol/kg (n=2), 0.05 mmol/kg (n=2), 0.025 mmol/kg (n=1), 0.0125 mmol/kg (n=1), and 0.006 mmol/kg (n=1) via the right cephalic vein. Following intravenous contrast administration, intravenous fluids (0.9% sodium chloride, Baxter Healthcare, Deerfield IL), at a standard anesthetic flow rate dose of 5 mL/kg, were administered. Morphologic images were reviewed by a board-certified radiologist and a second-year imaging resident. Animals were included only if morphologic MR brain images were normal.

Contrast administration

A single, dose of gadodiamide was administered intravenously via a cephalic vein at various doses given below.

Table 4.1 Intravenous dosing scheme of gadodiamide (Omniscan) administered to the study population consisting of eight purpose-bred hound dogs

Number of dogs	Administered dose (mmol/kg)	Fraction of 0.1 mmol/kg dose
1	0.006	$\frac{1}{16}$
1	0.0125	$\frac{1}{8}$
2	0.025	$\frac{1}{4}$
2	0.05	$\frac{1}{2}$
2	0.1	1

The administered intravenous gadodiamide was followed by intravenous fluids (0.9% sodium chloride, Baxter Healthcare, Deerfield IL). A 3-D reconstructable, transverse T1-W FSPGR series was acquired following the administration of the contrast agent.

Following imaging, all dogs underwent cisternal cerebrospinal fluid centesis by a board-certified veterinary neurologist immediately following imaging and prior to anesthesia recovery. All dogs then received carprofen (4 mg/kg, Rimadyl, Zoetis, Florham Park, NJ) subcutaneously and recovered from anesthesia uneventfully.

Histopathology

Following imaging and recovery, all dogs were surrendered to an unrelated non-imaging terminal surgical laboratory under a separate institutional protocol. Animals were humanely euthanized following a second anesthetic event and terminal surgical laboratory, 3–7 days after administration of the contrast agent. Procedures performed during this surgical laboratory included enterotomies, small intestinal resection and anastomoses, and renal biopsies, but did not involve the central nervous system or brain in any way. The brains of each of the subjects were harvested no more than four hours following euthanasia, and in the interim, were kept on ice. Formalin-fixed neurologic tissue from the frontal, parietal, and piriform lobes, thalamus, cerebellum, brainstem, motor cortex, and hippocampus, were submitted for histopathologic evaluation to confirm the normal status of the tissue.

Data analysis

T1-W FSPGR transverse and sagittal images pre- and post-contrast administration were evaluated.

Lossless tagged image file format (TIFF) images of the transverse T1-W pre- and post-contrast images, all obtained at the same window level and width (*window level=2501, window width=498*), were anonymized and randomized using an available web-based random-number generator (www.random.org, accessed November 10, 2015). Images were then reviewed by two board-certified radiologists and a second-year imaging resident blinded as to the doses of contrast given and whether or not images were acquired in the pre- or post-contrast stage of imaging. Each participant evaluated the regions of interest that included regions of brain considered to enhance mildly to

moderately in normal people and dogs administered a GBCA. Images were then assigned a subjective and arbitrary score for the degree of enhancement perceived, at the following regions: olfactory bulb, dorsal sagittal sinus, cerebral cortex, third ventricle, lateral ventricle, thalamus, interthalamic adhesion, piriform lobe, pituitary, trigeminal nerve, mesencephalic aqueduct, cerebellum, fourth ventricle, and meninges. Images were subjectively scored as follows: 0=no contrast seen; 1=poor enhancement of normally enhancing structures (minimal contrast seen), 2=good enhancement of normally enhancing structures, and 3=excellent enhancement of normally enhancing structures (high contrast conspicuity).

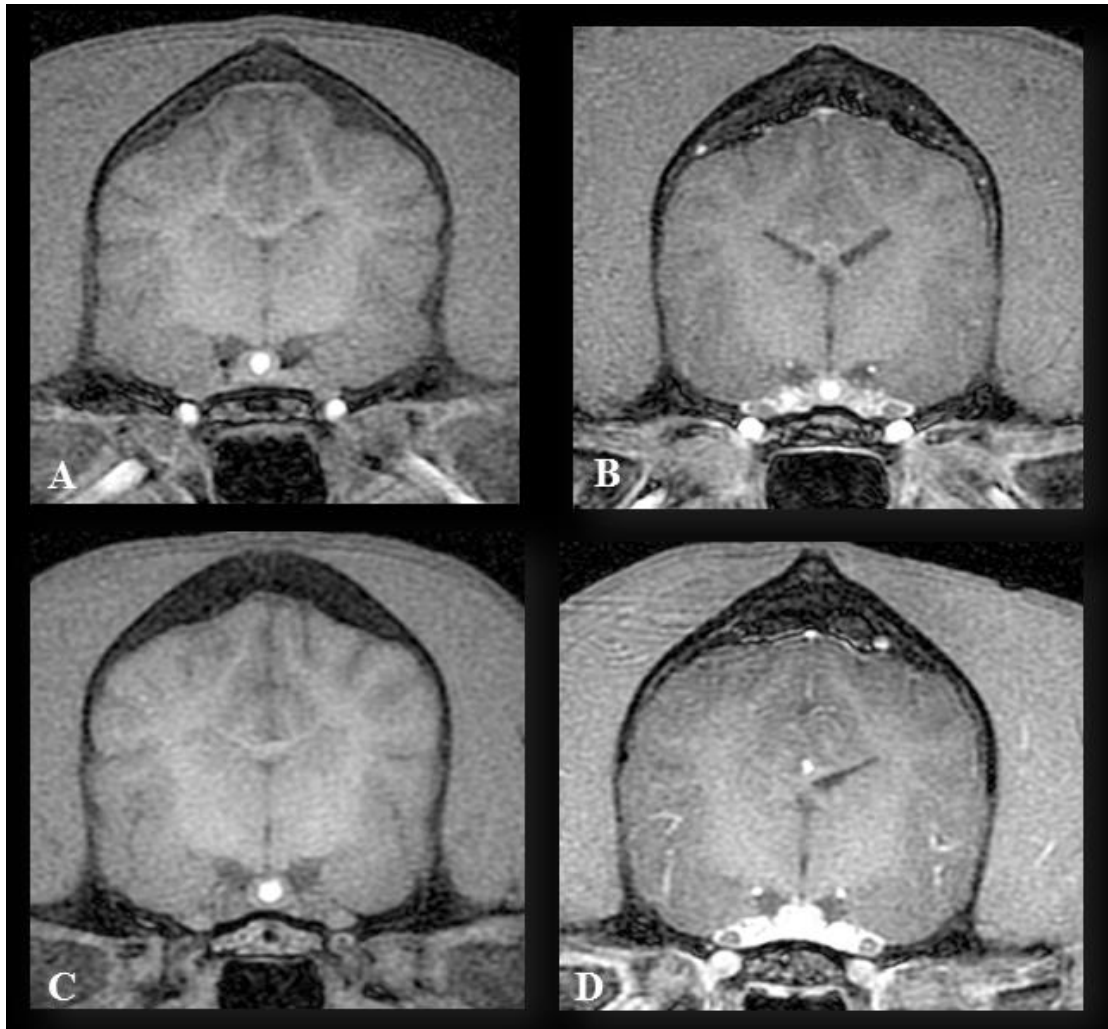


Figure 4.1 Tagged image file format (TIFF) images of T1-weighted transverse images following various doses of gadodiamide in four normal dogs

Dogs were given one of the following doses of contrast: A– 0 mmol/kg, B– 0.0125 mmol/kg, C– 0.025 mmol/kg and D– 0.1 mmol/kg (D). Images were scored by all three observers as a 0 (A), 1 (B), 2 (C), and 3 (D).

A novel computer program was created to analyze the images for the presence of contrast. Pixel intensity probability mass function (PMF) of graylevel* values were used as features. Features were optimized with Fisher's Linear Discriminant Analysis. Linear classifier decided for each image either no-enhancement or enhancement using Leave-

one-out analysis. Images were converted to grayscale (pixel values 0 to 255) for the analysis.

Statistical analysis

Kappa statistics were used to evaluate the performance of the two board-certified radiologists and imaging resident compared to each other as well as compared to the known pixel intensity for those regions, which was used as the gold standard. In addition, an interclass correlation coefficient (ICC) was performed to evaluate agreement between the three observers. All statistics were performed by a board-certified veterinary epidemiologist, using SAS for Window 9.4 (SAS Institute, Inc., Cary, NC, USA).

Gadolinium based contrast use by the American College of Veterinary Radiology: a survey

In order to more accurately determine the use of GBCAs in the veterinary radiology community, the author designed a survey regarding the use of GBCAs in the veterinary radiology community. This survey was distributed to Diplomates of the American College of Veterinary Radiology (ACVR) via an e-mail May 10, 2016 and results were accepted until October 10, 2016.

The questions were as follows:

1. Do you routinely use gadolinium chelated contrast agents as part of your MRI studies?
2. What contrast agent do you use?
3. What dose of contrast do you typically give?
4. Have you noticed any adverse reactions to gadolinium chelated contrast agents in your patients?

5. If yes, can you please describe these reactions?

All participant respondents remained anonymous.

Results

Conventional and advanced MRI examinations were successfully performed in all dogs and deemed normal by a board-certified veterinary radiologist and board-certified veterinary neurologist. Advanced protocols demonstrated normal brain diffusion and perfusion. All images were of excellent diagnostic quality and none were excluded from the image scoring. No complications were observed in any dog secondary to the phlebotomy, gadolinium contrast administration, MRI examinations or cerebrospinal fluid centesis. All hepatic and renal serum biochemistry values were normal in all dogs. Infectious disease titers for *Ehrlichia canis*, *Rickettsia rickettsii*, *Borellia burgdorferi*, and *Babesia canis* were negative, all dogs tested heartworm negative, and CSF cytology results were unremarkable in all animals. All dogs exhibited normal MR brain morphology with normal patterns of contrast enhancement and all animals recovered uneventfully from anesthesia.

Agreement

Initially, 5 reviewers were included in the study, including two board-certified radiologists, a second-year imaging resident, first-year imaging resident, and imaging intern. The results from the first-year imaging resident and imaging intern were excluded from analysis due to these two reviewers inadvertently revealing results to each other. When the remaining three results were analyzed, agreement between the board-certified radiologists (reviewers 1 and 2) was good (Kappa=0.64). Agreement was also good

between both board-certified radiologists and the imaging resident (reviewers 1 and 3, and 2 and 3; Kappa score=0.57 and 0.66, respectively). The interclass correlation between the 3 reviewers was excellent (ICC=0.79). When images were considered by score and reviewer, the two radiologists were very similar, while the less experienced imaging resident tended to score the images higher (or over interpret the degree of contrast dose present).

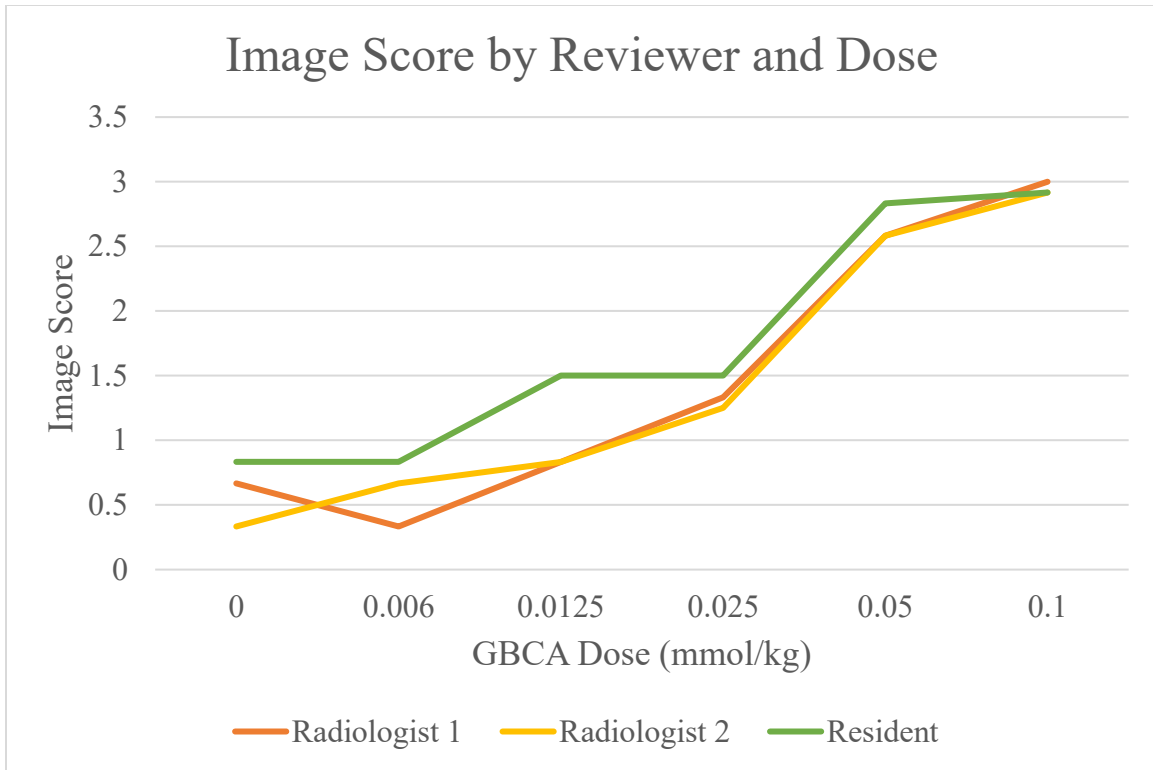


Figure 4.2 Image score by dose (in mmol/kg) and by reviewer.

Images scores were assigned to randomized, lossless, TIFF images by 3 reviewers (of varying levels of experience). A subjective assignment of scoring was performed by each of the participating individuals. Subjective scoring by reviewer, dose and correlation to actual intravenous dose administered (mmol/kg), is shown in graphical representation. Arbitrarily assigned, subjective image scoring was based on a scale of 0–3, with 0=no contrast seen; 1=poor enhancement of normally enhancing structures (minimal contrast seen), 2=good enhancement of normally enhancing structures, and 3=excellent enhancement of normally enhancing structures [high contrast conspicuity]. Notice the radiologists' scores are very similar, while the resident tended to score images higher than that of the radiologists. Notice also, fair to good agreement at the 0.125 mmol/kg dose, and excellent agreement at 0.05 and 0.1 mmol/kg, respectively.

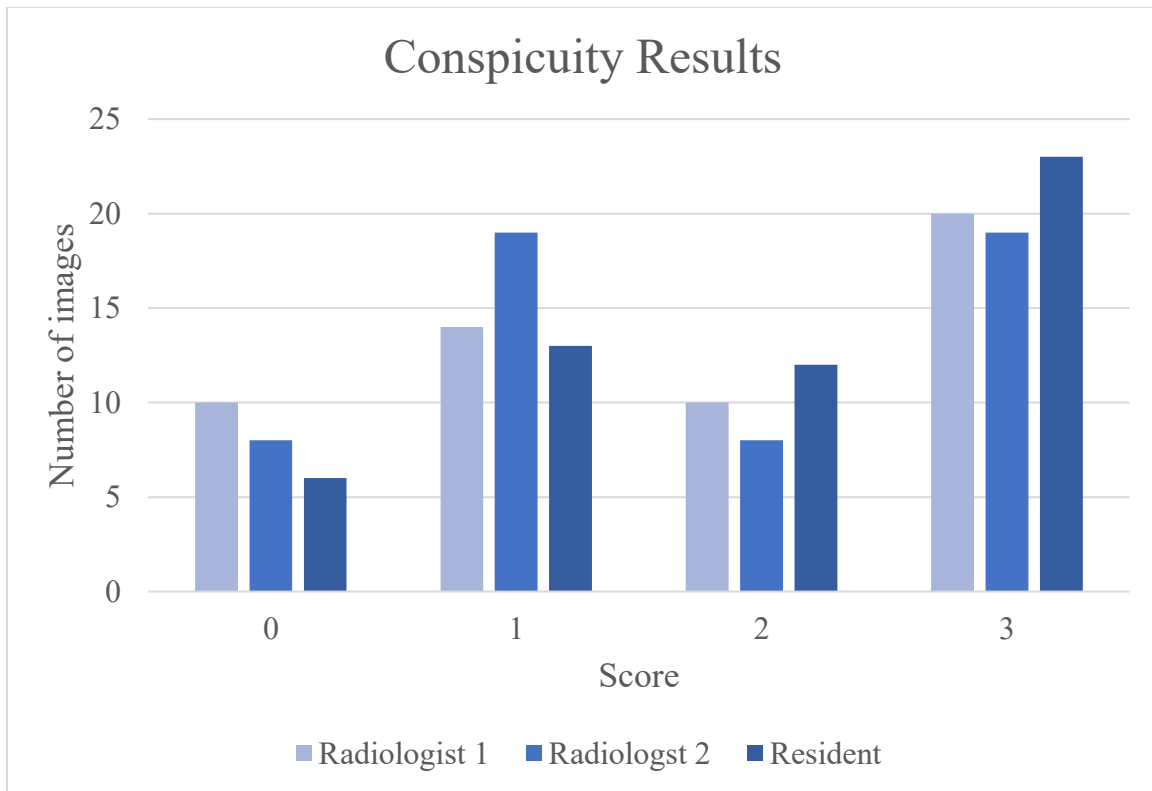


Figure 4.3 Number of images given each score by reviewer

Number of images scored 0, 1, 2, or 3 as scored by each reviewer (Radiologist 1, Radiologist 2, and radiology resident). Again notice the resident tended to score images higher than the radiologists. Notice the relatively good agreement for the number of doses that scored a 3 or excellent conspicuity. All reviewers over-interpreted the 0.5 mmol/kg dose as a 0.1 mmol/kg.

A total of 24 images were scored as 0, 46 were scored as 1, 30 were scored as 2, and a total of 62 images were scored as 3 (excellent conspicuity). Twenty-six of the images scored as a 3 from dogs administered the 0.05 mmol/kg dose, which corresponds to 42% of the images scored as 3 and 72% of the 0.05 mmol/kg images. Thirty-four of the images scored as a 3 were from dogs administered the 0.1 mmol/kg dose, which corresponds to 55% of the images scored as 3 and 94% of the 0.05 mmol/kg images. All images were reviewed in the same ambient conditions, on the same computer set to the same brightness level. Window and leveling capabilities were absent for all images.

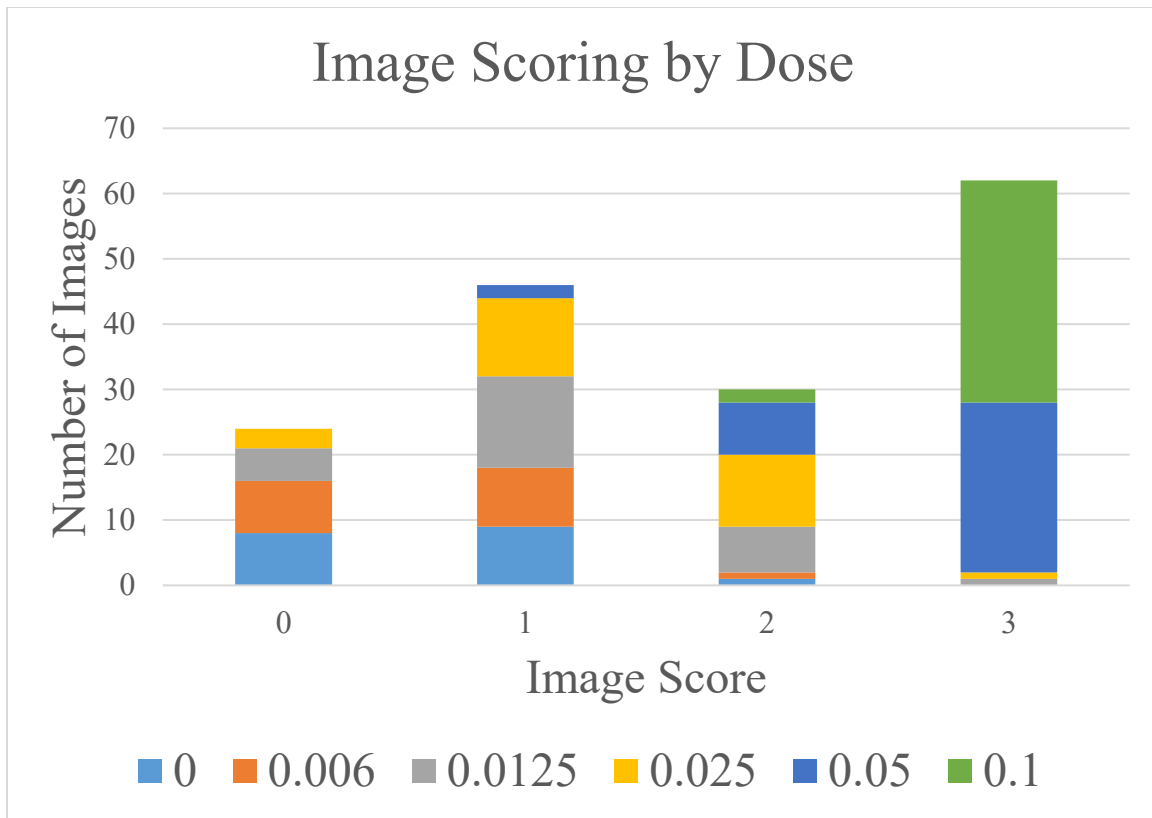


Figure 4.4 Images scored by dose by three reviewers

Image scoring presented by dose. Note that the majority of images scored a 3 (excellent conspicuity) were from dogs administered either a 0.05 mmol/kg dose (blue) or a 0.1 mmol/kg dose (green), comprising 72% of dogs receiving the 0.05 mmol/kg dose and 94% of the dogs receiving the 0.1 mmol/kg dose.

The novel custom automated detection software scored 48/48 (100%) images with contrast as contrast enhanced, and scored 2/6 (33.3%) of the images without contrast as non-enhanced. Thus the program had a false positive rate of 66.6% and a false negative rate of 0%. Upon review, it was determined that the computer was erroneously reading phase-encoding artifact (and subsequent arterial flow hyperintensity) as contrast enhancement. When phase-encoding artifacts were removed from the image, the computer classified 6/6 (100%) of the images without contrast as non-enhanced, decreasing the false positive rate to 0%.

Survey results

There were a total of 26 responses to the survey. Given 605 active diplomates in the ACVR, this is a response rate of 4.3%. Twenty-five of 26 respondents (96%) reported using GBCAs in their practice. The most commonly used agents were gadopentetate (Magnevist, 13/25, 52%), gadodiamide (Omniscan, 5/25, 20%), and gadobenate (Multihance, 4/25, 16%). Gadoteridol (ProHance) was reported twice (8%) and gadoversetamide (OptiMARK) was reported once (4%). The most commonly used dose was 0.1 mmol/kg with a dose range of 0.1–0.15 mmol/kg documented.

Twenty-three of 25 respondents reported seeing no adverse events associated with GBCA use (88.5%). The reported adverse events included bradycardia, tachycardia, hypertension, and allergic-type reactions. One event of hypotension was severe and resulted in euthanasia of the patient.

Discussion

Adverse effects

No adverse reactions to the gadodiamide injections were seen in the current study population. This was expected, as there are only sporadic reports of reactions to GBCA administration in veterinary medicine, and the incidence of reactions in people is very low, ranging from 0.06% to 0.11%.^{123,126,128,133}

Conspicuity

When each image was graphed by score and reviewer, both boarded radiologists were very similar in their scoring. The less experienced radiology resident tended to score images higher than the radiologists; this is likely due to the relative inexperience with

MR images of the resident compared to the more experienced radiologists. However, the overall trend of scoring was similar across all three reviewers, indicating that despite the resident generally scoring images higher than the radiologists, the scoring between the images was consistent amongst all reviewers. The interclass correlation coefficient of 0.79 indicated excellent agreement amongst the three reviewers.

When broken down into the described 0–3 categories, the majority of both the 0.1 mmol/kg (94%) and the 0.05 mmol/kg (72%) doses were scored as a 3, or “excellent conspicuity.” Results from this pilot study indicate that 0.05 mmol/kg gadodiamide was subjectively assessed as excellent and thus, should be considered as a viable, fractional clinical dose for brain imaging since it provides adequate conspicuity of normally enhancing brain structures in a healthy sub-population of young, purpose-bred dogs. Importantly, this study included the subjective assessment of normally enhancing structures in healthy dogs. Enhancement in the brain is the result of one of two separate primary processes: intravascular or vascular, and interstitial or extravascular enhancement.¹⁷¹ Following intravenous administration, the blood concentration of GBCAs rises rapidly. The concentration creates a gradient across the capillary endothelial membrane, and in regions with relatively free capillary permeability, contrast accumulates in the perivascular interstitial fluid. In the brain, the blood brain barrier (BBB) prevents this leakage normally. Thus, the structures which normally enhance are those outside of the BBB, including the meninges and choroid plexus of the ventricles. When the BBB is disrupted, however, as with a neoplastic or inflammatory condition, contrast is able to accumulate at the sites of disruption.¹⁷¹ Normal interstitial enhancement is directly related to alterations in the permeability of the BBB, while

intravascular enhancement is proportional to increases in blood flow or blood volume.¹⁷¹ Additionally, interstitial enhancement in MR requires both free water and gadolinium to be present; therefore, if a tissue does not contain free water, no contrast enhancement will be seen.¹⁷¹ Dura mater, for instance, is extra-axial and does not have a BBB, but it lacks sufficient water content for the required T1 shortening to show contrast enhancement.¹⁷¹

Study limitations

There were several limitations to this study. In this study, the author strove only to evaluate normally enhancing structures in healthy dogs, which is not duplicative of the typical clinical setting. Abnormal enhancement patterns of pathologic disease states were not evaluated or quantified. Thus, work beyond the limitations of a descriptive pilot study are required to verify the validity of this dose in clinical patients having a variety of central nervous system diseases. The study herein provides a basis for future investigation and comparison of the clinical efficacy of fractional dosing. Further, study population numbers were limited to only eight dogs, which limited the study power. The limited population size was partially due to the fact that this study was intended as a pilot study. This limitation was also due to the ethical and financial considerations inherent to veterinary MR research in dogs. Attempts to offset this limitation and increase power were made by including multiple images from each dog for the evaluation of normally enhancing structures and the multiple fractional doses. A larger number of dogs, investigating a larger but more targeted range of doses around the clinically accepted 0.1 mmol/kg dose, may have produced stronger results. However, dog numbers were limited by financial, ethical, and timing constraints. Further, a scale of computer assigned pixel

values can be assigned to a dose correlated reviewer viewing scheme where 0, 1, 2, 3, 4, etc. can be correlated to an assigned dose

The authors did not investigate the typically reported higher end of the dose range administered to people and companion animals (0.2–0.3 mmol/kg). The clinical protocols employed at the author’s institution do not include doses greater than 0.1 mmol/kg, and as excellent conspicuity of contrast is achieved at this dose, this study evaluated the conspicuity of equal and lower doses than those given to veterinary patients at the author’s institution. Similarly, the author chose to only investigate one GBCA, the linear agent gadodiamide. This agent was chosen because it is the agent used in clinical patients at the author’s institution in both veterinary patients and in people seen at the adjacent clinical practice that shares the 3T magnet. Although there are mild differences between T1 shortening times of different GBCAs (as shown in Figure 4.5), there is no literature that exists regarding the clinical performance of GBCAs which indicates that any one compound is superior to other GBCAs. Thus, it is unlikely that the choice to use only one GBCA negatively affected the results of this study. Reviews did not have the ability to manipulate the window or level of the images presented. Results may have been different had reviewers had the ability to alter the window and level, in that lower doses may have been deemed more adequate.

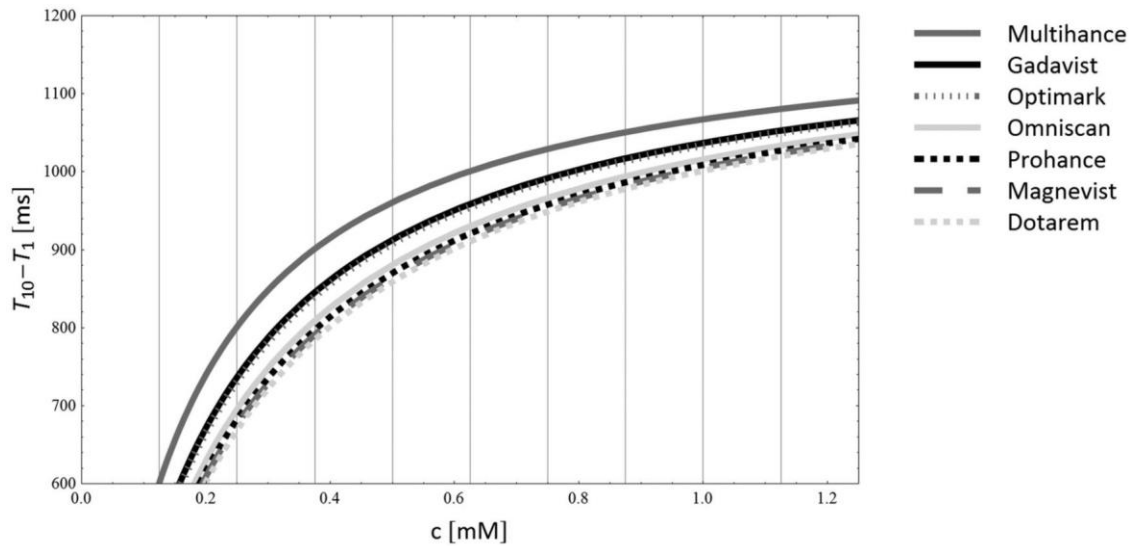


Figure 4.5 T1 shortening times of various GBCAs, as a function of their gadolinium concentration.

These times were calculated from relaxivities in blood, which was first reported by Roher et al in 2005.¹⁷² Image from Kanal et al 2014.¹⁷³

Finally, there is no current “gold standard” against which to judge the performance of the reviewers to validate the findings described. The described computer program is currently able to determine if contrast was administered at a high rate of success, however these results say nothing about levels of conspicuity. Proprietary software is currently being devised with novel computer algorithms for the evaluation of contrast enhanced images using pixel intensity for which to compare results of the current study, as well as future results from clinically diseased patients. The eventual goal is to evaluate images for the degree and presence of contrast enhancement following fractional dose administration that may be below human levels of detectability. The human eye is only able to detect 30 shades of grey, and humans are thus unable to see many of the available shades present on a computer screen.¹⁷⁴ Such work may mitigate the need for

normal, current dose protocols and will aid in the evaluation of computer, radiologist and resident performance.

Conclusions

In conclusion, the results show that the 0.05 mmol/kg and 0.1 mmol/kg doses of gadodiamide provide excellent conspicuity of normally enhancing structures in healthy dogs. There was an excellent interclass correlation coefficient for the three reviewers, and thus, excellent agreement. Based on these results, the author proposes fractional dosing for veterinary, clinical, contrast-enhanced MR examinations in general, inclusive of patients who may be at an increased risk for adverse events. No risk factors have been definitely discovered in companion animals, likely due to the sporadic nature of the case reports describing these events. Although conjectural, as limited literature exists, a potential at risk population might include individual animals having a previous history of an adverse event, asthma or other chronic respiratory diseases, or renal compromise as is true in people. Future work with the 0.05 mmol/kg dose is needed to evaluate the clinical viability of this dose for the evaluation of various intracranial and extracranial disease states, including those that arise from neoplasia, inflammation, infection and injury.

CHAPTER V
INVESTIGATION OF NEURONAL DEPOSITION OF GADOLINIUM IN NORMAL
DOGS FOLLOWING A SINGLE INTRAVENOUS EXPOSURE TO VARIOUS
DOSES OF GADODIAMIDE

Study purpose

Gadolinium tissue deposition has been demonstrated in both people and murine models. Tissue deposition has been demonstrated in cadaveric samples of brain, bone and skin in clinical human patients with numerous disease states, including neoplasia, hepatic cirrhosis, and systemic lupus erythematosus; and in mice receiving large, non-clinical doses of gadolinium.^{113,155} No studies exist determining if this deposition is seen in healthy non-murine, animals receiving a single, clinical (or subclinical) dose. The purpose of this portion of the study was to evaluate the neuronal deposition of varying (subclinical) fractional doses of a single, *in vivo* administration of intravenous gadodiamide, in 13 healthy canine subjects (having normal hepatic and renal function), with a 14th dog serving as a control following the administration of an intravenous placebo.

Hypothesis

The author and cohorts hypothesized that neural deposition would be seen in the brains of all dogs receiving intravenous gadodiamide, regardless of the dose administered, that no deposition would be seen in a control dog given an equal volume

saline bolus and that the gadolinium deposition would demonstrate both dose dependency and regional affinity.

Methods and materials

Design and execution of *in vivo* portions of this study and subsequent surgical laboratories, were subject to institutional review board oversight, (Institutional Animal Care Use Committee protocol numbers 15012, 12065, and 15075 and 16010). Financial support was provided by Dr. Gambino through the Department of Clinical Sciences; and by grants from Mississippi State University and the American College of Veterinary Radiology CT and MR society. In addition, Dr. Gambino provided direction and oversight of all aspects of the current study concept, design, drafting, revision, final approval and the acquisition, analysis, interpretation and full control of all data.

Study design and animal subject population

Fourteen, healthy, live purpose-bred hound dogs were evaluated following a single, IV exposure to gadodiamide (range 0.006 mmol/kg–0.1 mmol/kg) or saline. Eight of these dogs were the dogs described in Chapters II and IV above. All dogs had a physical and neurophysical examination performed by the institutional laboratory animal veterinarian, diagnostic imaging resident, and board-certified neurologist, complete blood count (CellDyn 3700, Abott Diagnostics, Santa Clara, CA), serum biochemistry (Vet Axcell, Alfa Wasserman Inc, West Caldwell, NJ), and negative serum occult heartworm antigen testing. Dogs were divided into 3 groups. As part of another study, dogs of group 1 underwent testing for infectious disease serum titers for *Ehrlichia canis*, *Rickettsia rickettsii*, *Borellia burgdorferi*, and *Babesia canis* (ProtaTek Reference Laboratory, Mesa

AZ), MRI examination, cerebrospinal fluid centesis (CSF), analysis and cytology and West Nile virus titers from CSF (Diagnostic Center for Population and Animal Health, Lansing MI). Blood sample collection for all testing was performed 1 day (group 1) or 8 weeks (groups 2 and 3), (median=1, mean=24.6, IQR=55), prior to GBCA exposure. Eight dogs in group 1 underwent brain MRI with a single, IV gadodiamide injection as follows: 0.006 mmol/kg (1 dog), 0.0125 mmol/kg (1 dog), 0.025 mmol/kg (2 dogs), 0.05 mmol/kg (2 dogs) or 0.1 mmol/kg (2 dogs). Dogs of group 1 underwent cisternal cerebrospinal fluid (CSF) centesis following contrast enhanced MRI (CEMRI). Five dogs in group 2 received IV gadodiamide as follows: 0.0125 mmol/kg (1 dog), 0.025 mmol/kg (1 dog), 0.05 mmol/kg (2 dogs), and 0.1 mmol/kg (2 dogs). Dogs in group 2 did not have testing for infectious disease titers and did not undergo preemptive MRI or subsequent cisternal CSF centesis. Group 3 was comprised of a single control dog that received a single, placebo volume of 3 mL saline (0.9% sodium chloride, Baxter Healthcare, Deerfield IL), and did not receive a GBCA.

Group 1 dogs were humanely euthanized within 3–7 days following the single exposure, whereas dogs of group 2 and 3 were humanely euthanized within 8.3–8.9 hours of the single exposure to gadodiamide or saline injection. Euthanasia was accomplished via intravenous barbiturate overdose in all animals. Neuronal tissues from the frontal, parietal, and piriform lobes, thalamus, cerebellum, brainstem, motor cortex, and hippocampus were evaluated histopathologically to confirm normal brain status in all groups, as described in Chapter II. Additionally, 1 cubic cm brain samples from the parietal and piriform lobes, thalamus, cerebellum, frontal lobe white matter and brainstem were harvested from all dogs and was analyzed post mortem with inductively-coupled

plasma mass spectrometry ICP-MS, scanning electron microscopy (SEM) and transmission electron microscopy (TEM) to evaluate for neuronal gadolinium deposition. All evaluators were blinded as to the doses administered to each of the dogs.

Exclusion criteria included abnormal neurophysical examination, CBC, blood chemistry, urinalysis, positive infectious disease titers, positive HTW-Ag test, abnormal brain MRI findings, pre-existing history of IV GBCA administration or an adverse event following the IV GBCA administration. Additionally, any subjects having complications related to anesthetic and imaging events, CSF centesis, surgical interventions (group 2), or a mean arterial blood pressure below 60 mmHg during the anesthetic event following the gadodiamide administration (group 2), were excluded.

MRI imaging and GBCA administration

All dogs had similar premedication, anesthetic induction protocols for two antemortem anesthetic events prior to euthanasia. Dogs were premedicated with acepromazine (0.01 mg/kg, PromAce, Fort Dodge Animal Health, Overland Park, KS) and hydromorphone (0.1 mg/kg, Dilaudid, West-Ward, Eatontown, NJ) intramuscularly (IM). For MR imaging (group 1) and/or surgical procedures (groups 1–3), general anesthesia was induced with IV propofol (2.3 mg/kg, PropoFlo, Abbot Animal Health, Abbott Park, IL) and were maintained on an admixture of isoflurane (Attane, Piramal Healthcare, Bethlehem, PA) inhalant anesthesia and oxygen according to standard clinical institutional protocols under supervision of the anesthesia service. Dogs recovered uneventfully from the first anesthetic events.

All study subjects underwent CT scout scanning with a 64 detector helical CT (Lightspeed VCT 64-slice, GE Healthcare, Milwaukee, WI) scanner as a whole body

metal (implanted or ingested) screening prior to MRI of the brain. MRI was acquired using a 3T magnet (Signa 3T Excite, General Electric Healthcare, Milwaukee, WI). All animals were scanned in sternal recumbency with a quadrature knee coil (M1385AM, IGC [Intermagnetics General Corporation], Latham, NY). A typical clinical conventional MR imaging protocol was performed in multiple image planes to include the following: sagittal T1-weighted (T1-W) Fluid Inversion Recovery (FLAIR); dorsal T2-weighted (T2-W); sagittal and transverse T1-W fast spoiled gradient echo (FSPGR); transverse T2-W FLAIR, T2* fast gradient echo (FGRE), transverse diffusion tensor (DTI); transverse diffusion weighted imaging with apparent diffusion coefficient mapping (DWI, ADC); and transverse time-of-flight (TOF) imaging; and a 3-D reconstructable, transverse T1-W FSPGR series following the intravenous administration of a gadolinium chelated contrast agent, gadodiamide (Omniscan, 0.5 mmol/mL, General Electric Healthcare, Milwaukee, WI). Typical conventional MRI acquisition protocol was as follows: 512x512 matrix, 2 number of signal averages, 140 mm reconstruction diameter, and 2.4 mm slice thickness and interval, respectively. Please refer to Appendix C for more information regarding MR sequence parameters.

As part of the MRI examination, eight dogs (group 1) received a single IV dose of gadodiamide at one of the following doses: 0.006 mmol/kg (1 dog), 0.0125 mmol/kg (1 dog), 0.025 mmol/kg (2 dogs), 0.05 mmol/kg (2 dogs) or 0.1 mmol/kg (2 dogs), via the right cephalic vein, for contrast enhanced MRI. Intravenous fluids (5 mL/kg/hr, 0.9% sodium chloride, Baxter Healthcare, Deerfield IL) were administered following the injection. In the immediate post-imaging interim, dogs were transferred to an animal recovery bay for cisternal cerebrospinal fluid centesis, which was performed by a board-

certified veterinary neurologist prior to recovery. A single subcutaneous injection of carprofen (4 mg/kg, Rimadyl, Zoetis, Florham Park, NJ) was administered and dogs recovered uneventfully.

Six additional dogs (groups 2 and 3) had tibial osteotomy procedures for an unrelated non-steroidal anti-inflammatory drug medication trial during the first anesthetic event and did not undergo preemptive CT or MRI. Sixty-two days following the initial anesthetic and surgical event, dogs of group 2 were anesthetized for the second event, a terminal surgical laboratory, in similar fashion, upon which IV gadodiamide was administered as follows: 0.025 mmol/kg (1 dog), 0.05 mmol/kg (2 dogs), 0.1 mmol/kg (2 dogs) and a placebo dose of IV saline (2.5 mL, 0.9% sodium chloride, Baxter Healthcare, Deerfield IL), via the right cephalic vein, followed by IV fluids (5 mL/kg/hr, 0.9% sodium chloride, Baxter Healthcare, Deerfield IL). The single dog in Group 3 underwent similar anesthetic protocols as dogs of group 3, however saline (3mL, 0.9% sodium chloride, Baxter Healthcare, Deerfield IL), was administered IV, as a placebo, rather than gadodiamide. CSF centesis and the administration of periprocedural carprofen, were not performed in dogs of group 2 and 3.

All dogs were subsequently surrendered to the unrelated, ethically preapproved, terminal surgical laboratories. Surgical interventions performed in all dogs at the time of the second anesthetic events for a terminal teaching laboratory were primarily gastrointestinal in nature, with no surgeries involving disruption of the blood brain barrier (BBB). Following the laboratory, dogs were humanely euthanized via intravenous injection under general anesthesia (4.5 mL/kg, Beuthanasia-D Special, Schering-Plough Animal Health Corp., Kenilworth, NJ).

Tissue processing and histopathology

Fourteen dogs underwent necropsy immediately following euthanasia with brain harvesting and sectioning performed by a single board-certified veterinary pathologist. Transverse samples were collected for histopathology from each of following regions in all dogs: the frontal, parietal, and piriform lobes, thalamus, cerebellum, brainstem, motor cortex, and hippocampus. The tissues were processed routinely, embedded in paraffin wax, sectioned at 4 microns and stained with hematoxylin and eosin for microscopic examination. For dogs of group 1, whole-brain specimens were removed at necropsy and immersion fixed in 10% neutral buffered formalin for 4-weeks. Bihemispheric, 1 cubic centimeter brain tissue samples from the frontal lobe white matter, parietal lobe, piriform lobe, thalamus, cerebellum, and brainstem were then submitted for ICP-MS. For dogs of groups 2 and 3, 1 cubic centimeter brain samples were collected from frontal lobe white matter, parietal lobe, piriform lobe, thalamus, cerebellum, and brainstem, immersion fixed in 10% neutral buffered formalin. Additional samples from the frontal lobe white matter, parietal lobe, piriform lobe, thalamus, cerebellum, and brainstem, were placed in Karnovsky's fixative (2% paraformaldehyde + 2.5% gluteraldehyde in 0.1 M sodium cacodylate buffer). Finally, thin slices of brain from the frontal lobe white matter, parietal lobe, piriform lobe, thalamus, cerebellum, and brainstem of the contralateral hemisphere were collected and frozen fresh at -80 degrees Celsius.

Fixed brain samples from dogs of group 1, and fresh frozen and fixed samples from dogs of group 2 and 3, were submitted for ICP-MS evaluation. Combined, a total of 120 brain tissue samples were evaluated for gadolinium quantification from the aforementioned lobes of interest.

For dogs of group 1, mean formalin fixation time for samples prior to ICP-MS was 200 days (range=150–278 days). For dogs of group 2 and 3, formalin sample time for samples prior to ICP-MS was 22 days. Median fixation time in electron microscopy fixative, prior to SEM and TEM, was 36 hours. Formalin-fixed brain samples from dogs of group 1 and fresh and formalin-fixed brain samples from dogs of group 2 and 3, respectively, were archived in the author's institutional bio-specimen repository. Formalin-fixed brain tissue samples from dogs with the highest lobar gadolinium depositions from both groups were submitted for SEM and TEM for gadolinium identification.

Inductively-coupled plasma mass spectrometry gadolinium analysis

Ex vivo brain samples from all dogs were analyzed and quantified for gadolinium deposition using ICP-MS at the Diagnostic Center for Population and Animal Health at Michigan State University by a board-certified toxicologist. The selected regions were trimmed from fixed tissue and briefly wicked with a Kimwipe (Kimberly Clark Professional, Roswell, GA) before being placed in sterile transfer tubes. The aforementioned lobar samples from all dogs were individually labeled, stored, and refrigerated in individual tissue vials during shipment. One cubic centimeter, formalin-fixed samples from the white matter of the frontal lobe, parietal lobe, piriform lobe, thalamus, cerebellum, and brainstem of each of the dogs were submitted and were dried for approximately 20 hours at 95° Celsius in a gravity convection oven (Lindberg/Blue M model G01305A, VWR, Radnor, PA). The laboratory was blinded to the contrast doses corresponding to each of the samples. Each standard solution (200 µL), spiked control and unknown sample was pipetted and diluted with 5mL of a solution containing 0.5%

EDTA and Triton X-100, 1% ammonia hydroxide, 2% propanol and 20 ppb of scandium, rhodium, indium and bismuth as internal standards. An Agilent 7500ce Inductively Coupled Plasma - Mass Spectrometer (Agilent Technologies, Santa Clara, CA) was used for the analysis. The ICP-MS was tuned to yield a minimum of 6000 counts per second (cps) sensitivity for 1 ppb yttrium (89 atomic mass units), < 1.0% oxide level as determined by the 156/140 mass ratio and < 2.0% double charged ions as determined by the 70/140 mass ratio. Gadolinium was calibrated using a 5 point linear relationship of the analyte:internal standard response ratio. Bismuth (209) was used as an internal standard. Helium was used as a collision gas to control polyatomic interferences to gadolinium. The gadolinium and internal standard mix was sourced from an outside laboratory (Inorganic Ventures, Christiansburg, VA). The limit of detection for gadolinium using this method is 0.0001188 part per billion.

Scanning and transmission electron microscopy with electron probe microanalysis

SEM was performed in conjunction with TEM and electron probe microanalysis at our institutional affiliate, The Institute for Imaging and Analytical Technologies, to characterize and quantify the distribution of gadolinium deposits in brain tissue samples. Samples were fixed first in 10% neutral buffered formalin for 30 days. After primary fixation, small samples (~ 1mm square for TEM and ~ 1cm for SEM) were excised and placed into ½ Karnovsky's fixative (2% paraformaldehyde + 2.5 % glutaraldehyde) in 0.1 M sodium cacodylate buffer (pH 7.2) at 4° Celsius until further processing. After the secondary fixation, the samples were rinsed and dehydrated in a graded ethanol series.

The TEM samples were then infiltrated with Spurr's resin. Ultra-thin (~80 nm) sections were cut with a Reichert-Jung Ultracut E ultramicrotome (Reichert-Jung

Incorporated, Depew, NY) and were collected on 75 mesh formvar coated copper grids. Sections were stained with lead citrate and initially examined with a JEOL JEM-1230 TEM (JEOL USA, Peabody, MA) at 80 kV for image generation and orientation of potential gadolinium locations. Once key areas were identified, grids were reexamined at 200 kV with a JEOL JEM-2100 equipped with an Oxford EDS system (Oxford, Oxfordshire, UK) for elemental analysis.

For SEM these samples were chemically dried using hexamethyldisilazane (HMDS) and then further air dried. Dried samples were affixed to aluminum stubs using double sided carbon tape and viewed in a Zeiss EVO-50 VP SEM (Zeiss, Jena, Germany) at 10 kV and 40 Pa using the back-scattered detector for imaging and Bruker EDS system for elemental analysis.

Statistical analysis

The effect of dose on the concentration of gadolinium deposits within in the brain was assessed using linear mixed-effects models with PROC MIXED in SAS for Window 9.4 (SAS Institute, Inc., Cary, NC, USA) by a board-certified veterinary epidemiologist. For fixed tissues, a separate analysis was conducted for group 1, group 2, and group 1 and 2 combined. For the individual group analyses, dose, lobe, and the dose by lobe interaction were the fixed effects in the model. In that case, dose was the only fixed effect. Dose, group, lobe, and the dose by group, dose by lobe, and lobe by group interaction terms were the independent variables in the combined group analyses. For group 2, another analysis was conducted which compared the fresh and fixed tissues. Dose, lobe, tissue type and all two-way interactions were the fixed effects in the model. Dose was considered a continuous variable and was included as a covariate in all models.

Dog identity was included as a random effect in all models. If the interaction terms were not significant, they were sequentially removed with the term with the largest p-value removed and the model refit. Differences in least squares means with the Simulate adjustment for multiple comparisons were determined for significant main effects or interaction terms. Diagnostic plots of residuals for each outcome were assessed to ensure the assumptions of the statistical method had been met. An alpha level of 0.05 was used to determine statistical significance.

Results

Subject population

Fourteen young, purpose-bred, canine research subjects of similar age and weight (n=8 in group 1, n=5 in group 2, and n=1 in group 3), satisfied inclusion criteria for the study. All dogs were healthy, had brain tissue that was deemed normal based on gross and histologic examinations and were exposed to a single intravenous low-dose of gadodiamide *in vivo* prior to humane euthanasia. Hepatobiliary and renal serum biochemistry values, as well as the gadodiamide dosing scheme used in this study population, are summarized in Tables 5.1 and 5.2. No dogs were excluded. Dogs had no historical or current evidence of brain disease and were deemed healthy based on physical and neurophysical examination. Dogs were therefore presumed to have a normal and intact BBB prior to all interventions. The median weight of the subjects at the time of enrollment, administration of the GBCA agent, and humane euthanasia, was 23.75 kg (range=17.5–32 kg, mean=23.76 kg, IQR=8.65), and median age was 8.5 months (range=5–13 months, mean=8.6 months, IQR=5). Five dogs were intact males, 8 were intact females, and 1 was a spayed female.

All dogs had minimum database baseline CBC and serum biochemistry results within reference ranges for the species (as given in Table 5.1) and negative serum occult HTW-Ag tests.

Table 5.1 Hepatobiliary and renal serum biochemistry values for all dogs of groups 1, 2, and 3.

Group subject number	Alk Phos (U/L, reference range 11–140 U/L)	ALT (UL, reference range 10–90 U/L)	T Bili (mg/dl, reference range 0.2–0.6 mg/dL)	BUN (mg/dl, reference range 8–24 mg/dL)	Creat (mg/dl, reference range 0.5–1.4 mg/dL)
<i>Group 1</i>					
1	120	12	0.6	9	0.6
2	130	10	0.3	8	0.8
3	138	13	0.2	8	0.6
6	135	16	0.3	12	0.81
4	86	28	0.4	9	0.87
7	73	36	0.3	10	0.78
5	92	27	0.3	10	0.14
8	90	34	0.2	8	0.76
<i>Group 2</i>					
1	84	15	0.2	17	0.98
2	67	51	0.2	18	1.09
3	58	22	0.3	16	1.07
4	50	20	0.2	19	1.04
5	62	34	0.4	19	0.96
<i>Group 3</i>					
1	80	20	0.2	16	1.07

All dogs from all groups had normal hepatobiliary and renal values.

The 8 dogs of group 1 had negative serum titers for *Ehrlichia canis*, *Rickettsia rickettsii*, *Borellia burgdorferi*, and *Babesia canis* and CSF West Nile virus titers. MRI of eight dogs (group 1) demonstrated normal brain morphology, signal intensity pre-contrast administration, and normal patterns of enhancement following the IV gadodiamide administrations with no evidence of BBB disruption, deemed as such by a board-certified veterinary radiologist and 3rd year imaging resident. CSF cytology in the 8 dogs of group 1 were within normal reference ranges (protein quantification <30 mg/dL with nucleated < 5 cells/uL). Testing verified that this population purpose-bred canine subjects were negative for such infections and that exposure to infectious agents did not occur while in containment in the southeastern region where they were enrolled. Serum biochemistry tests, including renal and hepatobiliary serum chemistry tests, and CBC, were within reference range in all subjects.

Dogs of groups 1 and 2 underwent a single, IV gadodiamide exposure. Following pre-enhanced MRI, dogs of group 1 received various low doses of IV gadodiamide 3–7 days (mean=5.4, median=5, IQR=1.5) prior to humane euthanasia. For group 1, cisternal CSF centesis occurred under general anesthesia following conventional MRI, GBCA administration and CEMRI (as described in detail in Chapter II). Dogs of group 2 similarly received various low doses of IV gadodiamide 8.3–8.9 hours (mean=8.6 hours, median=8.5 hours, IQR=0.175) prior to humane euthanasia. All dogs underwent all procedures without complication, including humane euthanasia. Post mortem, the brains of the subjects were harvested no more than 3.5 hours (range=1–3.5 hours) following humane euthanasia and were kept on ice during that interim. Samples were placed in

formalin fixation and archived for 101–278 days (mean=157.8 days, median=150.5 days, IQR=86) as shown in Table 5.2.

Table 5.2 Doses of gadodiamide as administered to dogs with information regarding tissue state, timing of sample collection and total time between tissue collection (and necropsy) and gadodiamide administration for all dogs.

Group subject number	Dose of GBCA (mmol/kg)	Total volume of GBCA administered (mL)	Time between imaging and tissue collection (hours)	Time of formalin tissue Fixation (days)	Time of tissue in fresh frozen state (days)	Time between tissue collection / necropsy and ICP-MS
<i>Group 1</i>						
1	0.006	0.2	168	278	52	278
2	0.0125	0.45	120	276	52	276
3	0.025	1.0	72	274	52	274
6	0.025	0.88	96	158	52	156
4	0.05	2.5	144	157	52	158
7	0.05	2.3	168	156	52	151
5	0.1	4.0	120	151	52	157
8	0.1	4.0	144	150	52	150

Table 5.2 (Continued)

<i>Group 2</i>									
1		0.025	1.5	8.5	69	32	101		
2		0.05	3.4	8.8	69	32	101		
3		0.05	2.9	8.5	69	32	101		
4		0.1	6.1	8.7	69	32	101		
5		0.1	5.9	8.6	69	32	101		
<i>Group 3</i>									
1		0.0	0.0	8.6	69	32	101		

Effect of gadolinium exposure on tissue deposition

Brain tissue remained histopathologically and grossly normal following gadodiamide administration, and did not show any evidence of associated pathology under light microscopy. Elemental gadolinium deposition following a single intravenous exposure occurred at all doses administered, including the lowest fractional dose (approximately 1/16th of the 0.1mmol/kg dose), in all dogs except for the control. All dogs exposed, regardless of dose, demonstrated elevated levels of intracranial gadolinium in the 6 prescribed lobar regions with concentrations ranging from 1.7 to 162.5 ng Gd/g of brain tissue for group 1 and 67.3 to 1216.4 ng Gd/g of brain tissue for group 2 (Table 5.3). The highest mean gadolinium concentrations were seen within the cerebellum (mean 252.5 ng/g, range 3.2–659.0 ng/g, IQR 373.7), parietal (mean 275.8 ng/g, range 19.7–911.7 ng/g, IQR 351.8), and piriform lobes (mean 200.1 ng/g, range 22.1–839.0 ng/g, IQR 313.2). Retained gadolinium in the brains of these healthy canine subjects, quantified using ICP-MS, is shown in Table 5.3.

Table 5.3 Gadolinium deposition by lobe for all dogs of each group

Deposition by lobe of brain (ng gadolinium/ g brain tissue)						
Group and Subject number	Brainstem	Cerebellum	Frontal lobe	Parietal lobe	Piriform lobe	Thalamus
<i>Group 1</i>						
1	27.53	32.7	20.9	42.05	38.94	19.02
2	4.193	10.92	10.82	7.883	15.47	7.838
3	7.645	24.41	10.03	19.71	27.53	13.22
4	20.59	80.68	13.4	51.02	50.02	39.42

5.3 (Continued)

5	54.53	162.5	32.29	79.67	83.12	51.93
6	10.65	28.89	1.707	20.14	22.14	15.52
7	20.13	63.35	21.6	29.97	33.51	29.35
8	39.85	94.81	36.18	62.99	54.44	49.34
<i>Group 2</i>						
1	917.5	220.8	68.6	308.2	335.2	67.3
2	550.0	382.6	95.3	343.2	375.1	185.2
3	1216.4	360.9	100.5	290.7	289.9	166.7

5.3 (Continued)

4	971.1	658.9	112.6	910.3	839.0	222.6
5	927.6	363.6	102.9	716.2	330.7	174.1
Group 3						
1	5.3	3.2	0	3.1	2.4	1.4

Deposition given in ng gadolinium/g brain tissue

Statistical model with group 1 and group 2 dogs

Gadolinium tissue concentration in fixed tissues was significantly affected by the group by lobe ($p < 0.001$) interaction in the analysis that combined group 1 and 2 dogs (Table 4). The least square means (lsmeans) of gadolinium concentrations for group 1 dogs were significantly less than group 2 dogs for brain stem ($p < 0.001$), cerebellum ($p = 0.025$), parietal lobe ($p < 0.001$), and piriform lobe ($p = 0.002$). There were no significant differences in lsmeans of gadolinium concentrations between groups for frontal lobe white matter ($p = 0.999$) or thalamus ($p = 0.975$). There were no significant differences of the lsmeans between lobes of the brain in group 1 dogs ($p > 0.999$). In group 2, gadolinium concentrations were greater in the brainstem than in the cerebellum ($p < 0.001$), frontal lobe white matter ($p < 0.001$), parietal lobe ($p < 0.001$), piriform lobe ($p < 0.001$), and thalamus ($p < 0.001$). The gadolinium concentrations in the cerebellums of group 2 dogs were significantly greater than in the frontal lobe white matter ($p = 0.019$) but were not significantly different than in the parietal lobe ($p = 0.942$), piriform lobe ($p = 1.000$), or thalamus ($p = 0.150$). Concentrations in the parietal lobe of group 2 dogs were significantly greater than in frontal lobe white matter ($p < 0.001$) and thalamus ($p = 0.003$) but were not significantly different from concentration in the piriform lobe ($p = 0.996$). Concentrations in the piriform lobe of group 2 dogs were significantly greater than in frontal lobe white matter ($p = 0.004$) and approaching the alpha level for thalamus ($p = 0.051$). Concentrations in the frontal lobe white matter and thalamus were not significantly different ($p = 0.999$). The group by dose interaction was also significant ($p < 0.001$) in the analysis that combined group 1 and 2 dogs. The regression plots of tissue concentration by dose for group 1 and group 2 dogs are presented in Figure 5.1.

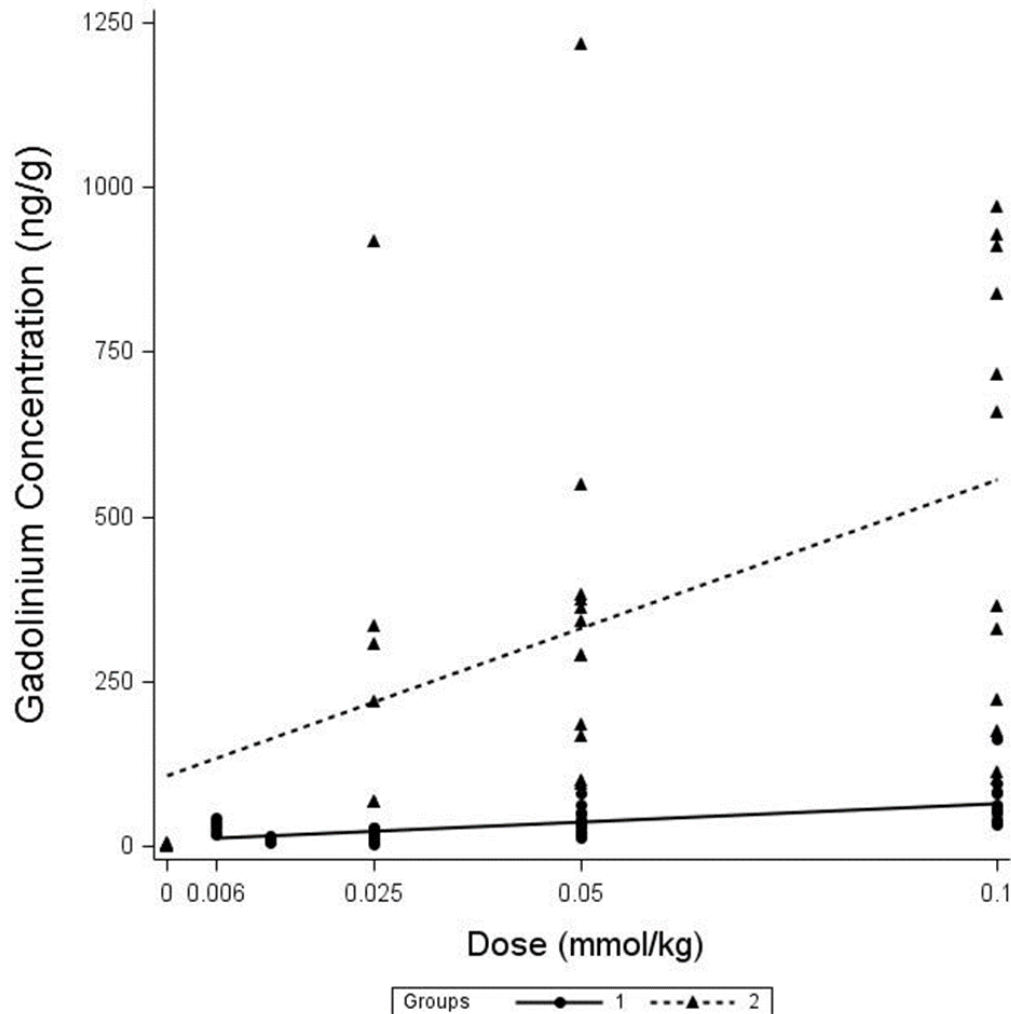


Figure 5.1 Regression lines of gadolinium concentrations (ng/g) by dose (mmol/kg) for group 1 and group 2 dogs.

The gadolinium concentrations are the values predicted by the linear mixed model with dose, group, lobe, and the group by lobe and group by dose interactions as fixed effects and dog identity as a random effect. Data points are the actual measured values of the gadolinium concentrations as determined by ICP-MS.

Model with group 1 dogs

Due to the significant interactions with group, data from group 1 and 2 dogs were analyzed separately. In group 1 dogs, gadolinium concentration in fixed tissue was significantly affected by the dose by lobe interaction ($p < 0.001$). Within the brain lobes,

the response to dose for cerebellum was significantly different than for the other brain lobes ($p < 0.001$). The regression plots of tissue concentration by dose for each of the lobes is shown in Figure 5.2.

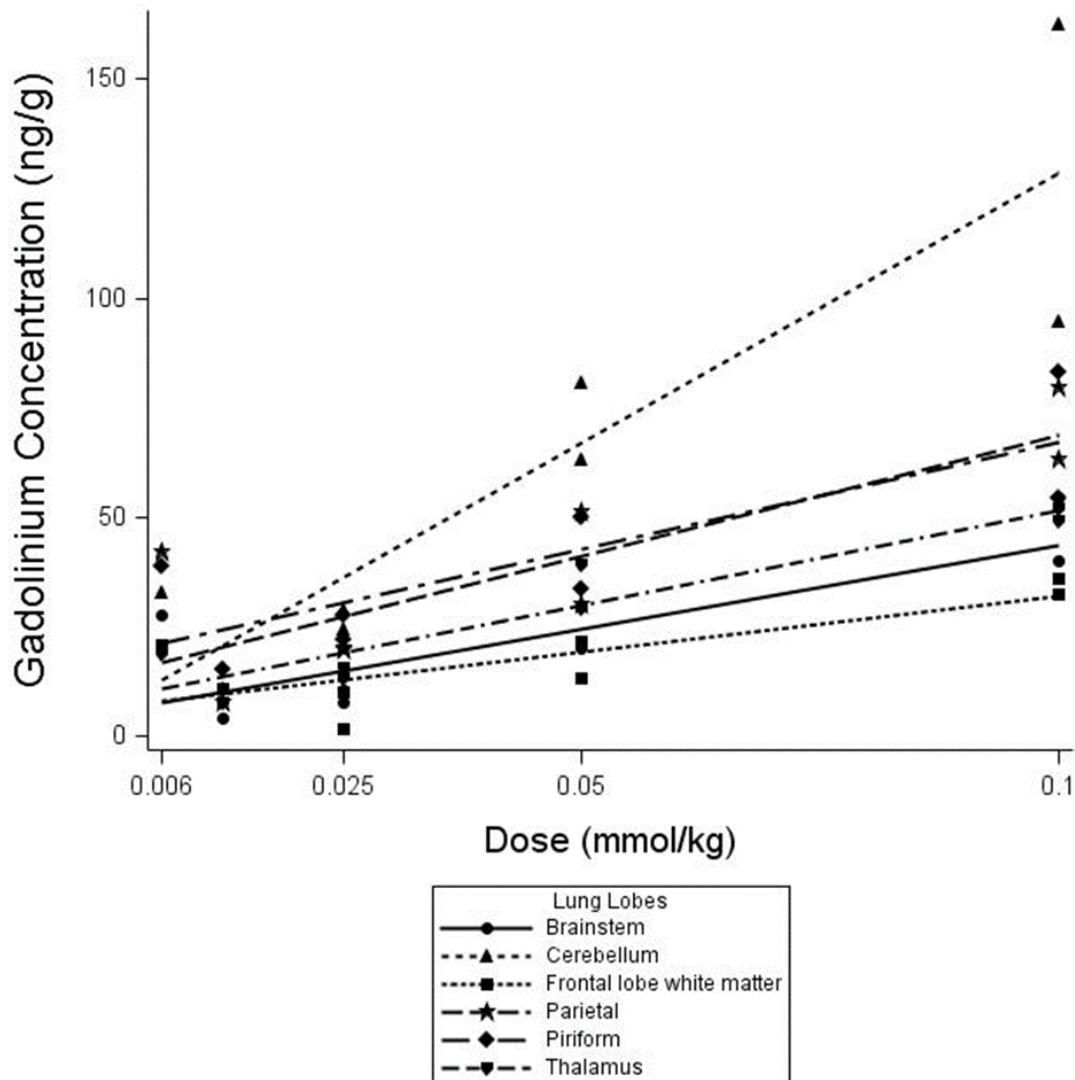


Figure 5.2 Regression lines of gadolinium concentrations (ng/g) by dose (mmol/kg) for each brain lobe of group 1 dogs.

The gadolinium concentrations are the values predicted by the linear mixed model with dose, lobe, and the lobe by dose interaction as fixed effects and dog identity as a random effect. Data points are the actual measured values of the gadolinium concentrations as determined ICP-MS.

Model with group 2 dogs

In group 2 dogs, gadolinium concentration in fixed tissue was significantly affected by lobe ($p < 0.001$) (Table 5). Gadolinium concentration were greater in the brainstem than in the cerebellum ($p = 0.005$), frontal lobe white matter ($p < 0.001$), parietal lobe ($p = 0.043$), piriform lobe ($p = 0.009$), and thalamus ($p < 0.001$). The gadolinium concentration in the cerebellums of group 2 dogs were not significantly greater than in the frontal lobe white matter ($p = 0.210$), parietal lobe ($p = 0.941$), piriform lobe ($p = 1.000$), or thalamus ($p = 0.465$). Concentrations in the frontal lobe white matter of group 2 dogs were significantly lower than in the parietal lobe ($p = 0.031$) but were not significantly different from those of piriform lobe ($p = 0.127$) or thalamus ($p = 0.995$). Concentrations in the parietal lobe of group 2 dogs were not significantly different than those in the piriform lobe ($p = 0.989$) or thalamus ($p = 0.104$). Gadolinium concentrations in the piriform lobe of group 2 dogs were not significantly different than concentrations in the thalamus ($p = 0.314$). Gadolinium tissue concentrations were also significantly affected by dose ($p < 0.001$), but there was not a significant dose by lobe effect ($p = 0.123$) as was seen in group 1 dogs. The regression plot of gadolinium concentration by dose for the group 2 dogs is shown in Figure 5.3.

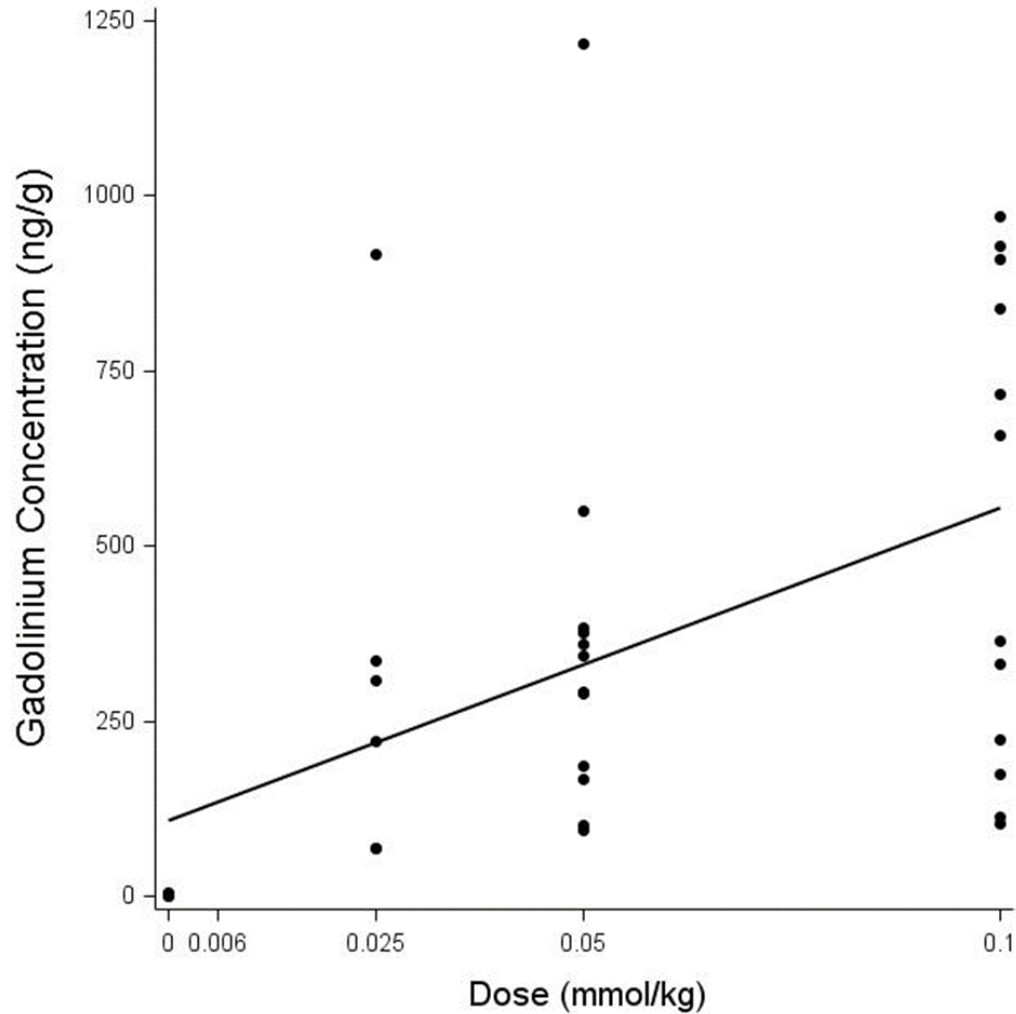


Figure 5.3 Regression line of gadolinium concentrations (ng/g) by dose (mmol/kg) for group 2 dogs.

The gadolinium concentrations are the values predicted by the linear mixed model with dose and lobe as fixed effects and dog identity as a random effect. Data points are the actual measured values of the gadolinium concentrations as determined by ICP-MS.

Model with group 2 dogs comparing tissue type

No significant differences in the gadolinium concentrations were found between fixed and fresh tissues from group 2 dogs ($p=0.430$). There was a significant effect on concentrations by brain lobe ($p<0.001$), irrespective of tissue type or dose (Table 5.3).

Gadolinium concentrations were not significantly greater in the brainstem than in cerebellum ($p=0.068$) or parietal lobe ($p=0.266$). They were significantly greater in the brainstem than in frontal lobe white matter ($p<0.001$), piriform lobe ($p=0.007$), and thalamus ($p<0.001$). The gadolinium concentrations in the cerebellum were significantly greater than in the frontal lobe white matter ($p=0.016$) but not in parietal lobe ($p=0.987$), piriform lobe ($p=0.955$), or thalamus ($p=0.097$). Concentrations in the frontal lobe white matter were significantly lower than in the parietal lobe ($p=0.003$) but were not significantly different from those of piriform lobe ($p=0.144$) or thalamus ($p=0.982$). Concentrations in the piriform lobe were not significantly different than those in the parietal lobe ($p=0.673$) or thalamus ($p=0.474$). Gadolinium concentrations in the parietal lobe were significantly greater than concentrations in the thalamus ($p=0.019$). Gadolinium tissue concentrations were also significantly affected by dose ($p=0.003$). The regression plot of gadolinium concentration by dose from the model which included tissue type and lobe for the group 2 dogs is shown in Figure 5.4.

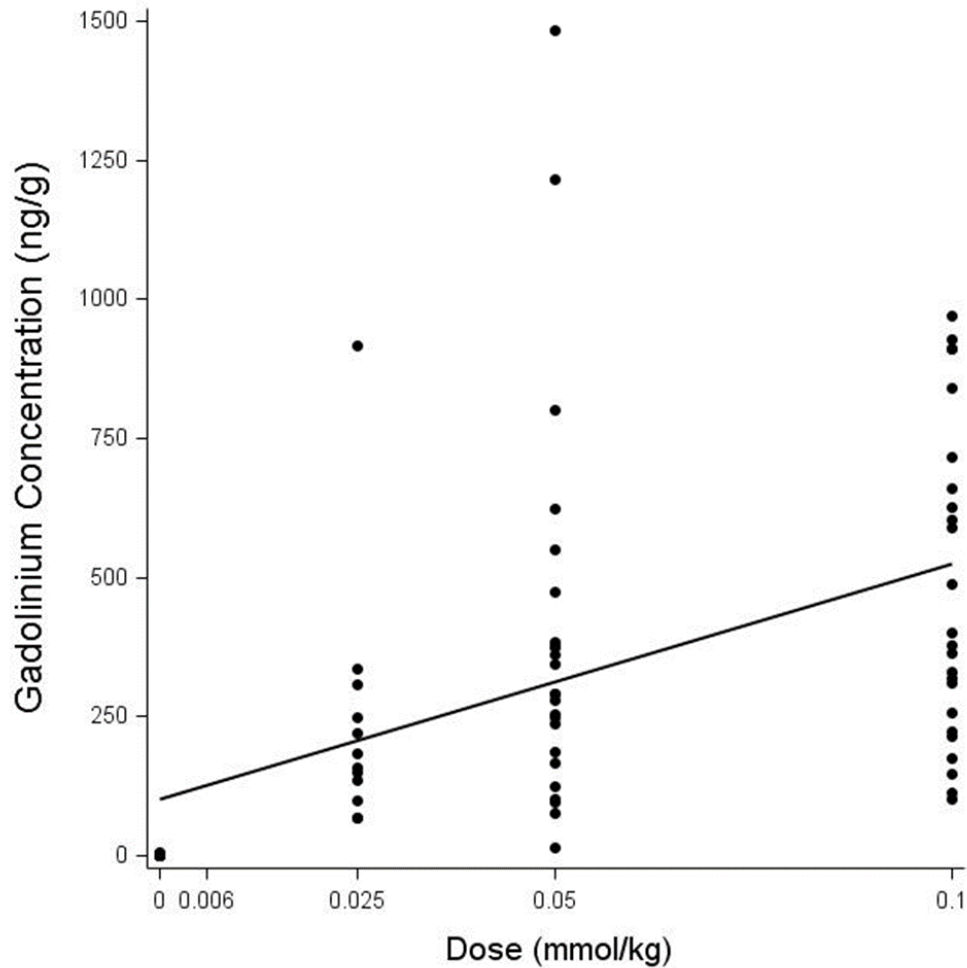


Figure 5.4 Regression line of gadolinium concentrations (ng/g) by dose (mmol/kg) for group 2 dogs.

The gadolinium concentrations are the values predicted by the linear mixed model with tissue type, dose and lobe as fixed effects and dog identity as a random effect. Data points are the actual measured values of the gadolinium concentrations as determined by ICP-MS.

For dogs of group 1, gadodiamide dose administered was strongly positively correlated with parenchymal gadolinium tissue concentration (R-square 0.73); however, for dogs of group 2, dose was not correlated with parenchymal gadolinium deposition.

There was no statistical correlation between age and deposition, weight and deposition, or

gender and deposition. The deposition by lobe and deposition by dose did not correlate between dogs of group 1 and group 2 for either fresh or fixed brain tissue.

Localization of gadolinium within neuronal tissue and assessment of histologic change

When evaluated with SEM, gadolinium was not detected in any of the tissue samples. Six lobar samples from dogs administered either 0.1 mmol/kg (n=2) or 0.05 mmol/kg (n=1) gadodiamide were evaluated with TEM. TEM demonstrated several angular, irregularly shaped structures with a mean length of 1009 nm (range 683–1360 nm), throughout the examined tissue. These structures displayed sharp margins. For group 1 dogs, all structures were within the vascular endothelial cells; for group two dogs, however, some were membrane bound within the neuropil. This is likely consistent with cellular pinocytosis.¹⁰⁰ These structures demonstrated an L-series K-edge of 2.111, consistent with gadolinium, and corresponded to approximately 0.19% of the weight of the sample. The membrane around the gadolinium confirmed they were intracellular within the neuropil, however exact cell types containing the gadolinium could not be determined due to the sample being unstained to avoid contamination. Other elements found in the samples included carbon, oxygen, sodium, magnesium, silicon, sulfur, chlorine, cobalt, nickel, copper, and lead.

Discussion

The author reports herein gadolinium deposition in brain tissue of healthy dogs with normal renal and hepatobiliary function following a single IV exposure of fractional gadodiamide doses. No previous studies have explored the neural deposition of gadodiamide in dogs, nonhuman primates or in people lacking evidence of serious

systemic disease and multiorgan failure following a single administration of a GBCA. Herein the author describes some of the features of neuronal deposition following the intravenous deposition of fractional doses of gadolinium (gadodiamide), ranging from 0.006–0.05 mmol/kg, which are well below the recommended (and reported) human and companion animal dosing schemes.

Gadolinium deposition

Gadolinium deposits were found within the brains of all healthy canine subjects evaluated, at all doses, following a single IV administration of the non-ionic linear GBCA, gadodiamide. Brain tissue deposits were noted after administration of doses lower than the established recommended human dose range in all but the control dog. These depositions were seen within the vascular endothelium in 3-7 days (in the case of group 1 dogs) and within the neuropil in 8.3–8.9 hours (in the case of the group 2 dogs) post-intravenous exposure to gadodiamide. When compared to *ex vivo* studies in people, results of this study show the pattern of deposition in brain tissue of dogs of group 1 closely followed those recently described in people, specifically dose dependency in the thalamus, white matter of the frontal lobe, and cerebellum.^{105,166} Gadolinium deposition occurred despite the fact that, in the evaluated population of dogs, dosing and administration were limited to a single, 0.1 mmol/kg or fractional dose. This information complements earlier studies that describe deposition of gadolinium within the human brain of repeatedly scanned clinical patients having both single and multiple doses of a GBCA for CEMRI despite the presumption of normal BBB integrity.^{113,166} Although all of the patients in those studies had systemic illnesses, many had normal renal and hepatobiliary function and normal estimated GFR.^{105,166} Prior studies have used ICP-MS

to show gadolinium deposition in the bone from patients undergoing total hip arthroplasties and to report gadolinium deposition in the femora of patients with normal renal function.^{165,175} Further, ICP-MS was used to quantify gadolinium in the skin in 13 patients suffering from nephrogenic systemic fibrosis, and resulted in a mean gadolinium concentration of 71.4 $\mu\text{g/g}$ in these patients.¹⁴⁸ Additionally, studies investigating intracranial gadolinium deposition in people administered both linear and macrocyclic agents were quantified using ICP-MS.^{105,113,166} Historically, investigations in people having parenchymal depositions had serious systemic illness and succumbed to their diseases regardless of whether or not hepatobiliary and renal function tests were normal.^{105,113,166} Results of the current study confirms that intracranial gadolinium deposition occurs in the vascular endothelium and neuropil of the brains of healthy dogs, with normal hepatic and renal function, as early as 3 days and 8 hours, respectively, following IV injection. Previous work in murine models confirmed deposition in healthy subjects of these species; however, this deposition occurred following 20 injections at 0.6 mmol/kg, whereas the current study shows deposition following a single injection of a fractional dose ranging from 0.006–0.1 mmol/kg.¹⁵⁵

Gadolinium deposition did not occur in the fresh tissues of the control dog in this study via ICP-MS. In the fixed samples in the same dog, however, trace amounts of gadolinium were quantified within the parietal lobe (3.1 ng/g), piriform lobe (2.4 ng/g), and thalamus (1.4 ng/g) lobes. This finding is in concert with recent results from other studies in which control patients (having had no previous exposure to gadolinium by way of GBCA administration for CEMRI, and brain sample quantification by way of ICP-MS), demonstrated trace amounts of gadolinium deposition (up to 0.2 ng/g) in numerous

brain regions.¹¹³ The results from the control dog in the current study were, as in the previous study, orders of magnitude lower than the results from the exposed dogs. The investigating physicians of the previous study attributed this finding to small environmental exposures.¹¹³ Given inability to document gadolinium deposition in fresh tissues from the same (control) patient, specific consideration in this study is also given to contamination during preparation for fixation and/or (mechanical) residuals during any step of pre-processing on surfaces or at any point during ICP-MS.

Dose dependency

The degree of gadolinium deposition in the canine subjects of this study was dose dependent for all lobes in all dogs of group 1, following a linear regression with an R-square value of 0.73. These dogs were given the drug 3–7 days prior to humane euthanasia suggesting that once administered, deposition may begin to occur, at any dose, sooner than 48 hours following administration. Contrary to expectations, the results of group 2 contradicted the lobar affinity and dose deposition profiles of those of group 1 in that dose dependency was not observed, and a linear regression could not be fit to these data. This result can be attributed to the difference in sampling timing between the two groups of dogs. Dogs in group 1 were exposed to gadolinium 3–7 days prior to euthanasia, whereas dogs in group 2 were exposed to gadolinium only 8.3–8.9 hours prior to euthanasia. Previous pharmacokinetic studies in both people and animals, using numerous GBCAs, have suggested an extracellular distribution of gadolinium, with 90–99% of the gadolinium being excreted unchanged in the urine within 72 hours of administration, and the remaining being cleared via hepatic clearance in the bile.^{100,101,176}

The findings of the current study and other recent studies in people demonstrating

deposition in both the brain and the bone, suggests a more complicated pharmacokinetic behavior than what was previously believed.^{165,166,175} Although conjectural, and an idea that warrants further investigation, it is possible that some degree of redistribution of gadolinium or gadolinium chelate occurs sometime between 8 and 48 hours following intravenous administration, which may have resulted in the difference in deposition pattern seen between the two groups of dogs in this study.

The author found that the brains of dogs administered a single, fractional dose of gadolinium contained an average of 0.028% of the total dose (group 1=0.02%, group 2=0.04%) over the 6 lobes of brain evaluated per gram of brain mass, representing only a small portion of the total accumulation for a given dog within the brain.

Prior studies

No published studies are available for which to compare the results of the current study. The current study complements historical observations of several studies in which intracranial gadolinium deposits were present in people having had single or multiple doses of GBCAs.^{105,113,156,166,177} Similarly, deposition of gadolinium occurred in all healthy dogs having no clinical evidence of hepatobiliary or renal dysfunction. The results herein provide direct evidence that gadolinium begins to deposit within the neuropil regardless of dose and following a single 0.1 mmol/kg or fractional dose exposure to gadodiamide compared to the control subject that received a placebo small volume of saline. The control also served to validate quantification methods and provide a comparison for SEM and TEM evaluation. The presence of gadolinium in the neuropil within hours (range 8.3–8.9 hours) following the administration of fractional doses demonstrates that deposition may not be limited to that acquired by way of repository

accumulations in the bone matrix by way of slow release and organ reuptake of a sequestered pool of gadolinium.^{165,175} In addition, the results herein support potential early widespread interstitial brain parenchymal exposure (between 8.8–8.9 hours) and vascular endothelial (at 3–7 days) and biodistribution of the unexcreted fraction of gadolinium residuals, and represent the likelihood of more complex pharmacokinetics than what is currently understood. Furthermore, the presence of gadolinium in the normal brain tissue of dogs with no physical or MR imaging evidence of BBB disruption challenges the current understanding of how GBCAs interact with an intact BBB in healthy subjects with no historical or current brain afflictions, or other systemic diseases.

Physiology

The integrity of the BBB and its permeability is affected to varying degrees by multiple disease processes, which is why purpose-bred, healthy dogs with no current or historical evidence of brain disease were evaluated in this study. When the BBB is disrupted, or when abnormal vascularity is present, gadodiamide can accumulate within lesions such as neoplasms, abscesses, and subacute infarcts.¹⁷⁸ McDonald et al evaluated formalin-fixed, cadaveric samples of brain (from regions of brain that were at a minimum of 2 cm from external beam radiation exposed tissue, or 4 cm from a brain lesion) obtained from gadolinium exposed people with historical multiple gadodiamide administrations with x-ray microanalysis/densitometry.¹⁶⁶ That study presumed normal BBB integrity and found that 18%–42% of the administered gadolinium had crossed the BBB with deposition into the neural tissue interstitium.¹⁶⁶ The remainder of the agent was sequestered in non-uniform fashion within the endothelial wall of neuronal capillaries in large clustered foci, similar to results from groups 1 and 2 in the current study.¹⁶⁶

The mechanism by which gadolinium deposits within the normal brain is poorly understood. Brain-wide paravascular or glymphatic CSF and interstitial fluid (ISF) exchange for clearance of solutes and waste using dynamic CEMRI is described in murine models.¹⁷⁹ Gadolinium allows for the identification of waste influx at key anatomical influx nodes, specifically the pituitary and pineal gland recesses.¹⁷⁹ In addition, kinetic parameters that characterize influx and clearance routes of paramagnetic contrast agents are defined, and glymphatic CSF and ISF exchange and solute clearance is generally described.¹⁷⁹ CSF secretion and reabsorption is not limited to traditional modeling of CSF secretion and the historical understanding of kinematics wherein only the antegrade flow of CSF occurs.¹⁸⁰

In mice, a large portion of subarachnoid CSF recirculates throughout the brain parenchyma along paravascular spaces and exchanges with the interstitial fluid along such routes, and through the interstitium, by way of transglial water movement through astrocytic aquaporin-4 (AQP4) water channels, facilitating the clearance of interstitial solutes.¹⁸⁰ The retrograde paravascular influx of paramagnetic contrast agents from the subarachnoid space rapidly enters the brain parenchyma by way of Virchow-Robin spaces along the para-arterial channels.¹⁸⁰ In the author's opinion, these regions and pathways provide not only a conduit for solute uptake from the brain, but potentially one for deposition to the brain parenchyma. It is plausible, although unproven, that the clearance pathways captured by gadolinium enhanced MRI may elucidate the potential pathway of parenchymal exposure and therein, deposition (Jennifer Gambino, personal communication, January 17, 2017).

Important factors to consider that may or may not contribute to the deposition of gadolinium within the parenchyma are the physical state of gadolinium at the time of parenchymal exposure, the physiologic mechanisms or events that drive ionization (which may be unique to individual patient and disease state and over all sequestration), deposition, and neuroanatomic affinity of the elemental gadolinium and the chelate. These details remain incompletely understood.¹⁶⁶ Further, the physical state of the element cannot be speciated in tissue by currently described methods.^{105,113,166} Chelates are historically considered stable pharmaceutical entities. Results of the current, and other recent historical studies support the contrary.^{113,166} GBCAs do not bind to human serum proteins *in vitro* and have no biotransformation (or evidence of metabolism) occurring in urine and fecal matter.^{89,181} In a murine model, radiocarbon tracing of the GBCA ligand demonstrated that, for a given organ compartment, elimination of the compound depends on the respective organ with clearance of gadolinium and the ligand being identical (when measured independently).^{89,182} Thus, the conclusion that disassociation does not take place is erroneously based on a premise that lacks more specific speciation of the excreted individual components (the ligand and the ion, respectively). Further, it is highly plausible that *in vitro* findings cannot be translated over to the *in vivo* pharmacokinetics of these agents.^{89,183}

In general, GBCAs are analogous to iodinated radiographic agents in that they have rapid renal excretion (unchanged) by way of glomerular filtration, a short half-life (1–2 hours), and greater than 90% of an administered dose can be recovered from the urine 3 hours following IV administration.⁸⁷ In people and animals, the pharmacokinetic parameters of gadodiamide are not well known, and detectable biotransformation or

decomposition of the agent is not previously reported.¹⁸⁴ GBCAs were, since the inception of their use, not thought to cross the intact blood brain barrier and thus were presumed not to accumulate in normal brain or in lesions that do not have an abnormal BBB such as cysts and mature post-operative scar tissue.¹⁸⁴ In normal subjects, when administered intravenously, gadodiamide conforms to a two-compartmental (extracellular) model with mean distribution and elimination half-lives (reported as a mean \pm SD) of 3.4 \pm 2.7 minutes and 77.8 \pm 16 minutes, respectively.¹⁸⁴ Within twenty-four hours following administration, gadodiamide is eliminated almost entirely in the urine (95.5% \pm 5%), with nearly identical renal and plasma clearance rates of 1.7 and 1.8 mL/min/kg, respectively, and a volume of distribution similar to that of extracellular water (approximately 200 \pm 61 mL/kg).¹⁸⁴

Study limitations

The current study had several limitations. The sample numbers were small, and dogs evaluated were young and limited to the age range we described. The number of dogs was limited by number of available dogs for terminal surgical laboratories, the ethical and monetary expense of purpose-bred dogs and cost of MR evaluation. These factors often preclude large prospective studies of this nature in veterinary medicine. Limitations in subject number lead to limitations in the choice of dosing scheme(s) investigated. A larger subject pool would have likely reduced the variability of measurements amongst samples and would have lent greater power to the study. Additionally, the author did not investigate the typical higher end of the dose range administered to people and companion animals (0.2–0.3 mmol/kg). Clinical protocols for GBCA use as established by the author's institution do not exceed doses beyond 0.1

mmol/kg in people or companion animals undergoing CEMRI. Thus, the author chose to evaluate levels of accumulation for frequently administered doses of the veterinary patients seen at the author's institution. Only one control dog was available for verification of analyses. The author concludes that a negative control sufficiently addresses the potential for natural and/or environmental exposure in these dogs and verifies the techniques used. Levels of gadolinium deposition were not quantified in entirety (i.e. grams of Gd/entire brain) for each of the subjects, nor was deposition of gadolinium in other organs evaluated. This limitation was due to limited financial resources, and there was concern that if these analyses were performed, the testing may undermine attempts to discover data supporting dose dependency, neurotropic changes and regional neuroaffinity. Because the current study was limited to a single linear GBCA, the findings herein are likely not directly applicable to non-linear or macrocyclic GBCAs. Although preliminary hepatobiliary and renal function of all dogs was normal, estimated GFR (eGFR) calculation, nuclear scintigraphy or computed tomographic GFR estimation were not performed. A relevant eGFR estimate equation is not available across the breeds or veterinary species and the author had no reason to suspect underlying renal insufficiency in this population based on laboratory and clinical evaluation. Further, urine specific gravity and urinalyses results were not obtained in the evaluated dogs. Regardless, the author had no reason to believe any of the dogs had impaired renal function. Finally, the physical chelation state of the neuronal gadolinium deposited in these dogs was not determined. This is a technological limitation, as speciation of neuronal gadolinium deposits in formalin-fixed tissue is not currently available.^{89,166}

Conclusion

In conclusion, a single, full or fractional, IV administration of gadodiamide is associated with dose dependent deposition in the neuropil of neuronal tissues, unrelated to renal and hepatobiliary function. The author and cohorts were able to determine that the gadolinium was membrane bound and therefore within the neuropil. The exact cell type, however, could not be determined due to secondary mechanical distortion of the cell, using an unstained sample and not focusing the electron microscope to preserve the sample. Although a goal of the study was to describe the deposition and lobar affinities for gadodiamide administered at two time points in healthy dogs, the histological phenotype of deposited gadolinium was not found.

Admittedly, the discovery of parenchymal brain gadolinium deposits are likely not pertinent to the clinical outcome of companion animals receiving GBCAs with regard to long-term deleterious cognitive or physiologic effects, and to date, extensive evidence and literature as to what those effects may be in people has yet to surface. Furthermore, it will likely not be feasible to assess subtle clinical signs related to low or clinical dose exposures to GBCAs in veterinary patients.

A goal of a separate study, however, (as described in Chapter IV) was to find lower clinical dosing schemes that would provide adequate conspicuity of normal brain structures with CEMRI given historical relationship of dose and dose dependent adverse events.¹⁴⁰⁻¹⁴² This led to the discovery that a single, fractional dose as low as 0.006 mmol/kg has the potential to deposit within the brains of healthy, otherwise uncompromised dogs. The findings of the study herein are translatable to people. Dogs have been diagnosed with approximately 300 of the 400 intracranial diseases described in

people, making them a viable model for human intracranial disease.¹⁸⁵ Currently, no evidenced based literature exists defining clinical syndromes attributable solely to gadolinium exposure in people or animals. The dog however, can serve as a viable *in vivo* translational model for future investigation of deposition profiles of various GBCAs and chelate agents. This study provides transformative data that may be relevant to the continued use of gadodiamide (and linear GBCAs) in routine CEMRI studies for both clinical purposes and for research in people.

Results from the current study may aid clinicians in discretionary decision making with regard to choice of GBCA (i.e. linear versus macrocyclic, or otherwise) and may mitigate future use of linear GBCAs in healthy human subjects participating in prospective MRI studies, in pediatric patients, and in those patients in which the use of a GBCAs is not essential to patient care, follow up or quality of life. Potential clinical implications or ramifications of gadolinium deposition and accumulation in the brain and other organs are yet to be determined. Future research following the outcomes of patients having already received these agents are warranted in order to determine if gadolinium retention poses a safety risk or causes long-term health consequences in both people and animals. The work herein may serve as an impetus for the following: evaluating other classes of GBCAs and the use of gadolinium nanoparticles for CEMRI, investigating novel and safer methods of chelation, investigating mechanisms by which GBCAs cross the BBB, and exploring alternative means of increasing the sensitivity and specificity of MR imaging while limiting the use of linear GBCAs to clinical cases necessitating the agents.

REFERENCES

1. Gavin P. Growth of clinical veterinary magnetic resonance imaging. *Veterinary Radiology & Ultrasound*. 2011;**52**: s2-s4.
2. Xu V, Chan H, Lin A, Sailasuta N, Valencerina S, Tran T, et al. MR spectroscopy in diagnosis and neurological decision-making. *Semin Neurol*. 2008;**28**: 407-422.
3. Young IR. *Methods in biomedical magnetic resonance imaging and spectroscopy*. Chichester ; New York: Wiley, 2000.
4. De Graaf RA. *In vivo NMR spectroscopy : principles and techniques*. Chichester, West Sussex, England ; Hoboken, NJ: John Wiley & Sons, 2007.
5. Rabi II. The Molecular Beam Resonance Method for Measuring Nuclear Magnetic Moments. The Magnetic Moments of. *Physics Review*. 1939;**55**: 526.
6. Curry TS, Dowdey JE, Murry RC. *Christensen's Physics of Diagnostic Radiology*: Lea & Febiger, 1990.
7. Bushberg JT. *The essential physics of medical imaging*. Philadelphia: Wolters Kluwer Health/Lippincott Williams & Wilkins, 2012.
8. Purcell E, Torrey H, Pound R. Resonance Absorption by Nuclear Magnetic Moments in a Solid. *Physical Review*. 1946;**69**: 37-38.
9. Bloch F. Nuclear Induction. *Physical Review*. 1946;**70**: 460-474.
10. Proctor WG, Yu FC. The Dependence of a Nuclear Magnetic Resonance Frequency upon Chemical Compound. *Physical Review*. 1950;**77**: 717-717.
11. Proctor WG, Yu FC. The dependence of a nuclear magnetic resonance frequency upon chemical compound [6]. *Physical Review*. 1950;**77**: 717.
12. Shaw TM, Elsken RH. Nuclear Magnetic Resonance Absorption in Hygroscopic Materials. *J Chem Phys*. 1950;**18**: 1113-1114.
13. Andrew ER. *Nuclear Magnetic Resonance*: Cambridge University Press, 1955.
14. Odeblad E, Lindstrom G. Some preliminary observations on the proton magnetic resonance in biologic samples. *Acta Radiologica*. 1955;**43**: 469-476.

15. Ernst RR, A AW. Application of Fourier Transform Spectroscopy to Magnetic Resonance. *Rev Sci Instrum.* 1966;**37**: 93-102.
16. Damadian R. Tumor detection by nuclear magnetic resonance. *Science.* 1971;**171**: 1151-1153.
17. Hinshaw W, Andrew E, Bottomley PA, Holland G, Moore W, Worthington B. Display of cross sectional anatomy by nuclear magnetic resonance imaging. *The British journal of radiology.* 1978;**51**: 273-280.
18. Hansen G, Crooks LE, Davis P, De Groot J, Herfkens R, Margulis A, et al. In vivo imaging of the rat anatomy with nuclear magnetic resonance. *Radiology.* 1980;**136**: 695-700.
19. Mansfield P, Pykett I, Morris P, Coupland R. Human whole body line-scan imaging by NMR. *The British journal of radiology.* 1978;**51**: 921-922.
20. Smith F, Hutchison J, Mallard J, Johnson G, Redpath T, Selbie R, et al. Oesophageal carcinoma demonstrated by whole-body nuclear magnetic resonance imaging. *Br Med J (Clin Res Ed).* 1981;**282**: 510-512.
21. Lanzer P, Botvinick E, Schiller N, Crooks L, Arakawa M, Kaufman L, et al. Cardiac imaging using gated magnetic resonance. *Radiology.* 1984;**150**: 121-127.
22. Skoch A, Jiru F, Bunke J. Spectroscopic imaging: Basic principles. *European Journal of Radiology.* 2008;**67**: 230-239.
23. Ruiz-Cabello J, Barnett BP, Bottomley PA, Bulte JWM. Fluorine ((19)F) MRS and MRI in biomedicine. *NMR in biomedicine.* 2011;**24**: 114-129.
24. Bitar R, Leung G, Perng R, Tadros S, Moody AR, Sarrazin J, et al. MR pulse sequences: what every radiologist wants to know but is afraid to ask. *Radiographics.* 2006;**26**: 513-537.
25. Rodenas S, Pumarola M, Gaitero L, Zamora A, Anor S. Magnetic resonance imaging findings in 40 dogs with histologically confirmed intracranial tumours. *Veterinary journal (London, England : 1997).* 2011;**187**: 85-91.
26. Wolff CA, Holmes SP, Young BD, Chen AV, Kent M, Platt SR, et al. Magnetic resonance imaging for the differentiation of neoplastic, inflammatory, and cerebrovascular brain disease in dogs. *Journal of veterinary internal medicine / American College of Veterinary Internal Medicine.* 2012;**26**: 589-597.

27. Young BD, Levine JM, Porter BF, Chen-Allen AV, Rossmeisl JH, Platt SR, et al. Magnetic resonance imaging features of intracranial astrocytomas and oligodendrogliomas in dogs. *Veterinary radiology & ultrasound : the official journal of the American College of Veterinary Radiology and the International Veterinary Radiology Association*. 2011;**52**: 132-141.
28. Palus V, Volk HA, Lamb CR, Targett MP, Cherubini GB. MRI features of CNS lymphoma in dogs and cats. *Veterinary radiology & ultrasound : the official journal of the American College of Veterinary Radiology and the International Veterinary Radiology Association*. 2012;**53**: 44-49.
29. Guzmán-De-Villoria JA, Mateos-Pérez JM, Fernández-García P, Castro E, Desco M. Added value of advanced over conventional magnetic resonance imaging in grading gliomas and other primary brain tumors. *Cancer Imaging*. 2014;**14**: 35.
30. Callot V, Galanaud D, Le Fur Y, Confort-Gouny S, Ranjeva J-P, Cozzone PJ. 1H MR spectroscopy of human brain tumours: a practical approach. *European Journal of Radiology*. 2008;**67**: 268-274.
31. Soares DP, Law M. Magnetic resonance spectroscopy of the brain: review of metabolites and clinical applications. *Clinical Radiology*. 2009;**64**: 12-21.
32. Hajek M, Dezortova M. Introduction to clinical in vivo MR spectroscopy. *European Journal of Radiology*. 2008;**67**: 185-193.
33. Barker PB, Bizzi A, De Stefano N. *Clinical MR spectroscopy: techniques and applications*: Cambridge University Press, 2010.
34. Ross B, Bluml S. Magnetic resonance spectroscopy of the human brain. *The Anatomical record*. 2001;**265**: 54-84.
35. Panigrahy A, Nelson M, Jr., Blüml S. Magnetic resonance spectroscopy in pediatric neuroradiology: clinical and research applications. *Pediatr Radiol*. 2010;**40**: 3-30.
36. Sibtain NA, Howe FA, Saunders DE. The clinical value of proton magnetic resonance spectroscopy in adult brain tumours. *Clinical Radiology*. 2007;**62**: 109-119.
37. Stadler KL, Ober CP, Feeney DA, Jessen CR. Multivoxel proton magnetic resonance spectroscopy of inflammatory and neoplastic lesions of the canine brain at 3.0 T. *Am J Vet Res*. 2014;**75**: 982-989.
38. Carrera I, Kircher PR, Meier D, Richter H, Beckman K, Dennler M. In vivo proton magnetic resonance spectroscopy for the evaluation of hepatic encephalopathy in dogs. *Am J Vet Res*. 2014;**75**: 818-827.

39. Shutter L, Tong KA, Holshouser BA. Proton MRS in acute traumatic brain injury: role for glutamate/glutamine and choline for outcome prediction. *Journal of neurotrauma*. 2004;**21**: 1693-1705.
40. Macri MA, D'Alessandro N, Di Giulio C, Di Iorio P, Di Luzio S, Giuliani P, et al. Region-specific effects on brain metabolites of hypoxia and hyperoxia overlaid on cerebral ischemia in young and old rats: a quantitative proton magnetic resonance spectroscopy study. *Journal of Biomedical Science*. 2010;**17**: 14.
41. Kingsley PB, Shah TC, Woldenberg R. Identification of diffuse and focal brain lesions by clinical magnetic resonance spectroscopy. *NMR in Biomedicine*. 2006;**19**: 435-462.
42. Carrera I, Richter H, Beckmann K, Meier D, Dennler M, Kircher PR. Evaluation of intracranial neoplasia and noninfectious meningoencephalitis in dogs by use of short echo time, single voxel proton magnetic resonance spectroscopy at 3.0 Tesla. *American Journal of Veterinary Research*. 2016;**77**: 452-462.
43. Power C, Moench T, Peeling J, Kong PA, Langelier T. Feline immunodeficiency virus causes increased glutamate levels and neuronal loss in brain. *Neuroscience*. 1997;**77**: 1175-1185.
44. Dennler M, Carrera I, Beckmann K, Ritz J, Rütten M, Kircher PR. IMAGING DIAGNOSIS—CONVENTIONAL AND FUNCTIONAL MAGNETIC RESONANCE IMAGING OF A BRAIN ABSCESS IN A GOAT. *Veterinary Radiology & Ultrasound*. 2014;**55**: 68-73.
45. Prost RW. Magnetic resonance spectroscopy. *Medical physics*. 2008;**35**: 4530-4544.
46. Teresi LM. *A Practicing Radiologist Guide to MR Spectroscopy of the Brain*, 2007.
47. Mason G. Magnetic resonance spectroscopy for studies of neurotransmission in vivo. *Psychopharmacology bulletin*. 2002;**37**: 26-40.
48. Alger JR. Quantitative Proton Magnetic Resonance Spectroscopy and Spectroscopic Imaging of the Brain: A Didactic Review. *Topics in magnetic resonance imaging : TMRI*. 2010;**21**: 115-128.
49. Carrera I, Richter H, Meier D, Kircher PR, Dennler M. Regional metabolite concentrations in the brain of healthy dogs measured by use of short echo time, single voxel proton magnetic resonance spectroscopy at 3.0 Tesla. *American Journal of Veterinary Research*. 2015;**76**: 129-141.

50. Ober CP, Warrington CD, Feeney DA, Jessen CR, Steward S. Optimizing a protocol for 1H-magnetic resonance spectroscopy of the canine brain at 3T. *Veterinary Radiology & Ultrasound*. 2013;**54**: 149-158.
51. Abdel-Aziz K, Solanky BS, Yiannakas MC, Altmann DR, Wheeler-Kingshott CA, Thompson AJ, et al. Age related changes in metabolite concentrations in the normal spinal cord. *PLoS One*. 2014;**9**: e105774.
52. Duarte JMN, Lei H, Mlynárik V, Gruetter R. The neurochemical profile quantified by in vivo 1H NMR spectroscopy. *NeuroImage*. 2012;**61**: 342-362.
53. Rae C. RE: Magnetic resonance spectroscopy of the brain: review of metabolites and clinical applications. *Clinical Radiology*. 2009;**64**: 1042-1043.
54. Algin O, Taskapilioglu O, Ocakoglu G, Yurtogullari S, Hakyemez B. Value of MRS in the evaluation of deep grey matter in multiple sclerosis. *Iranian Journal of Radiology*. 2010;**7**: 161-165.
55. Hsu S-H, Chou M-C, Ko C-W, Hsu S-S, Lin H-S, Fu J-H, et al. Proton MR spectroscopy in patients with pyogenic brain abscess: MR spectroscopic imaging versus single-voxel spectroscopy. *European Journal of Radiology*. 2013;**82**: 1299-1307.
56. Kayabas U, Alkan A, Firat AK, Karakas HM, Bayindir Y, Yetkin F. Magnetic resonance spectroscopy features of normal-appearing white matter in patients with acute brucellosis. *European Journal of Radiology*. 2008;**65**: 417-420.
57. Mohamed MA, Barker PB, Skolasky RL, Selnes OA, Moxley RT, Pomper MG, et al. Brain metabolism and cognitive impairment in HIV infection: a 3-T magnetic resonance spectroscopy study. *Magnetic Resonance Imaging*. 2010;**28**: 1251-1257.
58. Sailasuta N, Ross W, Ananworanich J, Chalermchai T, DeGruttola V, Lerdlum S, et al. Change in brain magnetic resonance spectroscopy after treatment during acute HIV infection. *PLoS ONE*. 2012;**7**: e49272-e49272.
59. Tomiyasu M, Aida N, Watanabe Y, Mori K, Endo K, Kusakiri K, et al. Monitoring the brain metabolites of children with acute encephalopathy caused by the H1N1 virus responsible for the 2009 influenza pandemic: a quantitative in vivo 1H MR spectroscopy study. *Magnetic Resonance Imaging*. 2012;**30**: 1527-1533.
60. Yeo RA, Gasparovic C, Merideth F, Ruhl D, Doezema D, Mayer AR. A longitudinal proton magnetic resonance spectroscopy study of mild traumatic brain injury. *Journal of neurotrauma*. 2011;**28**: 1-11.

61. Martin-Vaquero P, da Costa RC, Echandi RL, Sammet CL, Knopp MV, Sammet S. Magnetic resonance spectroscopy of the canine brain at 3.0 T and 7.0 T. *Res Vet Sci.* 2012;**93**: 427-429.
62. Umbehr M, Bachmann LM, Held U, Kessler TM, Sulser T, Weishaupt D, et al. Combined Magnetic Resonance Imaging and Magnetic Resonance Spectroscopy Imaging in the Diagnosis of Prostate Cancer: A Systematic Review and Meta-analysis. *European Urology.* 2009;**55**: 575-591.
63. Baltzer PAT, Dietzel M. Breast Lesions: Diagnosis by Using Proton MR Spectroscopy at 1.5 and 3.0 T—Systematic Review and Meta-Analysis. *Radiology.* 2013;**267**: 735-746.
64. Bohte AE, van Werven JR, Bipat S, Stoker J. The diagnostic accuracy of US, CT, MRI and 1H-MRS for the evaluation of hepatic steatosis compared with liver biopsy: a meta-analysis. *Eur Radiol.* 2011;**21**: 87-97.
65. Wang W, Hu Y, Lu P, Li Y, Chen Y, Tian M, et al. Evaluation of the diagnostic performance of magnetic resonance spectroscopy in brain tumors: A systematic review and meta-analysis. *PloS one.* 2014;**9**: e112577.
66. Steen RG, Hamer RM, Lieberman JA. Measurement of Brain Metabolites by 1H Magnetic Resonance Spectroscopy in Patients with Schizophrenia: A Systematic Review and Meta-Analysis. *Neuropsychopharmacology.* 2005;**30**: 1949-1962.
67. Sievert C, Richter H, Beckmann K, Kircher PR, Carrera I. COMPARISON BETWEEN PROTON MAGNETIC RESONANCE SPECTROSCOPY FINDINGS IN DOGS WITH TICK-BORNE ENCEPHALITIS AND CLINICALLY NORMAL DOGS. *Veterinary Radiology & Ultrasound.* 2017;**58**: 53-61.
68. Lynch K. Ex vivo proton magnetic resonance spectroscopy (1HMRS) of normal, reactive and malignant canine lymph nodes: evaluation of the choline metabolite as a marker for malignancy. University of Illinois at Urbana-Champaign, 2014.
69. Dickinson PJ, LeCouteur RA, Higgins RJ, Bringas JR, Larson RF, Yamashita Y, et al. Canine spontaneous glioma: A translational model system for convection-enhanced delivery. *Neuro-Oncology.* 2010;**12**: 928-940.
70. Potschka H, Fischer A, von Rüden E-L, Hülsmeier V, Baumgärtner W. Canine epilepsy as a translational model? *Epilepsia.* 2013;**54**: 571-579.
71. Zhang Y, Shen J. Regional and tissue-specific differences in brain glutamate concentration measured by in vivo single voxel MRS. *J Neurosci Methods.* 2014.

72. Robertson I. Optimal magnetic resonance imaging of the brain. *Veterinary radiology & ultrasound : the official journal of the American College of Veterinary Radiology and the International Veterinary Radiology Association*. 2011;**52**: S15-22.
73. Baker EH, Basso G, Barker PB, Smith MA, Bonekamp D, Horská A. Regional apparent metabolite concentrations in young adult brain measured by ¹H MR spectroscopy at 3 Tesla. *Journal of Magnetic Resonance Imaging*. 2008;**27**: 489-499.
74. Pouwels PJ, Frahm J. Regional metabolite concentrations in human brain as determined by quantitative localized proton MRS. *Magnetic resonance in medicine*. 1998;**39**: 53-60.
75. Michaelis T, Merboldt K, Bruhn H, Hänicke W, Frahm J. Absolute concentrations of metabolites in the adult human brain in vivo: quantification of localized proton MR spectra. *Radiology*. 1993;**187**: 219-227.
76. Komoroski RA, Heimberg C, Cardwell D, Karson CN. Effects of gender and region on proton MRS of normal human brain. *Magnetic Resonance Imaging*. 1999;**17**: 427-433.
77. Nagae-Poetscher LM, Bonekamp D, Barker PB, Brant LJ, Kaufmann WE, Horská A. Asymmetry and gender effect in functionally lateralized cortical regions: A proton MRS imaging study. *Journal of Magnetic Resonance Imaging*. 2004;**19**: 27-33.
78. Xu D, Vigneron D. Magnetic Resonance Spectroscopy for Imaging the Newborn Brain – A Technical Review. *Seminars in perinatology*. 2010;**34**: 20-27.
79. Gross B, Garcia-Tapia D, Riedesel E, Ellinwood NM, Jens JK. NORMAL CANINE BRAIN MATURATION AT MAGNETIC RESONANCE IMAGING. *Veterinary Radiology & Ultrasound*. 2010;**51**: 361-373.
80. Ono K, Kitagawa M, Ito D, Tanaka N, Watari T. Regional variations and age-related changes detected with magnetic resonance spectroscopy in the brain of healthy dogs. *Am J Vet Res*. 2014;**75**: 179-186.
81. Charles HC, Lazeyras F, Krishnan KRR, Boyko OB, Patterson LJ, Doraiswamy PM, et al. Proton spectroscopy of human brain: Effects of age and sex. *Progress in Neuro-Psychopharmacology and Biological Psychiatry*. 1994;**18**: 995-1004.
82. Alkan A, Burulday V, Oztanir N, Dogan M, Erbay MF, Kocak A, et al. Effects of contrast material on the metabolite ratios in single-voxel MR Spectroscopy of intraaxial brain tumors. *Medical Hypotheses*. 2012;**79**: 129-131.

83. Lin AP, Ross BD. Short-echo time proton MR spectroscopy in the presence of gadolinium. *Journal of computer assisted tomography*. 2001;**25**: 705-712.
84. Idée J-M, Port M, Robic C, Medina C, Sabatou M, Corot C. Role of thermodynamic and kinetic parameters in gadolinium chelate stability. *Journal of Magnetic Resonance Imaging*. 2009;**30**: 1249-1258.
85. Greenwood NN, Earnshaw A. *Chemistry of the Elements*: Elsevier Science, 2012.
86. Kuriashkin IV, Losonsky JM. CONTRAST ENHANCEMENT IN MAGNETIC RESONANCE IMAGING USING INTRAVENOUS PARAMAGNETIC CONTRAST MEDIA: A REVIEW. *Veterinary Radiology & Ultrasound*. 2000;**41**: 4-7.
87. Brady TJ, Reimer P. Contrast Agents in Whole Body Magnetic Resonance: an Overview. In: Young IR (ed): *Methods in Biomedical Magnetic Resonance Imaging and Spectroscopy*. Ann Arbor, MI: Wiley, 2000.
88. Caravan P, Ellison JJ, McMurry TJ, Lauffer RB. Gadolinium(III) Chelates as MRI Contrast Agents: Structure, Dynamics, and Applications. *Chem Rev*. 1999;**99**: 2293-2352.
89. Telgmann L, Sperling M, Karst U. Determination of gadolinium-based MRI contrast agents in biological and environmental samples: A review. *Analytica Chimica Acta*. 2013;**764**: 1-16.
90. Bau M, Dulski P. Anthropogenic origin of positive gadolinium anomalies in river waters. *Earth and Planetary Science Letters*. 1996;**143**: 245-255.
91. Liu J, Qu W, Kadiiska MB. Role of oxidative stress in cadmium toxicity and carcinogenesis. *Toxicology and applied pharmacology*. 2009;**238**: 209-214.
92. Rogosnitzky M, Branch S. Gadolinium-based contrast agent toxicity: a review of known and proposed mechanisms. *Biometals*. 2016;**29**: 365-376.
93. Laine M, Arjamaa O, Vuolteenaho O, Ruskoaho H, Weckström M. Block of stretch-activated atrial natriuretic peptide secretion by gadolinium in isolated rat atrium. *The Journal of Physiology*. 1994;**480**: 553-561.
94. Ray DE, Holton JL, Nolan CC, Cavanagh JB, Harpur ES. Neurotoxic potential of gadodiamide after injection into the lateral cerebral ventricle of rats. *AJNR American journal of neuroradiology*. 1998;**19**: 1455-1462.
95. Ray DE, Cavanagh JB, Nolan CC, Williams SC. Neurotoxic effects of gadopentetate dimeglumine: behavioral disturbance and morphology after intracerebroventricular injection in rats. *AJNR American journal of neuroradiology*. 1996;**17**: 365-373.

96. Roman-Goldstein SM, Barnett PA, McCormick CI, Szumowski J, Shannon EM, Ramsey FL, et al. Effects of Gd-DTPA after osmotic BBB disruption in a rodent model: toxicity and MR findings. *J Comput Assist Tomogr.* 1994;**18**: 731-736.
97. Feng X, Xia Q, Yuan L, Yang X, Wang K. Impaired mitochondrial function and oxidative stress in rat cortical neurons: implications for gadolinium-induced neurotoxicity. *Neurotoxicology.* 2010;**31**: 391-398.
98. Xia Q, Feng X, Huang H, Du L, Yang X, Wang K. Gadolinium-induced oxidative stress triggers endoplasmic reticulum stress in rat cortical neurons. *Journal of neurochemistry.* 2011;**117**: 38-47.
99. Valko M, Rhodes CJ, Moncol J, Izakovic M, Mazur M. Free radicals, metals and antioxidants in oxidative stress-induced cancer. *Chemico-biological interactions.* 2006;**160**: 1-40.
100. Aime S, Caravan P. Biodistribution of gadolinium-based contrast agents, including gadolinium deposition. *Journal of magnetic resonance imaging : JMRI.* 2009;**30**: 1259-1267.
101. Weinmann HJ, Laniado M, Mutzel W. Pharmacokinetics of GdDTPA/dimeglumine after intravenous injection into healthy volunteers. *Physiological chemistry and physics and medical NMR.* 1984;**16**: 167-172.
102. Carr D, Brown J, Bydder G, Steiner R, Weinmann H, Speck U, et al. Gadolinium-DTPA as a contrast agent in MRI: initial clinical experience in 20 patients. *American Journal of Roentgenology.* 1984;**143**: 215-224.
103. Lohrke J, Frenzel T, Endrikat J, Alves FC, Grist TM, Law M, et al. 25 Years of Contrast-Enhanced MRI: Developments, Current Challenges and Future Perspectives. *Advances in therapy.* 2016;**33**: 1-28.
104. Smith JA. Hazards, Safety, and Anesthetic Considerations for Magnetic Resonance Imaging. *Topics in Companion Animal Medicine.* 2010;**25**: 98-106.
105. Kanda T, Fukusato T, Matsuda M, Toyoda K, Oba H, Kotoku Ji, et al. Gadolinium-based Contrast Agent Accumulates in the Brain Even in Subjects without Severe Renal Dysfunction: Evaluation of Autopsy Brain Specimens with Inductively Coupled Plasma Mass Spectroscopy. *Radiology.* 2015;**276**: 228-232.
106. Shi H, Liu C, Ding HY, Li CW. Magnesium sulfate as an oral contrast medium in magnetic resonance imaging of the small intestine. *Eur J Radiol.* 2012;**81**: e370-375.

107. Kubicek V, Vitha T, Kotek J, Hermann P, Vander Elst L, Muller RN, et al. Towards MRI contrast agents responsive to Ca(II) and Mg(II) ions: metal-induced oligomerization of dota-bisphosphonate conjugates. *Contrast media & molecular imaging*. 2010;**5**: 294-296.
108. Brekenfeld C, Foert E, Hundt W, Kenn W, Lodeann K-P, GEHL H-B. Enhancement of Cerebral Diseases: How Much Contrast Agent Is Enough?: Comparison of 0.1, 0.2, and 0.3 mmol/kg Gadoteridol at 0.2 T with 0.1 mmol/kg Gadoteridol at 1.5 T. *Investigative Radiology*. 2001;**36**: 266-275.
109. Ramalho J, Semelka RC, Ramalho M, Nunes RH, AlObaidy M, Castillo M. Gadolinium-Based Contrast Agent Accumulation and Toxicity: An Update. *AJNR American journal of neuroradiology*. 2015.
110. Hao D, Ai T, Goerner F, Hu X, Runge VM, Tweedle M. MRI contrast agents: Basic chemistry and safety. *Journal of Magnetic Resonance Imaging*. 2012;**36**: 1060-1071.
111. Park K-W, Im S-B, Kim B-T, Hwang S-C, Park J-S, Shin W-H. Neurotoxic Manifestations of an Overdose Intrathecal Injection of Gadopentetate Dimeglumine. *Journal of Korean Medical Science*. 2010;**25**: 505-508.
112. Birchard KR, Busireddy KR, Semelka RC. *Critical Observations in Radiology for Medical Students*: Wiley, 2015.
113. Murata N, Gonzalez-Cuyar LF, Murata K, Fligner C, Dills R, Hippe D, et al. Macrocyclic and Other Non-Group 1 Gadolinium Contrast Agents Deposit Low Levels of Gadolinium in Brain and Bone Tissue: Preliminary Results From 9 Patients With Normal Renal Function. *Invest Radiol*. 2016;**51**: 447-453.
114. Konar M, Lang J. Pros and Cons of Low-Field Magnetic Resonance Imaging in Veterinary Practice. *Veterinary Radiology & Ultrasound*. 2011;**52**: S5-S14.
115. Yancey JM, Ackerman N, Kaude JV, Googe RE, Fitzsimmons JR, Scott KN, et al. Gadolinium-Dtpa Enhancement of Vx-2 Carcinoma of the Rabbit Kidney on T1 Weighted Magnetic Resonance Images. *Acta Radiologica*. 1987;**28**: 479-482.
116. Pettersson H, Ackerman N, Kaude J, Googe RE, Mancuso AA, Scott KN, et al. Gadolinium-DTPA Enhancement of Experimental Soft Tissue Carcinoma and Hemorrhage in Magnetic Resonance Imaging. *Acta Radiologica*. 1987;**28**: 75-78.
117. Frank JA, Choyke PL, Girton ME, Austin HA, Sievenpiper C, Inscoe SW, et al. Gadolinium-DTPA Enhanced Dynamic MR Imaging in the Evaluation of Cisplatin Nephrotoxicity. *Journal of Computer Assisted Tomography*. 1989;**13**: 448-459.

118. van Nesselrooij JHJ, Szeverenyi NM, Tillapaugh-Fay GM, Hendriksen FGJ. Gadolinium-DTPA-enhanced and digitally subtracted magnetic resonance imaging of estrogen-induced pituitary lesions in rats: Correlation with pituitary anatomy. *Magnetic Resonance Imaging*. 1990;**8**: 525-533.
119. Goldstein EJ, Burnett KR, Wolf GL, Wortman J, Joseph P, Sen S. Contrast enhancement of spontaneous animal CNS tumors with gadolinium DTPA: a correlation of MRI with x-ray CT. *Physiological chemistry and physics and medical NMR*. 1985;**17**: 113-122.
120. Gavin PR. Growth of clinical veterinary magnetic resonance imaging. *Veterinary radiology & ultrasound : the official journal of the American College of Veterinary Radiology and the International Veterinary Radiology Association*. 2011;**52**: S2-4.
121. Dennis R. Magnetic resonance imaging and its applications in small animals. *In Practice (0263841X)*. 1998;**20**.
122. Dennis R. Optimal magnetic resonance imaging of the spine. *Veterinary radiology & ultrasound : the official journal of the American College of Veterinary Radiology and the International Veterinary Radiology Association*. 2011;**52**: S72-80.
123. Dillman JR, Ellis JH, Cohan RH, Strouse PJ, Jan SC. Frequency and severity of acute allergic-like reactions to gadolinium-containing iv contrast media in children and adults. *American Journal of Roentgenology*. 2007;**189**: 1533-1538.
124. Hunt CH, Hartman RP, Hesley GK. Frequency and Severity of Adverse Effects of Iodinated and Gadolinium Contrast Materials: Retrospective Review of 456,930 Doses. *American Journal of Roentgenology*. 2009;**193**: 1124-1127.
125. Murphy KJ, Brunberg JA, Cohan RH. Adverse reactions to gadolinium contrast media: a review of 36 cases. *American Journal of Roentgenology*. 1996;**167**: 847-849.
126. Girard NM, Leece EA. Suspected anaphylactoid reaction following intravenous administration of a gadolinium-based contrast agent in three dogs undergoing magnetic resonance imaging. *Veterinary Anaesthesia and Analgesia*. 2010;**37**: 352-356.
127. Murphy KPJ, Szopinski KT, Cohan RH, Mermillod B, Ellis JH. Occurrence of adverse reactions to gadolinium-based contrast material and management of patients at increased risk: A survey of the American society of neuroradiology fellowship directors. *Academic Radiology*. 1999;**6**: 656-664.

128. Prince MR, Zhang H, Zou Z, Staron RB, Brill PW. Incidence of Immediate Gadolinium Contrast Media Reactions. *American Journal of Roentgenology*. 2011;**196**: W138-W143.
129. Pollard RE, Puchalski SM, Pascoe PJ. Hemodynamic and serum biochemical alterations associated with intravenous administration of three types of contrast media in anesthetized dogs. *American Journal of Veterinary Research*. 2008;**69**: 1268-1273.
130. Pollard RE, Puchalski SM, Pascoe PJ. Hemodynamic and serum biochemical alterations associated with intravenous administration of three types of contrast media in anesthetized cats. *Am J Vet Res*. 2008;**69**: 1274-1278.
131. Forsting M, Palkowitsch P. Prevalence of acute adverse reactions to gadobutrol—A highly concentrated macrocyclic gadolinium chelate: Review of 14,299 patients from observational trials. *European Journal of Radiology*. 2010;**74**: e186-e192.
132. Morcos S, Thomsen H. Adverse reactions to iodinated contrast media. *Eur Radiol*. 2001;**11**: 1267-1275.
133. Bruder O, Schneider S, Pilz G, van Rossum A, Schwitter J, Nothnagel D, et al. 2015 Update on Acute Adverse Reactions to Gadolinium based Contrast Agents in Cardiovascular MR. Large Multi-National and Multi-Ethnic Population Experience With 37788 Patients From the EuroCMR Registry. *Journal of Cardiovascular Magnetic Resonance*. 2015;**17**: 1-7.
134. Mair AR, Woolley J, Martinez M. Cardiovascular effects of intravenous gadolinium administration to anaesthetized dogs undergoing magnetic resonance imaging. *Veterinary Anaesthesia and Analgesia*. 2010;**37**: 337-341.
135. Katayama H, Yamaguchi K, Kozuka T, Takashima T, Seez P, Matsuura K. Adverse reactions to ionic and nonionic contrast media. A report from the Japanese Committee on the Safety of Contrast Media. *Radiology*. 1990;**175**: 621-628.
136. Davenport MS, Bashir MR, Pietryga JA, Weber JT, Khalatbari S, Hussain HK. Dose-Toxicity Relationship of Gadoxetate Disodium and Transient Severe Respiratory Motion Artifact. *American Journal of Roentgenology*. 2014;**203**: 796-802.
137. Davenport MS, Viglianti BL, Al-Hawary MM, Caoili EM, Kaza RK, Liu PSC, et al. Comparison of Acute Transient Dyspnea after Intravenous Administration of Gadoxetate Disodium and Gadobenate Dimeglumine: Effect on Arterial Phase Image Quality. *Radiology*. 2013;**266**: 452-461.
138. Jordan R, Mintz R. Fatal reaction to gadopentetate dimeglumine. *AJR American journal of roentgenology*. 1995;**164**: 743-744.

139. *ACR Manual on Contrast Media*, 2015.
140. Granata V, Cascella M, Fusco R, dell'Aprovitola N, Catalano O, Filice S, et al. Immediate Adverse Reactions to Gadolinium-Based MR Contrast Media: A Retrospective Analysis on 10,608 Examinations. *BioMed research international*. 2016;**2016**: 3918292.
141. Idee JM, Berthommier C, Goulas V, Corot C, Santus R, Hermine C, et al. Haemodynamic effects of macrocyclic and linear gadolinium chelates in rats: role of calcium and transmetallation. *Biometals*. 1998;**11**: 113-123.
142. Bokenes J, Hustvedt SO, Refsum H. Comparison of cardiovascular changes after administration of gadodiamide injection and gadopentetate dimeglumine in dogs. *Acad Radiol*. 1997;**4**: 204-209.
143. Kaewlai R, Abujudeh H. Nephrogenic Systemic Fibrosis. *American Journal of Roentgenology*. 2012;**199**: W17-W23.
144. Rydahl C, Thomsen HS, Marckmann P. High Prevalence of Nephrogenic Systemic Fibrosis in Chronic Renal Failure Patients Exposed to Gadodiamide, a Gadolinium-Containing Magnetic Resonance Contrast Agent. *Investigative Radiology*. 2008;**43**: 141-144.
145. Kuo PH, Kanal E, Abu-Alfa AK, Cowper SE. Gadolinium-based MR Contrast Agents and Nephrogenic Systemic Fibrosis. *Radiology*. 2007;**242**: 647-649.
146. Cowper SE, Robin HS, Steinberg SM, Su LD, Gupta S, LeBoit PE. Scleromyxoedema-like cutaneous diseases in renal-dialysis patients. *The Lancet*.**356**: 1000-1001.
147. Semelka RC, Commander CW, Jay M, Burke LM, Ramalho M. Presumed Gadolinium Toxicity in Subjects With Normal Renal Function: A Report of 4 Cases. *Invest Radiol*. 2016;**51**: 661-665.
148. Christensen KN, Lee CU, Hanley MM, Leung N, Moyer TP, Pittelkow MR. Quantification of gadolinium in fresh skin and serum samples from patients with nephrogenic systemic fibrosis. *Journal of the American Academy of Dermatology*. 2011;**64**: 91-96.
149. Sanyal S, Marckmann P, Scherer S, Abraham JL. Multiorgan gadolinium (Gd) deposition and fibrosis in a patient with nephrogenic systemic fibrosis—an autopsy-based review. *Nephrology Dialysis Transplantation*. 2011;**26**: 3616-3626.
150. Semelka R. Contrast Enhanced Body MR Imaging: Making Diagnoses While Managing Risks. *Safety of Gadolinium-Based Contrast Agents: A Four Part Webcast Series*, 2016.

151. Pollard RE, Pascoe PJ. Severe reaction to intravenous administration of an ionic iodinated contrast agent in two anesthetized dogs. *Journal of the American Veterinary Medical Association*. 2008;**233**: 274-278.
152. Pollard RE, Puchalski SM. REACTION TO INTRAARTERIAL IONIC IODINATED CONTRAST MEDIUM ADMINISTRATION IN ANESTHETIZED HORSES. *Veterinary Radiology & Ultrasound*. 2011;**52**: 441-443.
153. Roccatagliata L, Vuolo L, Bonzano L, Pichiecchio A, Mancardi GL. Multiple Sclerosis: Hyperintense Dentate Nucleus on Unenhanced T1-weighted MR Images Is Associated with the Secondary Progressive Subtype. *Radiology*. 2009;**251**: 503-510.
154. Kasahara S, Miki Y, Kanagaki M, Yamamoto A, Mori N, Sawada T, et al. Hyperintense dentate nucleus on unenhanced T1-weighted MR images is associated with a history of brain irradiation. *Radiology*. 2011;**258**: 222-228.
155. Robert P, Lehericy S, Grand S, Violas X, Fretellier N, Idee JM, et al. T1-Weighted Hypersignal in the Deep Cerebellar Nuclei After Repeated Administrations of Gadolinium-Based Contrast Agents in Healthy Rats: Difference Between Linear and Macrocyclic Agents. *Invest Radiol*. 2015;**50**: 473-480.
156. Errante Y, Cirimele V, Mallio CA, Di Lazzaro V, Zobel BB, Quattrocchi CC. Progressive increase of T1 signal intensity of the dentate nucleus on unenhanced magnetic resonance images is associated with cumulative doses of intravenously administered gadodiamide in patients with normal renal function, suggesting dechelation. *Invest Radiol*. 2014;**49**: 685-690.
157. Roberts DR, Chatterjee AR, Yazdani M, Marebwa B, Brown T, Collins H, et al. Pediatric Patients Demonstrate Progressive T1-Weighted Hyperintensity in the Dentate Nucleus following Multiple Doses of Gadolinium-Based Contrast Agent. *American Journal of Neuroradiology*. 2016.
158. Kanal E, Tweedle MF. Residual or Retained Gadolinium: Practical Implications for Radiologists and Our Patients. *Radiology*. 2015;**275**: 630-634.
159. Kanda T, Ishii K, Kawaguchi H, Kitajima K, Takenaka D. High Signal Intensity in the Dentate Nucleus and Globus Pallidus on Unenhanced T1-weighted MR Images: Relationship with Increasing Cumulative Dose of a Gadolinium-based Contrast Material. *Radiology*. 2014;**270**: 834-841.

160. Quattrocchi CC, Mallio CA, Errante Y, Cirimele V, Carideo L, Ax A, et al. Gadodiamide and Dentate Nucleus T1 Hyperintensity in Patients With Meningioma Evaluated by Multiple Follow-Up Contrast-Enhanced Magnetic Resonance Examinations With No Systemic Interval Therapy. *Invest Radiol.* 2015;**50**: 470-472.
161. Ramalho J, Castillo M, AlObaidy M, Nunes RH, Ramalho M, Dale BM, et al. High Signal Intensity in Globus Pallidus and Dentate Nucleus on Unenhanced T1-weighted MR Images: Evaluation of Two Linear Gadolinium-based Contrast Agents. *Radiology.* 2015;**276**: 836-844.
162. Kanda T, Osawa M, Oba H, Toyoda K, Kotoku Ji, Haruyama T, et al. High Signal Intensity in Dentate Nucleus on Unenhanced T1-weighted MR Images: Association with Linear versus Macrocyclic Gadolinium Chelate Administration. *Radiology.* 2015;**275**: 803-809.
163. Roberts DR, Holden KR. Progressive increase of T1 signal intensity in the dentate nucleus and globus pallidus on unenhanced T1-weighted MR images in the pediatric brain exposed to multiple doses of gadolinium contrast. *Brain & development.* 2016;**38**: 331-336.
164. Gibby WA, Gibby KA, Gibby WA. Comparison of Gd DTPA-BMA (Omniscan) versus Gd HP-DO3A (ProHance) Retention in Human Bone Tissue by Inductively Coupled Plasma Atomic Emission Spectroscopy. *Investigative Radiology.* 2004;**39**: 138-142.
165. Darrah TH, Prutsman-Pfeiffer JJ, Poreda RJ, Ellen Campbell M, Hauschka PV, Hannigan RE. Incorporation of excess gadolinium into human bone from medical contrast agents. *Metallomics.* 2009;**1**: 479-488.
166. McDonald RJ, McDonald JS, Kallmes DF, Jentoft ME, Murray DL, Thielen KR, et al. Intracranial Gadolinium Deposition after Contrast-enhanced MR Imaging. *Radiology.* 2015;**275**: 772-782.
167. Adin ME, Kleinberg L, Vaidya D, Zan E, Mirbagheri S, Yousem DM. Hyperintense Dentate Nuclei on T1-Weighted MRI: Relation to Repeat Gadolinium Administration. *AJNR American journal of neuroradiology.* 2015;**36**: 1859-1865.
168. Roman-Goldstein SM, Barnett PA, McCormick CI, Ball MJ, Ramsey F, Neuwelt EA. Effects of gadopentetate dimeglumine administration after osmotic blood-brain barrier disruption: toxicity and MR imaging findings. *AJNR American journal of neuroradiology.* 1991;**12**: 885-890.

169. Administration USFaD. FDA evaluating the risk of brain deposits with repeated use of gadolinium-based contrast agents for magnetic resonance imaging (MRI). Safety Announcement 2015 [cited 2015 July 30]; Available from: <http://www.fda.gov/Drugs/DrugSafety/ucm455386.htm>
170. Malayeri AA, Brooks KM, Bryant LH, Evers R, Kumar P, Reich DS, et al. National Institutes of Health Perspective on Reports of Gadolinium Deposition in the Brain. *Journal of the American College of Radiology*.**13**: 237-241.
171. Smirniotopoulos JG, Murphy FM, Rushing EJ, Rees JH, Schroeder JW. Patterns of Contrast Enhancement in the Brain and Meninges. *RadioGraphics*. 2007;**27**: 525-551.
172. Rohrer M, Bauer H, Mintorovitch J, Requardt M, Weinmann H-J. Comparison of magnetic properties of MRI contrast media solutions at different magnetic field strengths. *Investigative radiology*. 2005;**40**: 715-724.
173. Kanal E, Maravilla K, Rowley HA. Gadolinium Contrast Agents for CNS Imaging: Current Concepts and Clinical Evidence. *American Journal of Neuroradiology*. 2014;**35**: 2215-2226.
174. Kimpe T, Tuytschaever T. Increasing the Number of Gray Shades in Medical Display Systems—How Much is Enough? *Journal of Digital Imaging*. 2007;**20**: 422-432.
175. White GW, Gibby WA, Tweedle MF. Comparison of Gd(DTPA-BMA) (Omniscan) Versus Gd(HP-DO3A) (ProHance) Relative to Gadolinium Retention in Human Bone Tissue by Inductively Coupled Plasma Mass Spectroscopy. *Investigative Radiology*. 2006;**41**: 272-278.
176. Oksendal AN, Hals P-A. Biodistribution and toxicity of MR imaging contrast media. *Journal of Magnetic Resonance Imaging*. 1993;**3**: 157-165.
177. Radbruch A, Weberling LD, Kieslich PJ, Eidel O, Burth S, Kickingereeder P, et al. Gadolinium Retention in the Dentate Nucleus and Globus Pallidus Is Dependent on the Class of Contrast Agent. *Radiology*. 2015;**275**: 783-791.
178. Joslyn S, Sullivan M, Novellas R, Brennan N, Cameron G, Hammond G. EFFECT OF DELAYED ACQUISITION TIMES ON GADOLINIUM-ENHANCED MAGNETIC RESONANCE IMAGING OF THE PRESUMABLY NORMAL CANINE BRAIN. *Veterinary Radiology & Ultrasound*. 2011;**52**: 611-618.
179. Iliff JJ, Lee H, Yu M, Feng T, Logan J, Nedergaard M, et al. Brain-wide pathway for waste clearance captured by contrast-enhanced MRI. *The Journal of Clinical Investigation*. 2013;**123**: 1299-1309.

180. Iliff JJ, Wang M, Liao Y, Plogg BA, Peng W, Gundersen GA, et al. A paravascular pathway facilitates CSF flow through the brain parenchyma and the clearance of interstitial solutes, including amyloid beta. *Science translational medicine*. 2012;**4**: 147ra111.
181. Arbughi T, Bertani F, Celeste R, Grotti A, Sillari S, Tirone P. High-performance liquid chromatographic determination of the magnetic resonance imaging contrast agent gadobenate ion in plasma, urine, faeces, bile and tissues. *Journal of Chromatography B: Biomedical Sciences and Applications*. 1998;**713**: 415-426.
182. Kindberg GM, Uran S, Friisk G, Martinsen I, Skotland T. The fate of Gd and chelate following intravenous injection of gadodiamide in rats. *Eur Radiol*. 2010;**20**: 1636-1643.
183. Normann PT, Hals PA. In vivo stability and excretion of gadodiamide (GdDTPA-BMA), a hydrophilic gadolinium complex used as a contrast enhancing agent for magnetic resonance imaging. *European Journal of Drug Metabolism and Pharmacokinetics*. 1995;**20**: 307-313.
184. Omniscan [package insert]. Oslo, Norway: G.E. Healthcare, 2010.
185. Mata M, Gottschalk S. Man's Best Friend: Utilizing Naturally Occurring Tumors in Dogs to Improve Chimeric Antigen Receptor T-cell Therapy for Human Cancers. *Molecular therapy : the journal of the American Society of Gene Therapy*. 2016;**24**: 1511-1512.
186. Baker MA. Technical note – Considerations for MR imaging of small animals. *Radiography*. 2011;**17**: 171-174.

APPENDIX A
LIST OF ABBREVIATIONS

Ala – Alanine

B_0 – Main magnetic field or M_z (z) magnetization axis

BBB – Blood brain barrier

CEMRI – Contrast enhanced magnetic resonance imaging

Cho – Choline

Cr – Creatine

CSF – Cerebrospinal fluid

FID – Free induction decay

FLAIR – Fluid attenuation inversion recovery

FWHM – Full width half maximum

GABA – γ -amino butyric acid

GBCA – Gadolinium-based contrast agent

Gd – Gadolinium

Glu – Glutamate

Gln – Glutamine

Glx – Glutamate/glutamine complex

Gsh – Glutathione

^1H – Proton

Lac – Lactate

Lip – Lipids

mI – Myo-inositol

MR – Magnetic resonance

MRI – Magnetic resonance imaging

MRS – Magnetic resonance spectroscopy
MRSI – Magnetic resonance spectroscopic imaging
ms – milliseconds
MVS – Multi-voxel spectroscopy
NAA – N-acetyl aspartate
NEX – Number of signal averages
NMR – Nuclear Magnetic Resonance
PRESS – Point resolved spectroscopy
RF – Radiofrequency
STEAM – Stimulated echo acquisition mode
SVS – Single-voxel spectroscopy
T1 – Longitudinal relaxation time
T2 – Transverse relaxation time
Tau – Taurine
TE – Time to echo or echo time
TR – Time to repetition

APPENDIX B

MR SPECTROSCOPIC METABOLITES OF INTEREST

Table B.1 MRS metabolites of interest, spins, and clinical importance

Metabolite of Interest	ppm spin at 3T	Relevance
N-acetyl aspartate (NAA)	2.0	Most prominent peak. Quantitative for neuronal viability. Indicates grey matter neuronal number and white matter axonal density. Present only in neurons, axons, and dendrites.
Creatine (Cr)	3.0	2 nd tallest peak in the grey matter spectra. Brain energy marker.
Choline (Cho)	3.2	Complex peak of several choline containing membrane & brain inflammatory markers. Elevations occur with inflammation and malignancy. Cell membrane marker involved in synthesis and degradation.
Myo-inositol (mI)	3.5, 3.7	Pentose sugar, involved in the inositol triphosphate intracellular second messenger system. Osmolyte and astrocyte biomarker. Seen with abnormal metabolism or damaged membranes. Elevated with mannitol administration.
Lactate (Lac)	1.3	Product of anaerobic glycolysis (low levels in normal brains). Increased with hypoxic events, cell death and necrosis. Can be increased in brain tumors and infarction.

Table B.1 (Continued)

Lipids (Lip)	0.9–1.4	Normal component of scalp, skull & cell membranes. Increased with cell death. Can be a voxel contaminant.
Glutamine/Glutamate (Glx)	2.2–2.4	Excitatory neurotransmitters (glutamate is excitatory and plays a role in mitochondrial metabolism; glutamine plays a part in detoxification and regulates neurotransmitter activity).
Alanine (Ala)	1.48	Non-essential amino acid. Not usually present. Present in meningiomas
Taurine (Tau)	3.4	Osmoregulator and modulator of neurotransmitter action. Suggests aggressive tumor growth, as with medulloblastoma.

Spins of various brain metabolites (in ppm) acquired as part of a magnetic resonance spectrum, with their associated properties, clinical relevance, and use. *Adapted from Soares and Law (2009) and Baker et al (2010).*^{31,186}

APPENDIX C
BRAIN MRI PROTOCOLS

Typical MRI acquisition protocols

Typical conventional MRI acquisition protocol was as follows:

Matrix: 512x512

NEX (Number of signal averages): 2

Reconstruction diameter: 140 mm

Slice thickness: 2.4 mm

Slice interval: 2.4 mm

Dog 1-8 Sequences of Interest

Parameter	Pre-Contrast						Post-Contrast			MVS	
	T1-W FLAIR	T2-W	T1-W FSPGR	T2-W FLAIR	DWI	T2* FGRE	DTI	TOF 3D	T1 FSPGR 3D		SVS
TR (ms)	1157.9 - 1774.2	2650- 3966.7	8.2-8.3	7202- 7852	9000- 9400	320- 595	13400 -	33.3- 52.0	8.2-8.3	1500	1500
TE (ms)	8.0-8.2	97.1- 106.0	3.6-3.7	123.7- 126.1	82.5- 89.8	6-8	89- 95.9	3.2-5.9	3.6-3.7	30	30
Slice thickness (mm)	2.4	2.4	1.2	2.4	2.4	2.4	2.4	1.2	1.2	7.2-18	7.2-18
Interslice gap (mm)	2.4	2.4	0.6	2.4	2.4	2.4	2.4	0.3	0.6	7.2-18	7.2-18
NSA	1-2	1-2	0.5-1	2	2	1-2	2	1	1	8	2
Flip Angle	90°	90°	20°	90°	90°	18°	90°	15°	20°	90°	90°
Echo train	7-9	20-24	1	1	1	1	1	1	1	1	1
Echo number	1	1	1	1	1	1	1	1	1	1	1
Matrix (conventional)	512 x 512	512 x 512	512 x 512	512 x 512	256 x 256	512 x 512	256 x 256	512 x 512	512 x 512	1 x 1	0 x 0
Recon diameter (mm)	140- 160	120-160	140	140	140- 150	140	140	140- 160	140	140	120- 140
Phase field of view (%)*	90-100	90-100	90-100	100	100	100	100	75-100	90-100	100	100
Inversion time (ms)	525- 805	0	450	2000	0	0	0	0	450	0	0
Percent sampling	100	100	64.3-100	100	100	100	100	100	100	100	100
Pixel bandwidth (Hz)	122.1	122.1	122.1	122.1	1304.7	122.1	1304.	61.0- 122.1	122.1	9.8	3.9
Acquisition Matrix	0 x 0	0 x 0	0 x 0	0 x 0	160 x 160	0 x 0	0 x 0	0 x 0	0 x 0	1 x 1	0 x 0

FLAIR (fluid attenuated inversion recovery); FSPGR (fast spoiled gradient); FGRE (fast gradient recall echo); * (16 cm field of view)
Parameters reflect the range of parameters used for multiple image planes (transverse, sagittal, and dorsal).

Figure C.1 MRI acquisition parameters for the eight dogs described in Chapters II, IV, and group 1 of IV

Typical MR sequences

Table C.2 Typical minimum MR sequences and acquisition parameters acquired for all dogs in Chapters II and IV, and group 1 of Chapter V

Sequence	Echo Time [TE] (ms)	Repetition time [TR] (ms)	Flip angle (degrees)
Sagittal T1-W fast spoiled gradient echo (FSPGR)	3.7	8.3	20
Transverse T1-W fast spoiled gradient echo (FSPGR)	3.7	8.3	20
Transverse T2-W fluid attenuation inversion recovery (FLAIR)	126.1	7777	90
Transverse T2* fast gradient echo (FGRE)	6	545	18
Transverse T1-W fast spoiled gradient echo (FSPGR) post-contrast	3.7	8.3	90